



KfK 4817

Mai 1991

**Electrochemical Studies of the
Corrosion Behavior of the
Fine-Grained Structural Steel
DIN W. Nr. 1.0566 between
55 and 90° C in Simulated
Salt Brine Repository
Environments**

A. M. Farvaque-Béra, S. Leistikow
Institut für Materialforschung

Kernforschungszentrum Karlsruhe

KERNFORSCHUNGSZENTRUM KARLSRUHE

Institut für Materialforschung

KfK 4817

Electrochemical Studies of the Corrosion Behavior of the Fine-Grained
Structural Steel DIN W.Nr. 1.0566 between 55 and 90°C in Simulated
Salt Brine Repository Environments

A.M. Farvaque-Béra, S. Leistikow

Kernforschungszentrum Karlsruhe GmbH, Karlsruhe

Als Manuskript gedruckt
Für diesen Bericht behalten wir uns alle Rechte vor

Kernforschungszentrum Karlsruhe GmbH
Postfach 3640, 7500 Karlsruhe 1

ISSN 0303-4003

Electrochemical Studies of the Corrosion Behavior of the Fine-Grained Structural Steel DIN W.Nr. 1.0566 between 55 and 90°C in Simulated Salt Brine Repository Environments

At first basic literature data on corrosion of low-carbon steels in salt containing solutions are presented. Secondly, complementary to long-time immersion tests which are performed within the same KfK program, results of own electrochemical tests in similar solutions are given.

The electrochemical corrosion of the fine-grained structural steel DIN W.Nr. 1.0566 was tested between 55 and 90°C in three simulated salt brines of similar compositions as analyzed for the Gorleben repository environment. As test parameters the temperature, the salt brine composition, the stirring velocity and the oxygen content as well as the state of the steel surface were varied.

As experimental results of the above mentioned tests are presented: (1) the free corrosion potentials of the steel in three brines, (2) Tafel plots of current densities as measured potentiodynamically in the anodic and cathodic vicinity of the corrosion potentials and being representative for the rate of metal dissolution, (3) the surface morphology of the corroded specimens. As mechanisms - in the absence of oxygen - the cathodic reduction of water and the anodic dissolution of iron are considered to prevail the corrosion reaction. It is shown that the applied electrochemical techniques are able to determine within an accelerated procedure the most important corrosion parameters in respect to their influence on rate of metal dissolution and morphology of corrosion attack.

Elektrochemische Untersuchungen des Korrosionsverhaltens des Feinkornbaustahls DIN W.Nr. 1.0566 zwischen 55 und 90°C in simulierten Salzlaugen von Endlagerstätten

Aus der Literatur werden zuerst grundlegende Resultate von Korrosionsversuchen an niedrig kohlenstoffhaltigen Stählen in salzhaltigen Lösungen dargestellt. In Ergänzung von Immersionsversuchen, die innerhalb desselben KfK-Programms durchgeführt werden, werden sodann Ergebnisse eigener elektrochemischer Versuche in ähnlichen Lösungen vorgestellt.

Elektrochemische Korrosionsuntersuchungen am Feinkornbaustahl DIN W.Nr. 1.0566 wurden zwischen 55 und 90°C in drei Salzlösungen – ähnlicher chemischer Zusammensetzung wie sie für das Endlager Gorleben bestimmt wurden – durchgeführt. Als Parameter wurde die Temperatur, die Zusammensetzung, die Rührgeschwindigkeit und der Sauerstoffgehalt der Lösung sowie der Oberflächenzustand des Stahls variiert.

Als experimentelle Ergebnisse der oben erwähnten Versuche werden ausgewiesen: (1) die Freien Korrosionspotentiale des Stahls in drei Salzlösungen, (2) Tafel-Auswertungen der im anodisch-kathodischen Umfeld der Korrosionspotentiale potentiodynamisch gemessenen Stromdichte-Verläufe, die ein Maß für die Metallauflösung darstellen, (3) die Oberflächen-Morphologie der korrodierten Proben. Als Mechanismen werden - bei Abwesenheit von Sauerstoff - die kathodische Reduktion von Wasser und die anodische Auflösung von Eisen als für die Korrosionsreaktion vorherrschend angesehen. Es wird gezeigt, daß die angewandten elektrochemischen Techniken geeignet sind, die wichtigsten Parameter – hinsichtlich ihres Einflusses auf die Geschwindigkeit der Metallauflösung und die Morphologie des Korrosionsangriffs – in einem beschleunigten Verfahren zu bestimmen.

		Page
0	Abstract	
1	Introduction	1
2	Literature Survey on Corrosion Mechanisms	5
	2.1 Electrochemical Reactions	5
	2.2 Role of Environmental Variables	7
	2.3 Pitting Corrosion	11
3	Literature Survey on Corrosion Test Results	21
	3.1 Granitic and Basalt Groundwaters	21
	3.2 Sea Water and Marine Sediments	24
	3.3 Geothermal and Salt Brines	27
4	Electrochemical Corrosion Test Methodology	33
	4.1 Material Test Conditions	33
	4.2 Experimental Procedure	34
	4.3 Electrochemical Testing Procedures	34
	4.4 Preliminary Corrosion Results	45
5	Experimental Results	61
	5.1 Free Corrosion Potential	61
	5.2 Polarization Behavior	61
	5.3 Influence of Different Parameters on the Corrosion Behavior	68
	5.4 Influence of Temperature and Salt Brine Composition	73
6	Discussion	84
7	Conclusions	88
9	References	89

1. Introduction

The aim of the presented work is to determine by electrochemical methods the corrosion behavior of candidate overpack materials, suitable to fabricate nuclear waste packages for final storage in salt mines. A comparison of the radioactive waste disposal activities in different countries is given in Table 1.

Radioactive waste disposal, based on the concept of isolating radionuclides from the biosphere by combining geological with engineered barriers, is planned in Germany in deep rock salt formations. The candidate overpack materials must provide a long-term corrosion resistance (500-1000 years) against environmental attack. Although the salt in the vicinity of a waste package is expected to be relatively dry, the container surface is assumed to be exposed to saturated brine as a result of thermal migration of brine inclusions or under accidental ingress of water into the repository. Furthermore, the overall presence of air should prevail in the repository immediately following the emplacement of waste packages. Oxygen will be consumed by corrosion reactions without being replenished. Radioactive waste disposal design in deep rock salt formations and the induced potential disturbances of the environment are schematized in figure 1.

Two design concepts are considered for the overpack (1):

A corrosion-resistant and a corrosion-allowance design.

Both designs have the following advantageous and disadvantageous characteristics:

- The corrosion-resistant design generally relies on the passive oxide film formation, but under some conditions these films may break down locally, leading to local corrosion phenomena, as pitting corrosion or stress corrosion cracking.
- The corrosion-allowance concept is based on uniformly corroding material which is less susceptible to localized corrosion. In contrary to the corrosion resistant material it may be possible to lay out the wall thickness of the overpack according to the estimated uniform metal loss.

Initially emphasis of research was put on corrosion resistant materials, such as Titanium Grade 12 or Hastelloy C4 for salt repository environments. Ti Grade 12 and Hastelloy C4 exhibit a high degree of resistance against general corrosion and crevice corrosion in high temperature brines. But titanium alloys have a high affinity for hydrogen. A high amount of hydrogen can be adsorbed by formation of Ti-hydride. Embrittlement and desintegration of the metal structure take

Table 1: Comparison of the radioactive waste disposal activities in different countries (Sources: RWE, CEA)

Country	Formation	Location	Depth of Deposition	Radioactive Level of Waste	Research and Development Activities	Operation
Germany	Salt Salt Iron ore	Asse Gorleben Konrad Moorsleben	600-900 m 800-900 m 800-1300 m	l, m, tests h l, m, h l, m l	since 1965 since 1979 1975-1987	1967-1978 (2) ~2008 after 1993 in operation
Belgium	Clay	Mol	near the surface 200 m	l, m (4) m, h	since 1975	? after 2000
France	Clay Granite, Clay, Salt, Slate	La Manche Soulaines Neuvy-Bouin Sissonne Montcornet Montrevel Segré	near the surface subterraneous	l, m m, h	 since 1975	1969-1992 after 1991 after 2010
England	Clay Granite, Clay, Anhydrite	Sellafield ?	near the surface subterraneous	l l, m (4)	 since 1975	since 1959 after 1992
Japan	Clay Crystalline	Aomori Hokkaido	near the surface subterraneous	l (4) m, h	since 1976	after 1990 after 2000
Sweden	Granite	Stripa-Bergw. Forsmark Oskarshamn?	350 m near the surface 50 m under sea ~500 m	subterraneous laboratory l, m h (direct spent fuel disposal of FE)	since 1976	1980-1991 (3) since 1988 ~2020
Switzerland	Granite Anhydrite, Gneiss, Marl Crystalline	Grimsel several possibilities North	400-500 m 300-1000 m ~1200 m	subterraneous laboratory l, m (4) h	 since 1978	since 1984 (3) after 2000
USA	Sediment (Salz) Tuff	several possibilities New-Mexico Nevada	near the surface ~700 m subterraneous	l, m (4) m, h (milit.) m, h (civil)	since 1965 since 1980	since ~1950 canceled after ~2010

1) l = low, m = medium, h = high

2) since 1978: only Subterraneous Test Laboratory

3) Operation of subterraneous laboratory

4) Til maximum 1982, disposal in ocean (4500 m depth)

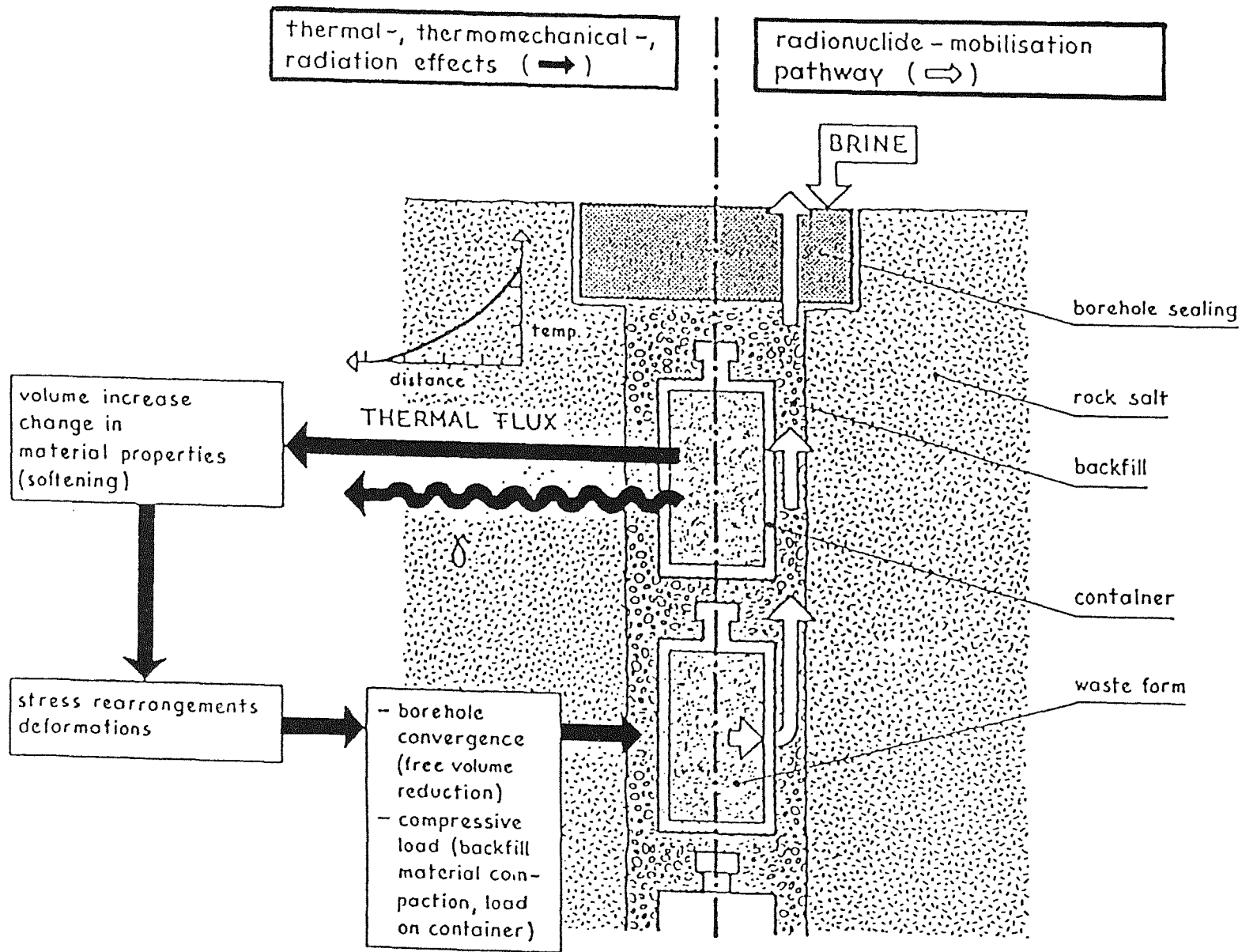


Fig. 1: Schematic Drawing of the Near-Field Barriers and their Interactions with the Host Rock (IAEA-CN-43/81)

place. It was also shown that Hastelloy C4, exposed to γ -dose rates of 10 and 100 Gy/h, underwent pitting and crevice corrosion (20 $\mu\text{m/a}$ at the maximum) (2). Consequently, the effort is now shifted towards corrosion - allowance materials like low-carbon steel. Their potential corrosion phenomena in salt repository environments are: general corrosion, localised corrosion, stress corrosion cracking, hydrogen embrittlement and microbial induced corrosion (3).

The objective of this task is to gain an understanding of the influence of the principal chemical and metallurgical variables on the corrosion behavior of the low-carbon steel DIN W.Nr. 1.0566 in salt brines and to identify its potential corrosion failure modes. Here attention is paid to general and potential localised corrosion. The influence of several parameters (temperature, salt brine composition, metal surface state etc.) has to be determined. Electrochemical methods are suitable to determine within a short-term of exposure the influence of various parameters on individual cathodic and anodic reactions or the overall corrosion process. Informations of this type are difficult to obtain by any other method of corrosion testing and has to be regarded as complementary to others of more engineering character.

This report covers the following items:

- A survey on the literature of corrosion of low-carbon steels in salt containing aqueous solutions,
- the methodology of our electrochemical tests,
- first results on corrosion of the fine-grained structural steel in different salt brines within a temperature range of 35 to 90°C and finally,
- a proposal for the continuation of these electrochemical corrosion studies.

2. Literature Survey on Corrosion Mechanisms of Low-Carbon Steels in Salt Brines

2.1 Electrochemical Reactions

When the fine-grained structural steel is immersed in a corrosive, salt containing aqueous solution, the chemical/electrochemical interaction of the metal with the solution builds up an electrochemical potential at the steel/solution interface, called free corrosion potential. It causes the steel to corrode according to two different and equilibrated processes:

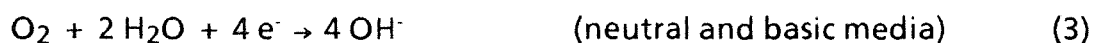
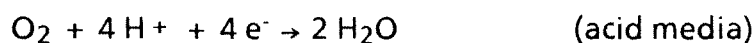
- at anodic sites metal dissolution takes place



- at cathodic sites, dependent on the pH, a reduction process occurs which results in the evolution of hydrogen



or in the reduction of dissolved oxygen / or water:



At the free corrosion potential, the cathodic and anodic current amplitudes are equal. The sum of these two currents, which is the measurable electrochemical cell current, is negligible.

For our corrosion studies, the rate of those cathodic and anodic reactions is of main interest. These reactions can show charge-transfer polarization (taking-off or giving-off of electrons is rate determining) or diffusion polarization (transport of a substance through the electrolyte to or from the electrode is rate determining). As shown in figure 2, the resulting polarization curves for electrodes showing charge-transfer polarization or diffusion polarization are very different. For example, the oxygen reduction reaction (3) shows diffusion polarization in nearly all practical cases: The transport of oxygen to the metal surface is rate-determining. Consequently, the oxygen content and its transport in a solution has a strong influence on the corrosion rate in neutral solutions. However in acid solutions, its influence is negligible since the cathodic corrosion process is dominated by the reaction (2).

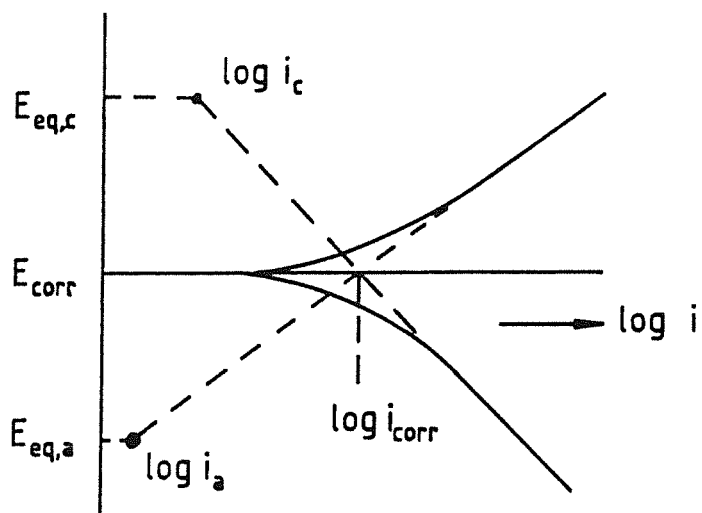


Fig. 2a: Polarisation diagram for binary electrode with charge-transfer polarisation of anodic reaction and cathodic reaction (4)

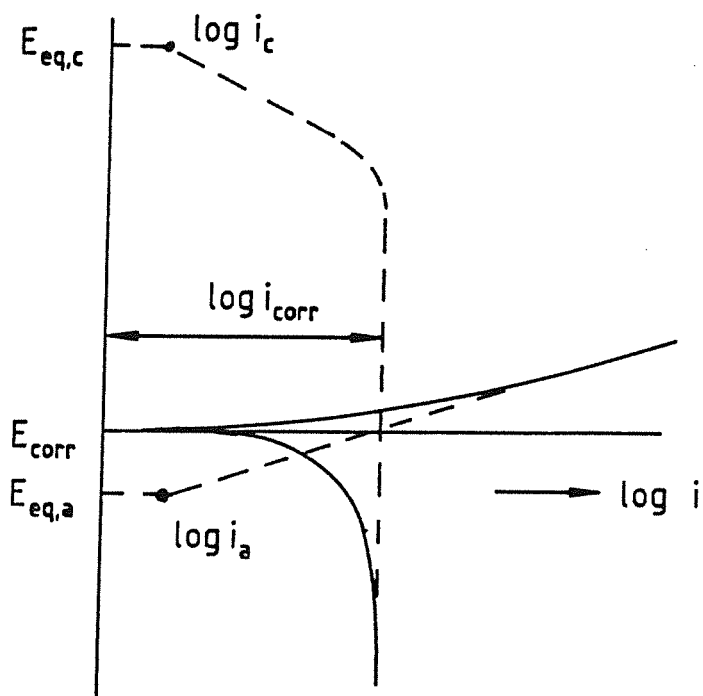


Fig. 2b: Polarisation diagram for binary electrode with charge-transfer polarisation of anodic reaction and diffusion polarisation of cathodic reaction (4)

2.2 Role of the Environmental Variables

As we just discussed it for the effects of p_H and oxygen content, the changes in the environmental conditions can completely modify the kinetics of steel corrosion. In the literature, some of these aspects are already well described:

- Oxygen: The corrosion rate can be influenced by the solubility of oxygen. Thus, in presence of oxygen, corrosion is diminished in neutral and high-concentrated solutions due to reduced oxygen solubility. Furthermore, oxygen accelerates the rate of general corrosion by depolarizing the cathodic reaction according to reaction (3) and may reduce the protection afforded by the corrosion product layer. Fe^{2+} ions are oxidized to Fe^{3+} which deposit as $Fe(OH)_3$ away from the metal surface. The rate of metal dissolution is controlled by the rate of oxygen supply to the metal surface. However, oxygen may also exert a beneficial effect on the corrosion by the formation of a truly passivating Fe_2O_3 surface layer. It is possible that oxygen will promote passivation on the majority of the metal surfaces, but also that relatively rapid corrosion will occur at local sites. This localized corrosion can be due to non-uniform transport of oxygen or due to inhomogeneities in the protective surface film. As oxygen will be consumed relatively quickly by the container material after the closure of nuclear waste packages in the salt mines and as it does not build up a reliable protective surface layer, already existing pits may rapidly coalesce. In this case, a rough, coalesced pit appearance of the steel surface (shallow pits) is observed.
- Temperature: The theoretical aspects of the temperature influence on the kinetics of electrochemical reactions were reviewed by Heusler [5]. The temperature dependence of the corrosion rate is given by an Arrhenius type function:

$$i = A \exp (-E_a / RT)$$

where i : corrosion current density (A/m^2)

E_a : Energy of activation (J/mole)

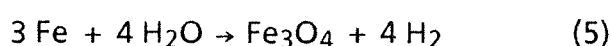
A : Preexponential factor (A/m^2)

T : Temperature (K)

R : Gas constant (J/mole K)

The acceleration of the corrosion rate with temperature is often balanced in neutral solutions by a decrease of the cathodic depolarization reaction

which is due to the inverse solubility of oxygen in the solution. In concentrated salt brines, an additional parameter must be considered: In presence of magnesium chloride, hydrolysis occurs which increases with temperature and induces a decrease of the pH in the solution. An important aspect of the temperature dependence under consideration is the assumption that the corrosion mechanisms does not change in the temperature range of interest. According to the Pourbaix diagram of the Fe-Cl-H₂O system at 25, 60, 100, 150°C (figure 3) iron tends to form two stable oxides Fe₂O₃ and Fe₃O₄ in high-temperature water. Westerman (6) reported that the passive film formed on cast iron at 100°C grows according to a parabolic rate law and that the overall reaction is:



In presence of magnesium chloride, complex (Fe, Mg) hydroxide corrosion products - such as amakinite - can be formed (6).

- p_H: In addition to the change in the cathodic process, the variation of the p_H in the solution influences the passivation process. Hydroxide layers, for example, are becoming more stable with increasing p_H. The p_H-dependence is important since the acidity of the brines is varying in the range of 2 to 8. Furthermore, the local p_H which develops at sites of attack on a passive film plays an important role in determining whether repassivation occurs on surfaces exposed by film disruption or not.
- Added substances: The presence of various substances (ions, neutral molecules) and of corrosion products may lead to acceleration or retardation of the metal dissolution rate. For example, the effect of different anions can be explained by differences in solubility of the corrosion products, an effect on the passivity of metal surface, the oxidizing character of the anion or complex formations. Particularly, chloride ions destroy the passive state (achieved by anodic polarization) by a direct action of forming soluble complexes and penetrating into protective films, where potentially pitting corrosion can be initiated.
- Brine flow velocity: The brine flow velocity has two important effects which accelerate the corrosion of the metal surface. At first, it increases the mass transport of chemical species to or away from the surface. At second, if the velocity is high enough, it may mechanically abrade the thin oxide layer, thus exposing continuously new metal surface to the brine.

Hydrogen: As hydrogen is formed during the corrosion reaction, its influence has to be determined. Diercks and Kassner [7] reported that in long-term, sealed capsule tests, the corrosion of carbon steel in acid chloride solutions is dependent on hydrogen pressure. The corrosion rate will vary with hydrogen fugacity according to

$$\frac{1}{[f_{H_2}]^{1/2}}$$

Furthermore they reported that hydrogen fugacity is a function of test temperature, time and specimen surface to brine volume ratio (S/V).

$$f_{H_2} = f \left[T^{2/3}, \exp\left(\frac{1}{T}\right), t^{2/3}, S/V^{2/3} \right]$$

- Pressure: As the nuclear waste packages can be exposed to an expected maximum pressure of about 130 bar, pressure dependence of the corrosion rate has to be determined. Heusler (5) measured a small influence: For example, the pressure dependence of the corrosion rate of iron in dilute sulfuric acid shows - when the pressure is increased from 1 to 1450 bar - an increase by a factor of 1.33.

In conclusion, the corrosion of low-carbon steels in high-temperature aqueous solutions depends on various environmental parameters and on the resulting corrosion mechanisms. The influence of the parameters must be determined experimentally. Active corrosion produces high corrosion rates. This process is thermally activated. If the chemistry of the environment can be maintained at a certain p_H and potential which places the metal in the passive area of the Pourbaix diagram, then the corrosion of the metal will follow parabolic or slow linear kinetics. If aggressive ions - such as chloride in salt brines - are added, or if the oxygen content or the acidity are changed, the corrosion rate increases due to active and uniform metal dissolution or local pitting corrosion.

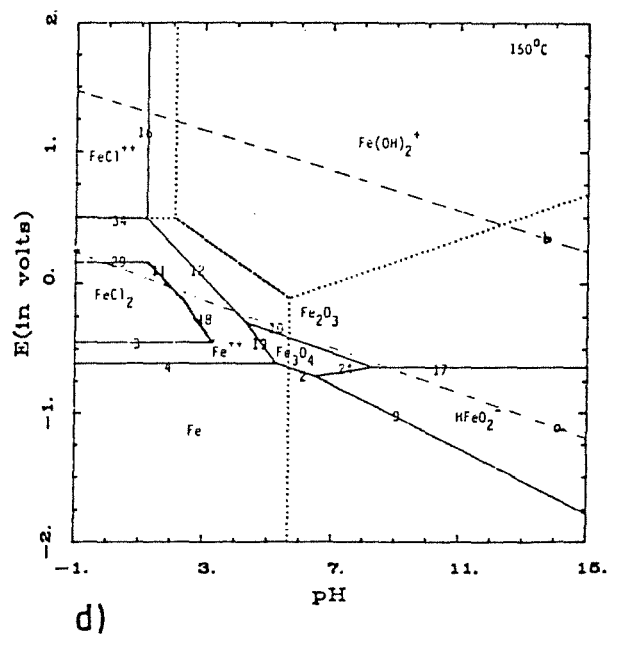
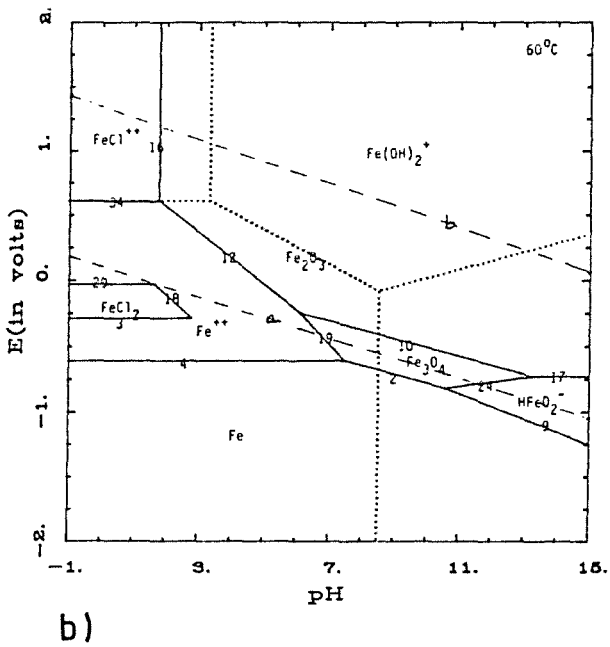
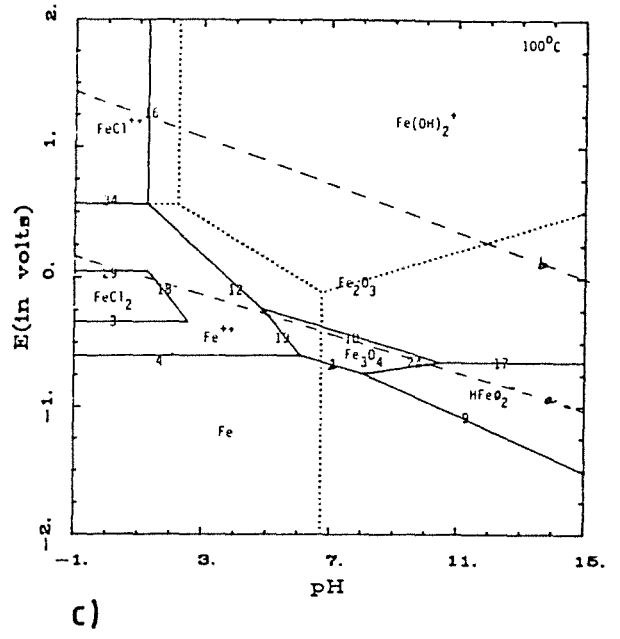
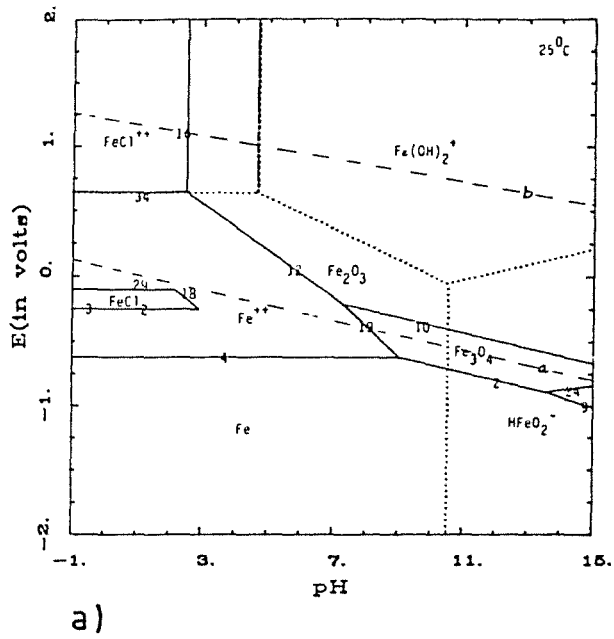


Fig. 3: Pourbaix Diagrams for the Fe-Cl-H₂O System
a) 25°C; b) 60°C; c) 100°C; d) 150°C (7)

2.3 Pitting Corrosion

As an introduction, it will be mentioned how Verink (9) has described the corrosion behavior of iron in aqueous solutions. As function of pH and the applied electrochemical potential, the iron surface shows immunity, general corrosion or passivity (Fig. 4).

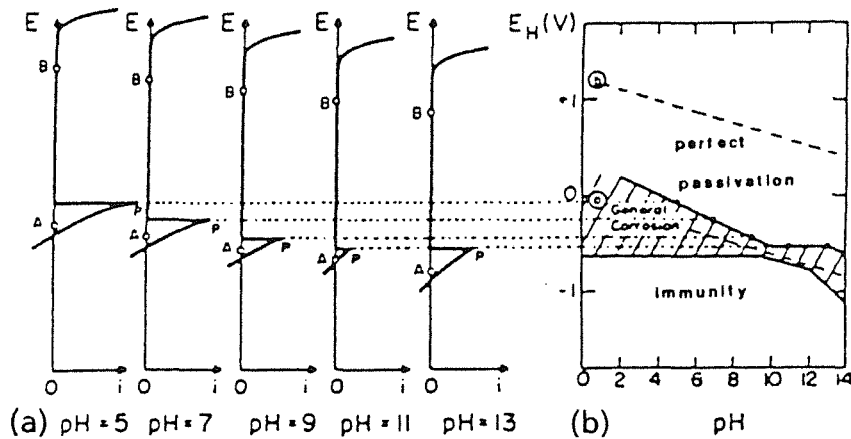


Fig. 4: a) Potentiokinetic polarization curves for Armco iron measured by the electrochemical hysteresis method at various pH
 b) Experimental potential/pH diagram based on electrochemical hysteresis data in Fig. 4a (9).

In the presence of chloride ions, the corrosion behavior of iron is changed, as shown in Fig. 5. As function of pH and electrochemical potential, imperfect passivation and pitting corrosion may occur.

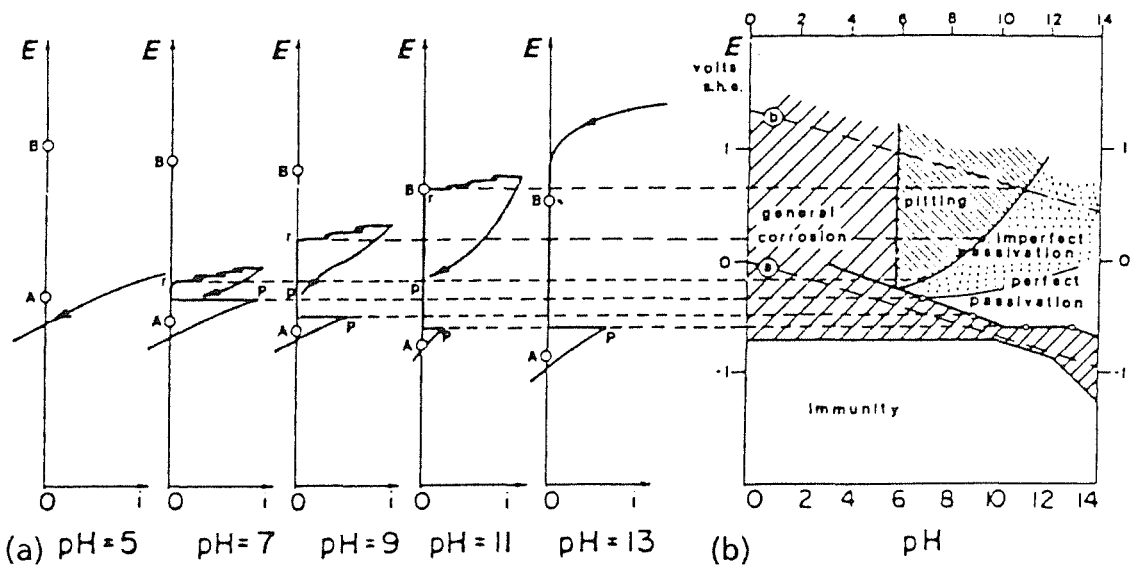


Fig. 5: a) Potentiokinetic polarization curves of Armco iron measured by the electrochemical hysteresis method in 10^{-2} m chloride solutions of various pH
 b) Experimental potential/pH diagram constructed from electrochemical hysteresis data in Fig. 5a (9).

The risk of pitting corrosion of the fine-grained structural steel DIN W.Nr. 1.0566 in salt brines must be enquired since it could lead to the perforation of nuclear waste packages long before it fails from general corrosion. Consequently a literature review on potential pitting corrosion of low-carbon steels in salt brine solutions was performed. It covers the testing procedures, pitting mechanisms, and influencing factors.

2.3.1 Pitting Corrosion of Low Carbon Steels

Description-Characteristics-Parameters

The characteristic features of pitting corrosion are well described by Kruger and Rhyne (10), Strehblow (11), and Szklarska-Smialowska (12). The localized corrosion is characterized by potential differences between the corroding and the unaffected area due to differences in local composition, oxygen concentration, pH, protective film coverage etc. (3). Pitting corrosion is usually observed when materials which exhibit active/passive behavior are exposed to the above mentioned conditions in a given environment. The process of pitting corrosion can be divided in two stages:

- an initiation and
- a propagation stage.

It is important to separate these two stages because each step can be the rate determining one. Their mechanisms probably differ from each other (13).

2.3.1.1 Initiation Process of Pitting Corrosion

The initiation process involves the local breakdown of a passive film which forms on the surface of the material. Damage of the passive films can lead to the formation of active corrosion centers, i.e. small areas of high anodic current density. Initiation generally occurs when the system is above a certain electrochemical potential, called the critical pitting potential (E_{pit}). Its value is diminished when aggressive anions, most notably Cl^- , are present. Susceptibility to pitting is also influenced by the chemical composition and microstructure of the material. An induction time separates the initiation of breakdown from the initiation of propagation by a pit.

Mechanisms of Pit Initiation

Several theories exist on the mechanisms of pit initiation. They are divided by Kruger and Rhyne (10) in three main mechanisms, which are governed by:

- Adsorbed ion displacement,
- Ion migration or penetration,
- Breakdown-repair.

Adsorbed ion displacement

These mechanisms describe the adsorption of aggressive anions by passive films. The breakdown occurs when:

- Oxygen- or hydroxyl-ions are displaced from the passive film by chemisorbed chloride ions. The displacement reaction results in the formation of chloride salt which dissolves (14).
- A small number of aggressive ions jointly adsorb on the surface of the passive film around a metal cation in the film and the cation is eventually removed from the film as a soluble complex (14, 15).

Ion migration or penetration

These mechanisms describe the penetration of aggressive anions through the film. The breakdown process is considered to be completed when the anions reach the metal-film interface.

- The passive films can contain pores suitable for aggressive ions diffusion.
- The anions migrate through the passive film by means of defects or by an ion exchange process.

The lattice structure of the film is locally altered by the inclusion of aggressive anions promoting further anionic attack (17).

Breakdown-repair

These mechanisms describe chemically-induced disruption of the passive film. It can be explained by the following two theories:

- The adsorption of aggressive anions on the passive film surface lowers the interfacial surface energy at the solution interface. This makes the film more susceptible to rupture due to stresses caused by mutual repulsion of adsorbed anions (18, 19).
- Rupture of the passive film results in a disorder of the passive layer which is perhaps enhanced by mechanical stresses (20). In presence of aggressive

anions, a competition develops between oxide film reformation (protective) and salt formation (non-protective) at the site of the rupture. A locally acidic environment may develop at the site of the film rupture (21). Hydrolysis, which occurs during the reaction between the bare metal and the environment, decreases the pH of the area. This decrease raises the thermodynamic stability of metal ions in solution, enhancing further dissolution of the metal.

Influence of Various Parameters on Pit Initiation Process

Electrochemical potential:

At potentials between E_{pit} (critical pitting potential) and E_{prot} (potential at which pits repassivate on reverse scan of a polarization curve), breakdown and repassivation are assumed to be competitive processes.

Material composition:





From iron-based materials it is known that the addition of Ni, Cr, Mo decreases the susceptibility to breakdown (22). The main effect of these elements is presumably the shift of the critical pitting potential to higher positive values. These elements favor the formation of passive films which are more stable, i.e. more difficult to penetrate.

Material microstructure:

Some studies on carbon steels (23) have shown that structural changes in the pearlite phase lead to a preferential attack of carbide or ferrite phases. That depends on pH, anodic potential, and the anions present in solution. The crystallographic orientation at the metal surface influences its tendency to breakdown (24). Defects - such as those introduced by deformation processes and welding or surface heterogeneities - influence the breakdown processes: The initiation of pitting in mild steels occurs preferentially at or near non-metallic inclusions (MnS primarily). It can be attributed to anodic-cathodic phenomena or discontinuities at the inclusion-matrix interface. Ives and Srivastava (25) have studied the role of non-metallic inclusions in the nucleation process of pitting in low-alloy steels in chloride containing solutions. They found that pits will fully develop only if the inclusions remain in place during the localized attack. They conclude that round, globular inclusions - which can easily fall out during attack - are less detrimental than irregular inclusions; non-metallic inclusions are necessary for the subsequent growth of pits. The sulfide phases of the inclusions are preferentially dissolved. The sulfide-free inclusions can behave cathodically

with respect to low-alloy steel matrix, leading to localized attack of the matrix. Pit nucleation processes were summarized by these authors as shown in figure 6:

Figure 6: PIT NUCLEATION PROCESSES /25/

<u>PHENOMENON</u>	<u>MECHANISM</u>	
	<u>Inclusion</u>	<u>Adjacent Matrix</u>
I)  Inclusions dissolves	Unstable	Unreactive or protected
II)  Inclusion dissolves selectively	Component phases unstable	Unreactive or protected
III)  Matrix (adjacent) dissolves	Cathodic site	Unstable
IV)  Disbonding at interface	Unreactive in bulk solution but dissolves within the crevice	

Environmental factors:

- Aggressive anions concentration: chlorides and all other halides and certain other anions (sulfides ...) induce pitting corrosion.
- Borate, phosphate, chromate, nitrate, hydroxyde, .. anions enhance the passivation process which, in the case of mild steel, may increase the susceptibility to localized corrosion.

- Oxygen concentration: It influences the breakdown process through its effect on the corrosion potential of the system. Oxygen acts as a cathodic depolarizer; this role is more important in pit propagation process. Oxygen may exert a beneficial effect by facilitating the formation of a truly passivating Fe_2O_3 surface layer. It is possible that oxygen will promote passivation on the main part of the metal surface, but that relatively rapid corrosion will occur at local sites. This localized corrosion can be due to non-uniform transport of oxygen or due to inhomogeneities in the protective surface film (26).
- Temperature: It is generally accepted that the tendency to breakdown increases with increasing temperature (27).
- pH : It shows only a weak dependence on the pH of the solution (27) since a lower pH enhances simultaneously breakdown and general corrosion. Rapid general corrosion depassifies the entire surface and renders breakdown inoperative. The local pH at sites of attack on the passive film plays an important role in determining whether repassivation or corrosion will occur on corroded surfaces or not.

2.3.1.2 Propagation Process of Pitting Corrosion

Propagation is the final damaging state of pitting. The following phenomena are characteristic for the propagation process:

- Pits act as anodes. Since the pit area is smaller than the cathodic area, the anodic current density in pits is high. Pits can also sometimes act as cathodes.
- The solutions inside the pits have a much different composition than the bulk solution (lower pH , more aggressive anions, lower oxygen content, higher concentration of metal ions). This corrosive environment develops because the mass transfer between the pit and the bulk solution is limited by the geometry of the growing pit.

Mechanisms of the Propagation Process

In order to balance the increasing concentration of positive ions (Fe^{2+} , H^+) in the pit, aggressive anions are drawn into the pit promoting further attack. The potential can rise in the pit which further stimulates anodic dissolution of the metal. A potential gradient develops between the active sites and the remaining

passive surface. The anodic dissolution reaction is: $\text{Fe} \rightarrow \text{Fe}^{2+}$. The migration of chloride and sulfate anions, for example, into the pits leads to the formation of FeCl_2 and FeSO_4 which hydrolyse to produce HCl and H_2SO_4 (27). The hydrolysis reaction is: $\text{Fe}^{2+} + 2 \text{H}_2\text{O} \rightarrow \text{Fe}(\text{OH})_2 + 2 \text{H}^+$. This reaction lowers the pH in the pit which inhibits repassivation of the pit surface.

The geometry of a forming pit is important since the mass transfer between the pit and the solution is influenced by geometrical constraints. Deposition of corrosion products at the mouth of the pit (due to the lower solubility of corrosion products in the higher pH environment outside the pit) can inhibit mass transfer. The localized corrosion period is also dependent on the passive film leakage current. The worst case for pitting corrosion is given when most of the surface is covered by an extremely protective surface film, thus making the maximum amount of cathodic current available to sustain local anodic sites which will develop (28). They will propagate according to the acid occluded cell mechanism. The following figure 7 shows an occluded cell near the site of a MnS inclusion on mild steel when exposed to an aerated chloride solution:

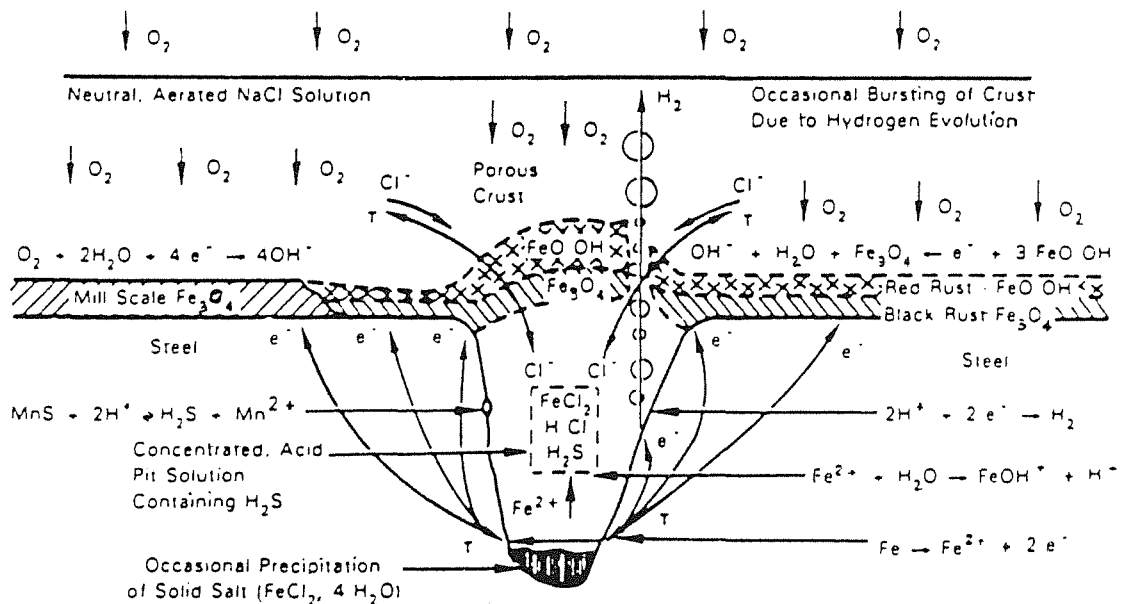


Fig. 7: A pit growing by the occluded cell mechanism (29)

Pits can sometimes repassivate and cease to propagate. Without a supply of cathodic current from the external surface, all of the cathodic reaction required to sustain the dissolution will have to occur within the active site. This will result in the consumption of acidity, which will no longer be regenerated by hydrolysis because there is no potential gradient to cause the migration of the aggressive

anions into the active sites. This forms a basis for an estimation of the rate of progress of the localized attack (28).

A second theory of pit propagation relies on the fact that the pit initiation is controlled by the formation of a non-protective film along the surface of a forming pit (20).

Parameters Influence on the Propagation Process

The most important factors influencing propagation of pitting corrosion are:

- Electrochemical potential,
- Material composition,
- Material microstructure,
- Geometry of the pit,
- P_H in the pit and the solution,
- Aggressive anions, and
- Oxygen concentration.

The oxygen concentration of the solution may directly affect the propagation rate as oxygen is a strong cathodic depolarizer. It may reduce the protection required by the corrosion product layer because it oxidizes Fe^{2+} ions to Fe^{3+} which precipitate as $Fe(OH)_3$ away from the metal surface. The rate of metal dissolution is controlled by the rate of supply of oxygen to the metal surface.

2.3.2 Pitting Corrosion Testing Procedure

Experimental tests are run on low carbon steels for nuclear waste repositories in salt formations in order to answer the following questions (30):

- Is pitting corrosion possible?
- Will it be initiated by rupture of a protective film?
- Can pitting corrosion be initiated when oxygen is present in salt brines (period during and following package closure)?
- Can non-uniform corrosion be sustained after all oxygen is consumed?

In the affirmative case:

- How long is the induction time for initiation of pitting?

- Is the propagation rate of existing pit greater than the general corrosion rate?
- Is the propagation rate high enough to permit the penetration of the waste package during its lifetime?

In addition - for choosing the proper test conditions - their duration should not be shorter than the induction time of pitting.

2.3.2.1 Description of Testing at the Free Corrosion Potential and by Electrochemical Polarization Techniques

A list of the experimental tests encountered in the literature is given here (30).

1) Immersion Tests

- Simple immersion tests of specimens for an extended period of time.
- Immersion tests of artificially pre-pitted specimens.
- Standard test (ASTM G 48-76): Immersion of specimens in a FeCl_3 solution which is supposed to simulate the environment in a propagating pit. It provides information on pitting corrosion only.
- Long-term immersion tests in which the electrochemical potential of the environment is constantly varied. It provides informations on pitting susceptibilities.
- Immersion tests in a gamma radiation field.

2) Electrochemical Test

These tests provide information on critical pitting and/or protection potentials (E_{pit} , E_{prot}). They are used to estimate the rate of pit propagation or re-passivation (10).

- In addition to tests of general corrosion mechanisms and rate determinations, potentiodynamic polarization is useful for determining pitting tendencies.
- Potentiostatic polarization tests are performed to determine E_{pit} and E_{prot} . Their results are more reliable than those obtained by potentiodynamic tests. However, these experiments can be very time-consuming.
- Galvanostatic techniques measure the electrode potential as function of time at constant current density. The interpretation of the results can be difficult due to periodic oscillations of the potential.

- The elaboration of corrosion behavior diagrams provides only an indication of passive film stability when the experiments are performed by scanning potentiodynamically over a wide range of potentials at a high scan rate and by several repetitions .
- Scratch techniques are applied to deform a specimen surface during immersion at constant potential and to measure the current response as a function of time. The biggest problem of these techniques are their reproductibility.
- The evaluation of the pit propagation curves permits the measurement of the pit propagation rate. It is obtained by measuring the general current density corrosion in the passive state and subtracting it from the current of general and pitting corrosion. This method requires the prior knowledge of E_{pit} and E_{prot} (measured by other test methods) which may not be valid in this test. The tribo-ellipsometric method provides information on repassivation and metal dissolution kinetics.
- Electrochemical noise measurements are used for studying dynamic breakdown repair processes and for measuring E_{pit} .
- Rotating ring disc electrode techniques provide informations on growth rates of pits.

2.3.2.2 Recommendation for Test Specimen Quality

The material specimens should represent the entire range of steel composition and microstructure. Welded specimens should be tested too as they present compositional and microstructural variations. Specimens of different heat treatments and varying degrees of cold work should be distinguished. Preoxidized specimens could be tested too as metal surface state is an important parameter.

3. Literature Survey on Corrosion Test Results

Corrosion test results of low-carbon steel corrosion in granitic, basalt groundwaters and in sea water are already part of the literature and are reviewed here.

3.1 Studies in granitic and basalt groundwaters

Heitz (31) tested the corrosion rate of unalloyed steels (carbon steels of very low content in Ni, Cr (Euronorm 20-74)) in granitic groundwaters and found that in a charge-transfer polarization process the E_a value is about to 30-60 KJ/mole; in a diffusion polarization process E_a value of about 10 KJ/mole has been obtained. A temperature increase from 25 to 120°C (for $E_a = 45$ KJ/mole) corresponds theoretically to an increase of the corrosion rate by a factor of 100 (32). Since the corrosion processes are often determined by the diffusion transport of ions, atoms or molecules through protective films, the temperature dependence becomes much lower. Simpson (33) studied the corrosion of unalloyed steel GS-40 (table 2 b) by immersion tests in granitic groundwaters ($pH \sim 9$) between 80 and 140°C. The results show that the corrosion rate at 140°C is lower than at 80°C. Pitting corrosion of low-carbon steel has been studied in synthetic granitic groundwater by Marsh et al. too (34-36). Three steels were included in the programme: a forged 0.2 % carbon steel, a cast steel, and a low-carbon forged steel (table 2 c, d, e). The chloride ion content of such groundwaters is much lower than in salt brines (Cl^- content: 35.5 ppm, HCO_3^- content: 244 ppm, SiO_3^{2-} content: 19 ppm). Their work has shown that passivation and pitting corrosion may occur in certain granitic groundwaters (pH 7-11). Preliminary electrochemical tests in Na_2CO_3 - $NaHCO_3$ - $NaCl$ solutions have shown that pitting can only occur at relatively high pH-values because the metal can passivate. Long-term corrosion measurements in granitic groundwaters indicate that pitting corrosion is favoured by oxygenated media and hypothetically will occur during the initial fraction of the container life. In order to evaluate the low-carbon steel thickness required for nuclear waste disposal in these granitic groundwaters, they develop a mechanistically based mathematical model of pit propagation, which will be compared with short-term experimental measurements.

Also electrochemical studies on low-carbon steel corrosion in basalt groundwaters, conducted at high temperature and pressure in autoclaves, are reported:

- Electrochemical studies on 1018 low-carbon steel (table 2 f) specimens - exposed

to high temperature conditions - have been performed in an autoclave and are reported by Beavers et al. (37). Their objective was to reproduce the corrosion data in basalt groundwaters at elevated temperatures (250°C) and to evaluate the influence of steel composition and microstructure as well as the composition of groundwaters on the corrosion behavior. 1000 h-autoclave exposures were performed using 1018 carbon steel specimens in simulated basalt groundwaters under stagnant deaerated conditions. The polarization resistance of the 1018 low-carbon steel specimens was measured by a two-electrode-technique as function of exposure time. Polarization resistance were found to decrease over the first 50 h of exposure, and to increase over the remaining 950 h, which indicates a decreasing corrosion rate with time. This was attributed to a possible passivation of the carbon steel.

Table 2: Chemical Composition (wt%) of Low-Carbon Steels

composition %	C	Si	Mn	P	S	Al
a: Fine-grained structural steel DIN W.Nr. 1.0566	0.17	0.44	1.49	0.021	0.04	0.045
b: Low-carbon steel	0.20	0.15	0.87	0.020	0.02	-
c: Forged 0.2% carbon steel	0.2	0.08	0.6	0.01	0.04	-
d: Cast steel	0.23	0.42	0.89	0.011	0.01	-
e: Forged low-carbon steel	0.05	0.06	0.15	0.01	0.02	-
f: 1018 low-carbon steel	0.18		0.72	0.007	0.010	-
g: 1020 carbon steel	0.18-0.23		0.30-0.60	<0.04	<0.05	-
h: Low-carbon steel	0.22	0.60	0.67	0.017	0.02	-
i: Type A212B carbon steel	0.36	0.18	0.62	0.012	0.03	-
j: Type A216 mild steel	0.16-0.23	0.45-0.58	0.6-0.71	0.014-0.018	0.01-0.02	-
k: Forged low-carbon steel BS 4360 43A	0.20	0.08	0.67	0.01	0.038	-

Beavers (37) observed pitting corrosion attack of the 1020 carbon steel (table 2 g) in various synthetic basalt groundwaters (chloride content 0.1 to 100 g/l, pH 6.0-9.3) in the presence of different ions (F^- , NO_3^- etc.) at 250°C under stagnant deaerated conditions. Shallow pits were found ($\leq 20 \mu m$) on most of the specimens after the exposure. These pits were associated with the breakdown of magnetite films found on the specimen surfaces. This observation is consistent with the results of the potentiodynamic polarization studies. In these studies, low-carbon steel was found to exhibit active/passive behavior in simulated basalt groundwater. The protection potential was found to be close to the free-corrosion potential, even under deaerated conditions, indicating a high probability of pit initiation. The results of the metallurgical studies showed that the variation of the steel composition or thermo-mechanical treatment did not have a marked effect on pitting corrosion resistance. Several tests were performed to study the effects of environmental variables on the corrosion behavior. It was found that the increase of the ion concentration of salt by a factor of 10 did not have an effect on the polarization curve. Similarly, the increase of the temperature from 90°C to 250°C did not markedly affect this behavior. It was shown that many of the environmental variables (species included in the groundwater, species that may intrude the repository or be generated by radiolysis . . .) have important single and combined effects on the electrochemical characteristics. The combined actions of two effects are normally not considered in the reviewed corrosion studies.

A low-carbon steel (table 2 h) was tested in simulated basalt groundwaters by Bakta and Solomon (38) using polarization and potentiostatic methods. The concentrations of dissolved oxygen were 3.1 (20°C) and 2.42 ppm (100°C) at 105 bar. Pitting corrosion was studied. The density of pits in numbers was found to be highest at 100°C. Under the investigated conditions the measured pit depth and shape was found to be independent of temperature. The polarization curves did not exhibit an active/passive behavior and therefore the pitting potentials are not well defined. This has been attributed to the metal, initially forming a weak oxide film which readily breaks down in corrosive environments. The authors report about variations of the measured polarization curves, however not in respect to their shape at the tested three temperatures. At all temperatures, the corrosion product was a mixture of γFe_2O_3 , Fe_3O_4 , and some traces of $FeOOH$.

3.2 Studies in Sea Water and Marine Sediments

Sea water is approximately 4 molar in chloride ions and does not contain significant concentrations of sulfide, heavy metals or silica. Heitz and Manner (39) found for mild steel (carbon content $< 0.25\%$) in artificial sea water that pitting occurred at levels > 20 ppb oxygen at temperatures $> 100^\circ\text{C}$. Mill scale (not removed prior to immersion in sea water) affects the nature of the attack of the mild steel (40, 41). Furthermore, Heitz and Manner reported that the corrosion rate of mild steel in deaerated sea water increased in the temperature range from 70 to 120°C by a factor of 3.5. Posey and Palko (42) observed no pitting corrosion on type A212B carbon steel (table 2 i) in deaerated 4m NaCl at pH 2 to 7 and temperatures 20 to 200°C . They showed that the corrosion rate increases for a temperature increase from 22 to 200°C at $p_H = 7$ from 0.01 to 1.27 mm/year. Nachmann and Duffy (43) using AISI 1008 steel showed similar results in deaerated sea water at $p_H = 7.5$. At 25°C the corrosion rate was 0.07 and at 100°C 0.42 mm/year. Lanza et al. (44) reported for mild steel (carbon content $\leq 0.25\%$) between 50 and 90°C in sea water an increase in corrosion rate by a factor of 1.5. Other investigators (45, 46) have measured for low-carbon steel in sea water a similar increase in corrosion rate as function of temperature. Grauer (47) reported E_a values from 12 to 24 kJ/mole for corrosion of unalloyed steel in sea water and in oxygen-free salt solution.

Marsh, Harker and Taylor (34) studied the pitting corrosion of forged 0.2% carbon steel (table 2 c) in marine sediments. They conclude that pitting corrosion is unlikely to occur for carbon steel nuclear waste containers in marine sediments. They explain that pitting corrosion takes place because of the appearance of an acidic electrolyte in the corrosion sites. These acidic sites can only be sustained if a positive potential gradient exists between them and the external metal surface. This requires two additional conditions:

- The carbon steel must form a protective oxide layer, since otherwise its rest potential will not rise above the active corrosion potential, which is negative to the H^+/H_2 or $\text{H}_2\text{O}/\text{H}_2$ equilibria (cathodic reaction). The formation of a truly protective passive film on the surface of the carbon steel is unlikely in an aggressive environment such as sea water.
- The environment must contain species, such as oxygen, with a thermodynamic redox potential more positive than H^+ ions or water. However, assuming that the formation of a passive film on the surface of the low-carbon steel is possible, the minimum requirement for the maintenance of a positive rest potential - capable of sustaining localised

corrosion - is that the cathodic reduction current should balance the anodic metal dissolution current flowing through the passive film. The cathodic oxygen reduction reaction is under mass transport control (diffusion of oxygen to the metal surface is rate determining). The period estimated to consume the oxygen in the first millimeters of marine sediments near the metal surface and hence the possible pitting corrosion period is short.

Posey et al. (42) have studied the effect of pH and temperature (25-200°C) on the corrosion rate of type A212B carbon steel (table 2 i) in deaerated 4 m NaCl solution. A refreshed, stirred titanium autoclave (figure 8 a) was used to permit electrochemical measurements. Corrosion rates were estimated by Tafel plots and polarization resistance measurements. The pressure of the autoclave was maintained between 15 and 35 bar.

Their results (figure 8 b) show clearly a change in the apparent activation energy of the overall corrosion process as a function of pH. Between pH 7 and 5, the corrosion rate does not depend on the pH but only on the temperature. The apparent activation energy of the overall corrosion process in the neutral pH range was 33 KJ/mole. On the other hand, in moderately acidic solutions (pH = 2-3), the apparent activation energy of the overall corrosion reaction was approximately 18 KJ/mole, a value which is consistent with a rate determining mass transport of H⁺ ions to the surface of the corroding metal. At pH = 4, a transition is observed between the two values of apparent activation energy. Up to approximately 75°C at this pH, the corrosion rate is controlled by the rate of convective diffusion of H⁺ ions to the electrode surface, while at higher temperatures, the rate is independent of stirring conditions and the cathodic process is mainly reduction of water to form molecular hydrogen. The data were described by a simple numerical correlation composed additively of pH-independent and pH-dependent terms.

These results agree qualitatively with results of other investigators (48) and provide the data base for the corrosion behavior of low-carbon steel in concentrated brines.

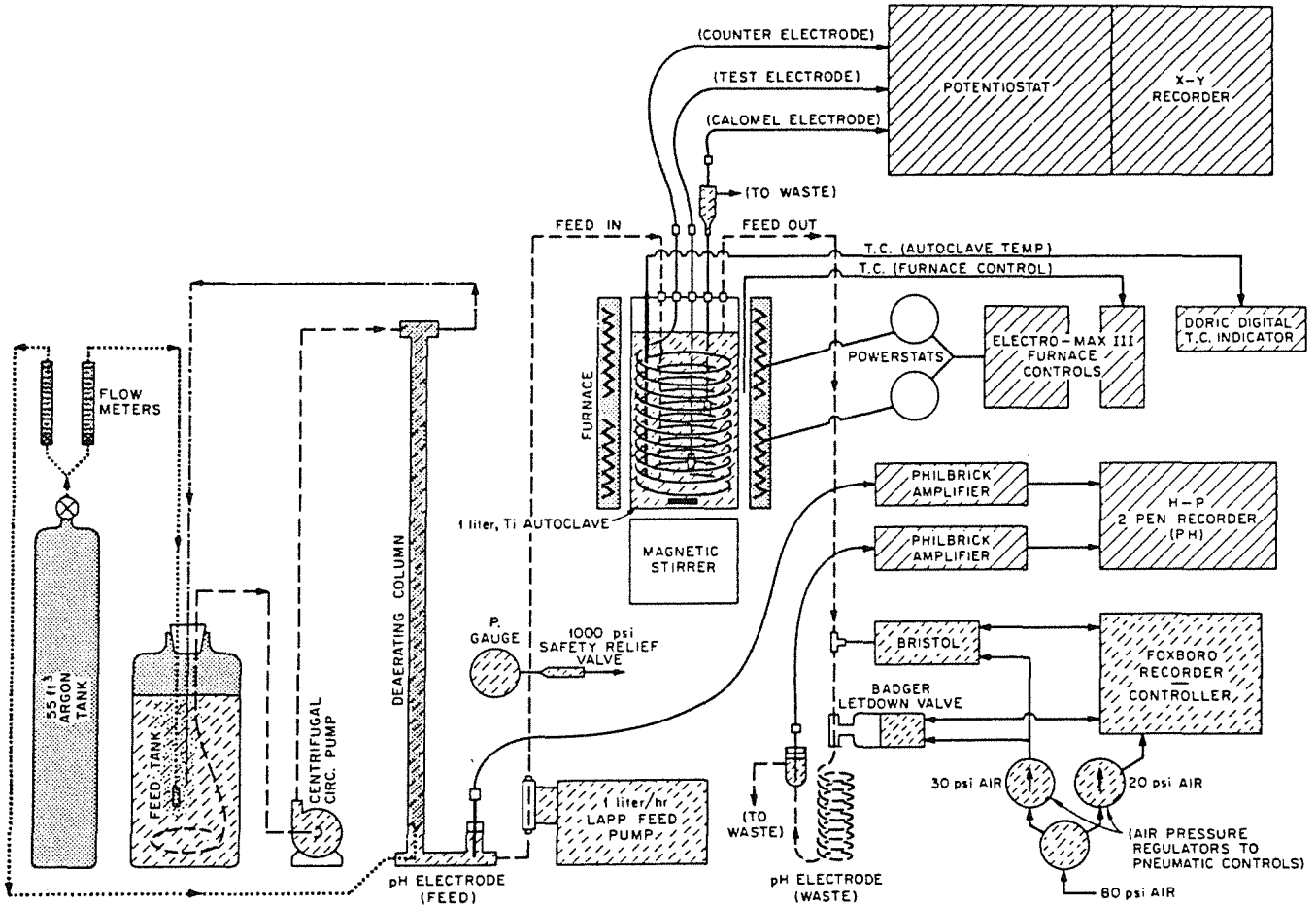


Fig. 8 a: Schematic diagram of refreshed, stirred titanium autoclave system for electrochemical studies (42).

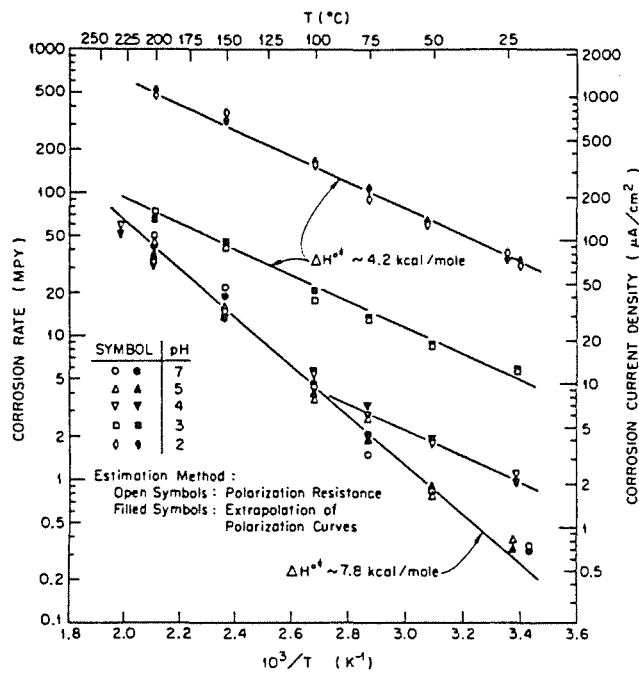


Fig. 8 b: Corrosion rate of A212B carbon steel in deaerated 4 m NaCl as a function of pH and temperature (42).

3.3. Corrosion results in brines

3.3.1 Studies in geothermal brines

Useful to be compared with our corrosion results in brines are experiments in solutions containing sodium and magnesium chlorides. The studied geothermal brines have been kept oxic and anoxic over a wide range of pH from room temperature to approximately 250°C. Some solutions contain also carbonate, bicarbonate, dissolved carbon dioxide, and sulfur. It was shown that pitting corrosion occurs in the geothermal brines, being directly related to the scale formation besides sulfur and heavy metal content of the brines. Brine solutions containing sulfur induce the formation of metal sulfide or iron-silicate sulfide-based scales on mild steel at elevated temperatures. These scales induce and enhance pitting corrosion. Mill scale - present prior to exposure - also affects pitting corrosion. It was also shown that dissolved oxygen increases the rate of pitting corrosion in geothermal brines. Goldberg and Owen (49) besides Cramer and Carter (50) report on pitting of low-carbon steel (table 2 b) and 1020 carbon steel (table 2 c) specimens respectively, in concentrated geothermal brines (chloride ions content: 118 to 185 g/l, pH = 4.8 to 5.7, T = 178 to 229°C).

Westerman et al. (51, 52) have studied the corrosion behavior of A216 mild steel (table 2 j) in hydrothermal brines (90 to 200°C, 5 to 30 bar). Specimens of A216 steel were used for both, as working electrodes and non-polarized (weight change) specimens, to evaluate the validity of the electrochemical corrosion rate determinations. Polarization resistance measurements were performed potentiostatically. Thus electric current densities were recorded during appropriate time intervals after application of a constant potential (8 to 10 mV in cathodic or anodic direction close to the corrosion potential). Potentiodynamic polarization curves were obtained at 0.2 and 1.0 mV/s. The tests were performed in solutions of constant 4.5 m Cl⁻ content under variation of the Mg²⁺/Na⁺ ratio. Results have confirmed that the corrosion rate of A216 mild steel in hydrothermal brines is a function of temperature. Furthermore, when the temperature increases, magnesium chloride hydrolysis causes a decrease of the pH in the solution and an increase of corrosion rate. The products of the hydrolysis of magnesium chloride affect the mechanism of the corrosion process. For example, Mg²⁺ ions might form a soluble complex with Fe²⁺ and appropriate anions which prevents the formation of iron corrosion products. Alternatively, Mg²⁺ ions might accelerate the dissolution of iron by the formation of intermediate reaction products. These types of direct chemical interactions between Mg²⁺, Fe²⁺ and

OH⁻ ions could explain the formation of complex Fe/Mg hydroxyde corrosion products, such as amakinite, instead of Fe₃O₄ magnetite.

3.3.2 Studies in salt brines

Tests undertaken to promote pitting corrosion have been conducted at Pacific Northwest Laboratory. They reported that there was until 1988 no indication of significant non-uniform corrosion (53). Natalie (3) noted that pitting corrosion was not observed in a simulated salt repository brine experiment, although the simulated salt repository brine applied did not contain significant concentrations of sulfur, silica or heavy metals. A three-year exposure of low-carbon steel to aerated wet salt at about 200°C in a salt mine at Avery Island in Louisiana resulted in heavy general corrosion without any evidence of pitting (54). Molecke, Ruppen and Diegle (55) conducted immersion tests of cast iron specimens in both aerated and deaerated brines and found no evidence of pitting corrosion. The tests were performed up to 150°C in deaerated brines and up to 90°C in aerated brines.

The polarization behavior of A216 mild steel (table 2 j) under deaerated conditions in 4.5 m NaCl and 2.0 m MgCl₂+0.5 m NaCl at 150°C has been investigated by Pool and Frydrych (56). No classic active/passive behavior was observed although the hysteresis of some polarization curves is characteristic for some systems which show pitting behavior. Potentiodynamic polarization scans (figure 9) have been performed by exposure of A216 mild steel specimens at 150°C to NaCl brines of various magnesium contents under anoxic conditions (30-50 ppb O₂) (3). They have not shown any strong tendency towards pitting. Although it can be argued that these curves show a weak trend towards increased pitting when magnesium ions concentration is decreased, none of the specimens appeared to be pitted and a pronounced hysteresis loop was not observed in the reverse scans. The data suggest that any pits which formed rapidly coalesced. This is consistent with the rough, coalesced-pit appearance (shallow pit) of mild steel specimens removed from brine immersion tests. Pit coalescence could theoretically occur if the pits were not surrounded by passive regions on the metal surface.

Reimus (13) concludes that the probability of severe pitting of mild steel in a salt repository can be considered to be low because mild steel shows very weak, if any, active / passive behavior in salt brines. Immersion tests have shown significant general corrosion on mild steels in salt brines but no tendency to pitting. It appears that those pits which form rapidly coalesce because of the non-passive nature of the unpitted surface. Marsh et al. (57) reported that pitting corrosion of

low-carbon steel is unlikely in salt brines since low carbon steel does not passivate itself.

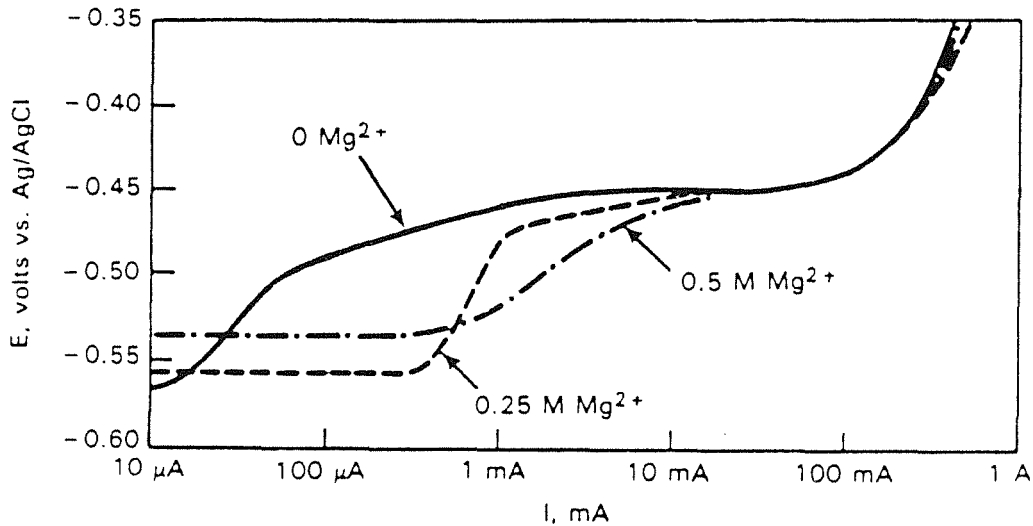


Fig. 9: Anodic Polarization Curves of A216 Mild Steel in NaCl-Brines of Various Mg^{2+} -Concentrations at 150°C (13)

Long-term immersion tests of unalloyed steels have been conducted in laboratory and in-situ experiments by Smailos et al. (58 to 61) using NaCl-rich and $MgCl_2$ -rich salt solutions at temperatures ranging from 90°C to 210°C with and without gamma irradiation (1 to 1000 Gy/h). Thus the corrosion behavior and rate determining influence of several parameters were characterized. Some of the experimental results are reported in figure 10. When the exposure temperature increases from 90°C to 170°C, the corrosion rate of these steels show an increase by a factor of 3 (from 35 to 100 $\mu m/year$). The temperature dependence in the range of 170°C to 200°C is much higher, the corrosion rate increases by a factor of 6. At 200°C a pressure increase from 9 bar to 130 bar in the Q-Brine showed no significant influence on the corrosion rate of the low-carbon steel. Gamma dose rates of 1 to 100 Gy/h or H_2S concentrations (from 25 to 200 mg/l) in the brines did not influence noticeably the corrosion rate of the steels. Under the test conditions, the fine-grained structural steel (table 2 a) has resisted against pitting and crevice corrosion as well as stress-corrosion cracking. Their results confirm that low-carbon steels are promising long-term corrosion resistant materials for packaging of nuclear waste.

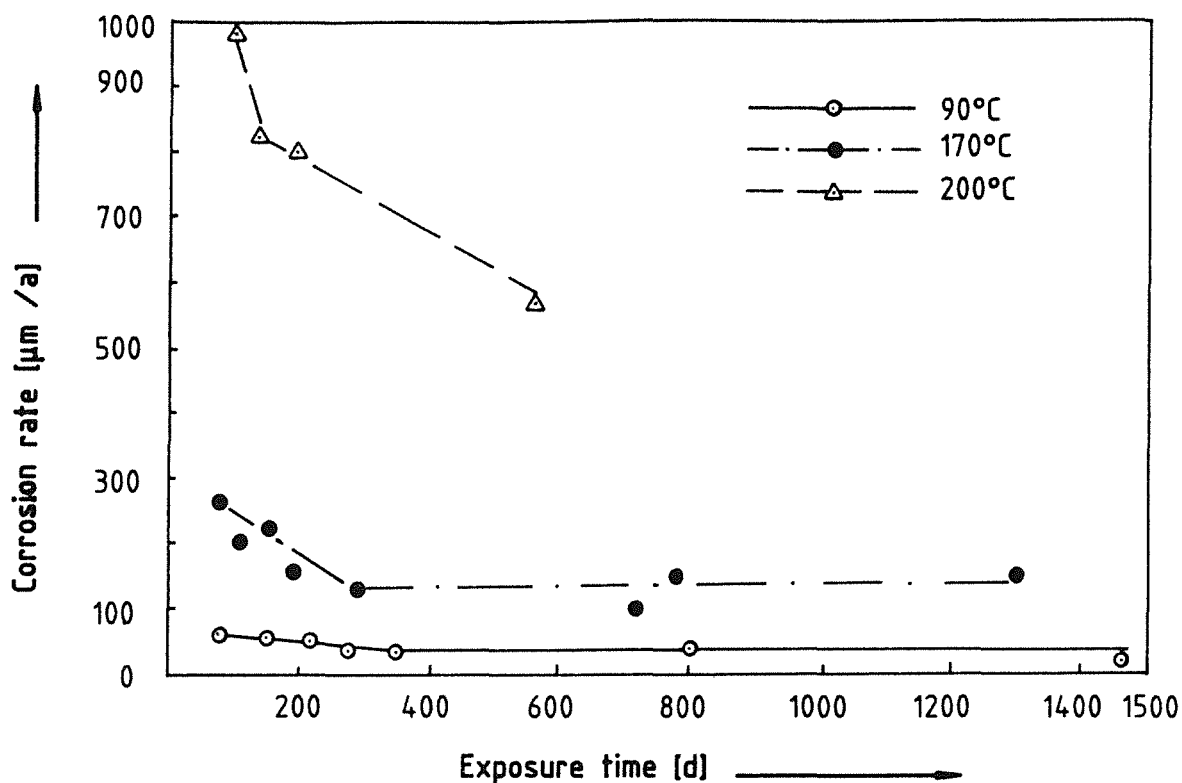


Fig. 10: Corrosion rate of fine-grained structural steel in a $MgCl_2$ -rich solution (61)

Heusler (62-63) studied by electrochemical methods the corrosion of iron and of unalloyed steel in salt containing solutions at high temperatures ($\leq 300^\circ C$) and high pressure (70 bar). The corrosion of iron follows a parabolic rate law which goes along with the formation of a magnetite film on its surface. The time constant does not depend on pH, increases little with chloride concentration and much more with the electrode potential. It reaches its maximum at approximately $250^\circ C$. After several test hours at the free-corrosion potential, the corrosion rate becomes constant, essentially it does not depend on electrode potential and shows little dependence on pH and chloride concentration. An activation energy of 41 KJ/mole and a corrosion rate of scarcely $10 \mu m/a$ were reported. Over a critical electrode potential which becomes more negative with increasing chloride concentration, the corrosion rate increase with electrode potential becomes quite high. Furthermore, the metal surface is no more uniformly corroded and partly protected against further corrosion attack by oxide film formation. In a high concentrated salt brine (6.3 m $MgCl_2$, 0.14 m NaCl, 0.05 m KCl), these conditions are observed near the free-corrosion potential and consequently the measured corrosion rate was relatively high. For studies at

extreme high pressures (up to 4 kbar) and temperatures (up to 250°C), a high pressure autoclave was constructed. Experiments are still going on.

Manfredi et al. (64) have recorded polarization curves and studied by that means the effect of pH on the corrosion of ASTM A216 low-carbon steel grade WCA (0.14% C) in saturated brine at 150°C. A drawing of their autoclave is given in figure 11. The corrosion rate of ASTM A216 carbon steel in saturated NaCl-brine at 150°C, measured over the entire range of pH and calculated by Tafel extrapolation, is plotted in figure 12.

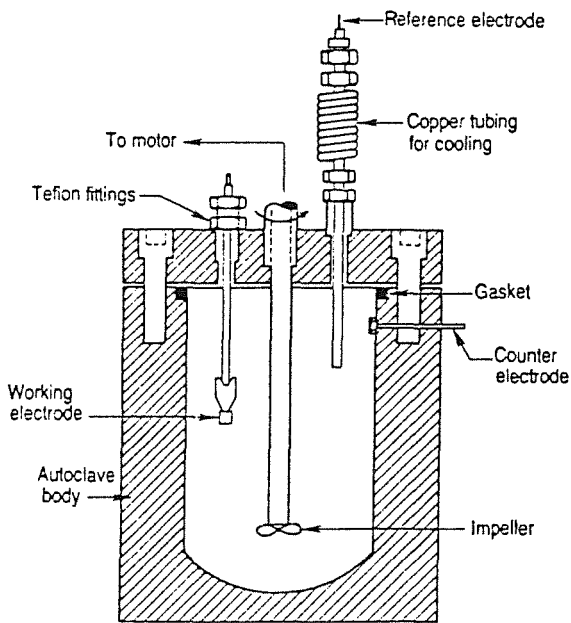


Fig. 11: Schematic illustration of the autoclave (64)

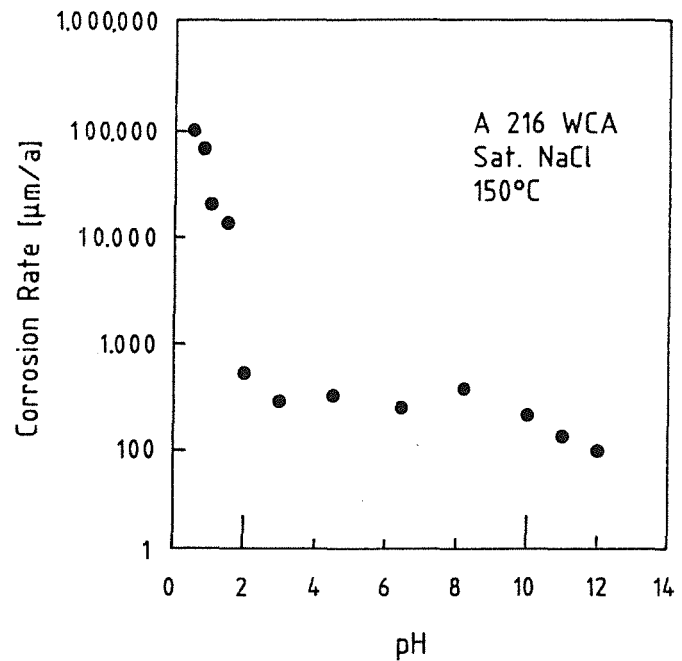


Fig. 12: Corrosion rates measured by Tafel extrapolation as a function of pH for ASTM carbon steel in saturated NaCl at 150°C (64)

These results show:

- High corrosion rate and a strong dependence of pH in acid solutions,
- Moderate corrosion rate, independent of pH in nearly neutral solutions,
- Low corrosion rate, but high susceptibility to localized corrosion as a result of the passivation of the low-carbon steel surface in alkaline solutions.

Schmitt (65) studied by electrochemical tests the corrosion behavior of the fine-grained structural steel DIN W.Nr. 1.0566 in 0.1 m KCl and Q-brine at 35, 55 and

90°C (figure 13). His results have also shown the important influence of the O₂-content and the pH on the corrosion rate. A rough, coalesced pit appearance of the low-carbon steel surface was observed (shallow pits).

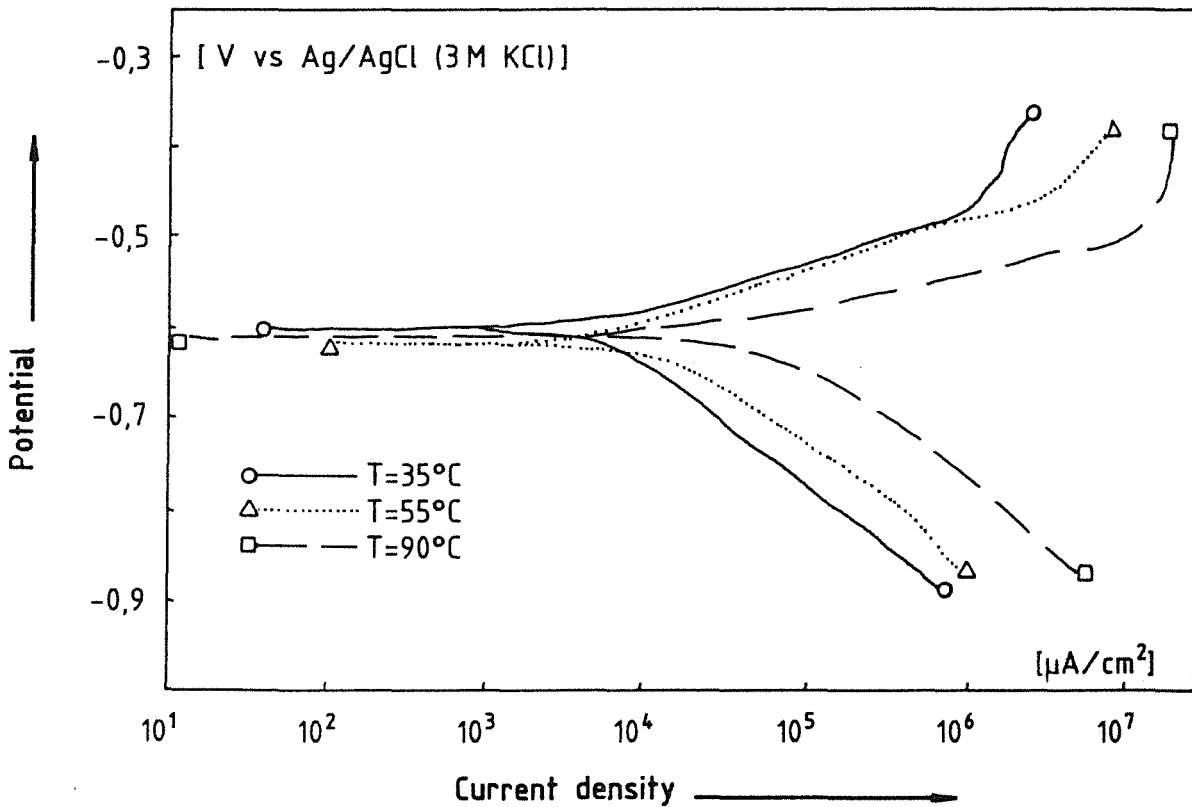


Fig. 13: Potentiodynamic curves obtained with the fine-grained structural steel No. 1.0566 in Q-Brine under aerated conditions (65)

3.4 Conclusions

The literature survey has shown that the following test parameters: temperature, MgCl₂ and O₂ content, pH and state of the metal surface have significant influence on the corrosion rate of low-carbon steels in brines. The experimental evidence indicate that non-uniform corrosion of low-carbon steel is possible if O₂ is present. But until now this type of corrosion has not been observed in salt brines under strictly anoxic conditions. As oxygen - present after emplacement of waste packages in the repository - will be rapidly consumed by corrosion reactions, the pit initiation period - if it exists at all - is short. Since pitting corrosion required the presence of a protective film on the metal surface, factors affecting the passivation process (impurities in salt brines, metal surface state)

must be taken in account. If the pits are not surrounded by highly protective passive regions as it is possible in such aggressive environments, pits may rapidly coalesce.

Our experimental studies therefore focus on the corrosion behavior of the fine-grained structural steel DIN W.Nr. 1.0566 in NaCl- and MgCl-rich salt brines under anoxic and oxic conditions. For instance, some of the specimens studied under anoxic conditions could be previously corroded under oxic conditions since it is of interest to know whether the low-carbon steel continues to corrode by pitting when all oxygen is consumed. Also it seemed to be valuable to examine the influence of different parameters as temperature, pH, salt brine composition, salt impurities (F^- , S^{2-} , . . .), and state of metal surface on steel corrosion..

4. Electrochemical Corrosion Test Methodology

4.1 Material test conditions

Electrochemical test methods were applied to study systematically the potential corrosion failure modes of the fine-grained structural steel DIN W.Nr. 1.0566 and the influence of environmental and metallurgical parameters by

- recording of the corrosion potentials of the steel in various salt brines as function of time,
- determination of its polarization behavior by recording of a potentiodynamic curve, i.e. the current density as function of the potential,
- post-examination of the corroded specimens.

Thus, in addition to long-term immersion tests, which are cited for the fine-grained structural steel in salt brines (58-61), electrochemical methods were applied. The reasons are

- they permit within an accelerated procedure to select the most important parameters in respect to their influence on the corrosion rate and can serve vice-versa as basis for further long-time immersion testing in the future, and
- they provide additional information on the corrosion mechanisms, because the cathodic and anodic processes are measured separately by polarization.
- The conditions under which passive behavior as well as local corrosion occur can be determined. Local corrosion could lead to the perforation of a nuclear waste package long before it fails from general corrosion.

The studied parameters are:

- Temperature (35°C - 90°C),
- Salt brine composition (as given in Table 3),
- Oxygen content,
- pH 2-8,
- Salt impurities: Br⁻, S²⁻, F⁻, ...
- Ratio of metal surface area to solution volume (S/V-ratio),
- Metal surface structure,
- Welding.

The experiments were conducted under normal pressure and otherwise constant conditions.

4.2 Experimental procedure

The equipment used for our electrochemical corrosion tests consists of a PAR Model 273 Potentiostat coupled to a computer data-acquisition system. The three-compartment-cell (figure 14) - which prevents the solutions in the different compartments of being mixed - contained a saturated Hg/Hg₂SO₄/SO₄²⁻ electrode and a platinum counter electrode. The chemical composition of the tested steel DIN W.Nr. 1.0566 is given in Table 2a. The material specimens were exposed at the working electrode position as disks of cylindrical shape (1.0 or 1.4 cm in diameter and 0.4 cm in length). For the surface preparation, the disks have been polished with 320, 800 and 1200-grit silicon carbide papers and cleaned with soap and water and then with isopropanol. The solutions were deaerated by purging with a fine stream of nitrogen or hydrogen prior to the start of electrochemical measurements for at least half an hour. A slow scan rate of the polarization test was applied (0.2 mV/s). The stirring conditions of the brine were kept constant. All given experimental potential values were measured versus the Hg/Hg₂SO₄/SO₄²⁻ reference electrode.

4.3 Electrochemical testing procedures

At first, the corrosion potential of the steel in the test solution is registered for at least half an hour, then the polarization behavior (active/passive characteristics) is determined by conventional polarization techniques.

Table 3: Chemical composition of the salt brines at 55°C

Weight %	MgCl ₂	KCl	NaCl	MgSO ₄	CaCl ₂	K ₂ SO ₄	CaSO ₄	H ₂ O	pH (25°C)
Brine 1 (Q-brine)	26,80	4,70	1,40	1,40				65,70	4,6
Brine 2	33,03	0,11	0,31		2,25			64,30	4,1
Brine 3			25,90	0,16		0,24	0,20	73,50	6,9
Z-Brine	36,40	0,67	0,20	0,87				61,86	
NaCl-H ₂ O			26,90					73,10	
NaCl-CaSO ₄ -H ₂ O			26,90				0,50	72,60	
KCl-H ₂ O		30,7						69,30	
CaCl ₂ -H ₂ O					57,40			42,60	

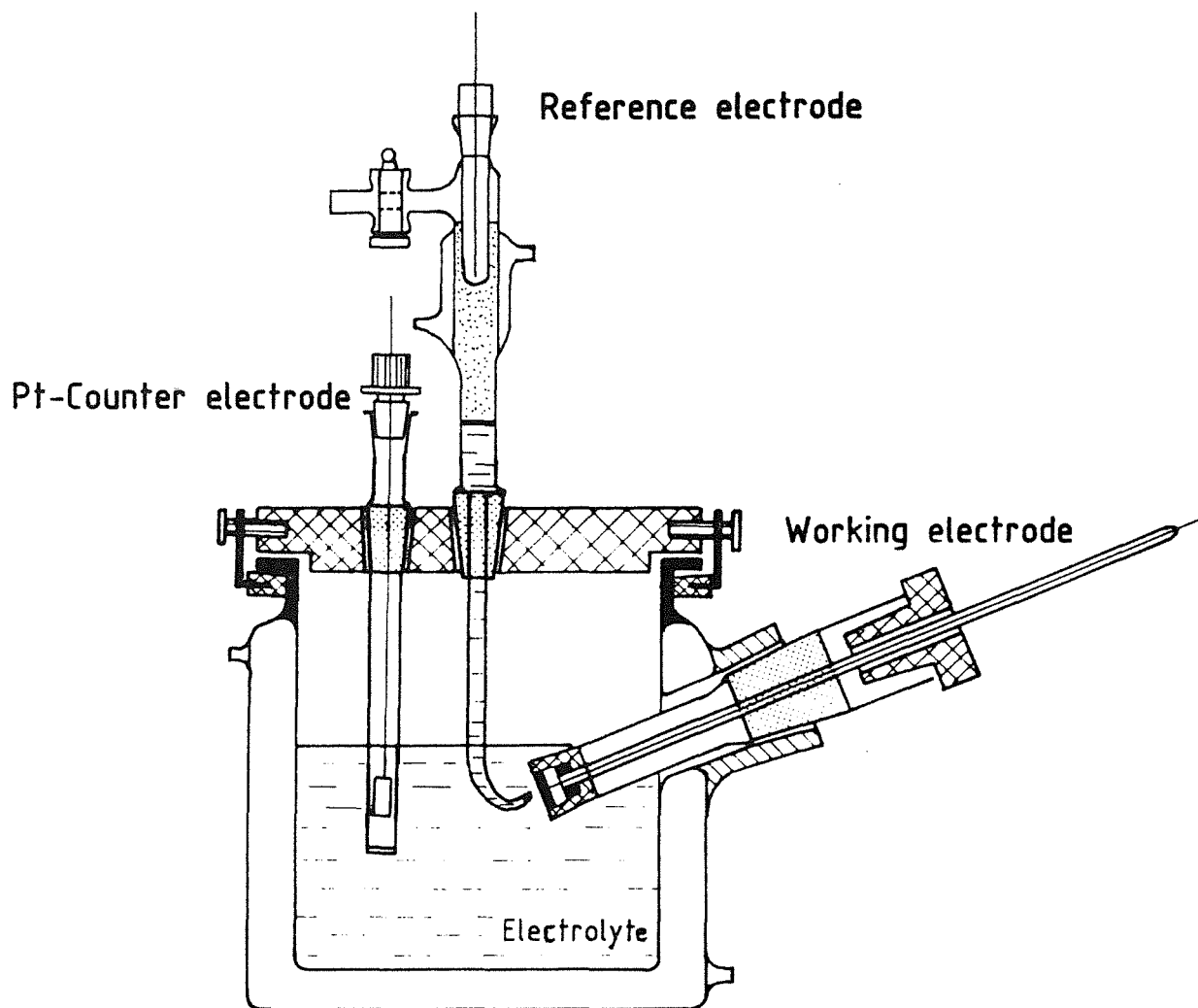


Fig. 14: Schematics of the electrochemical cell

4.3.1 Potentiodynamic Polarization

By potentiodynamic polarization, the polarity and magnitude of the current density between the metal specimen and an inert platinum counter electrode are measured as function of the electrochemical potential. A schematic of polarization curve showing several possible types of behavior is given in figure 15. For the active corrosion case, the anodic curve is linear when potential is plotted versus the logarithm of current density. The forward and reverse scans are coincident. The presence of a peak in the anodic portion of the curve followed by decreasing current, generally indicates the onset of passivation. The occurrence of hysteresis between the forward and reverse scans indicates pitting. Where the hysteresis loop is very large, the protection potential, E_{prot} , may be very close to the free corrosion potential E_{corr} , indicating a high probability of pitting in service.

In order to know how a metal will behave in practice, the polarization curves of the anodic and cathodic reactions can be used. One can then distinguish a number of possibilities for a passivating metal. The most important of those are shown in figure 16 (4).

- a) Spontaneous and stable passivity is obtained under the conditions given in figure 16 a. Here the cathodic reaction has a sufficiently high equilibrium potential, so that the curves intersect only in the passive region, and the corrosion current density i_{corr} is equal to current density in the passive range i_{pass} .
- b) At a lower equilibrium potential, two possibilities for the cathodic reaction (figure 16 b) exist:
 - A cathodic reaction with a large exchange current density ($i_{\text{oc}2}$) still makes it possible to obtain spontaneous and stable passivity.
 - For a cathodic reaction with a small exchange current density ($i_{\text{oc}1}$), it may happen that they are three intersections of the polarization curves. For practical purposes, the middle one is not important because it is electrically unstable. If the metal is passive to begin with it starts in point 1 and if undisturbed remains passive. But if the passive layer is locally damaged, the resulting active spots cannot be repassivated and corrode with a rate corresponding to point 3. Under these circumstances an active-passive element with a small anode and a large cathode exists. This situation leads to serious localized corrosion.

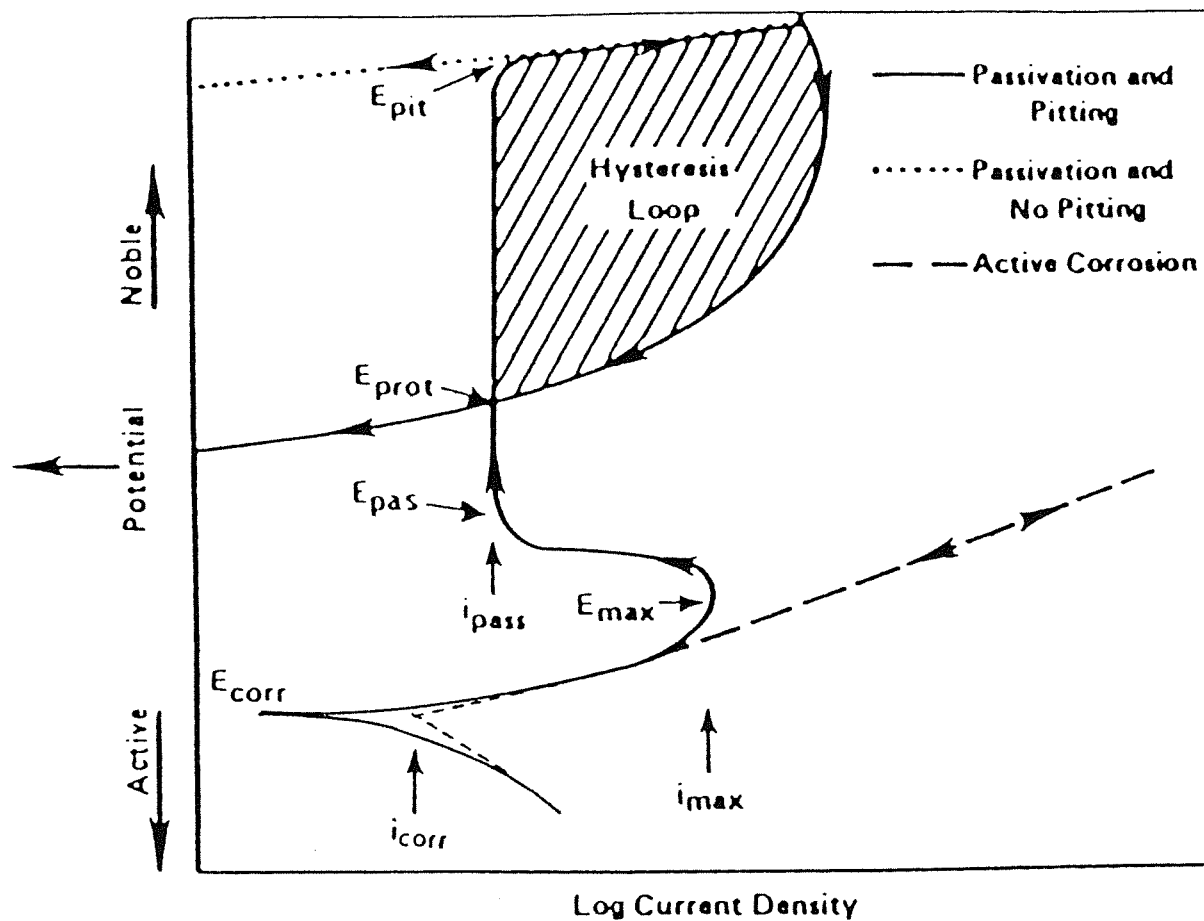


Fig. 15: Schematic diagram of typical potentiodynamic polarization curves showing important polarization parameters: E_{corr} = corrosion potential; E_{pit} = potential at which pits initiate on forward scan; E_{prot} = potential at which pits repassivate on reverse scan; i_{max} = current density at active peak; i_{pass} = current density in passive range. $\Delta E_{pit} = E_{pit} - E_{pass}$ (37)

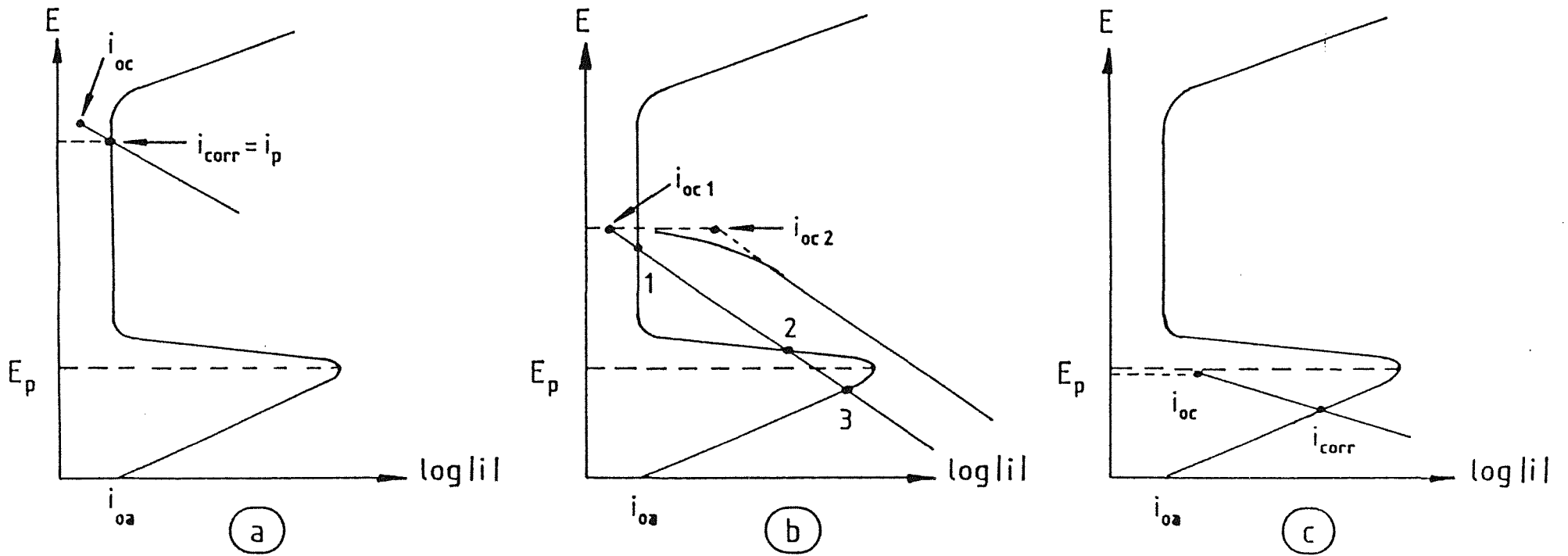


Fig. 16: Polarisation diagrams for a metal which can be passivated (4)

- a) Spontaneous and stable passivity
- b) Cathodic reaction with small and large exchange current density
- c) Corrosion of an active metal

- c) As it is shown in figure 16 c, for a cathodic reaction of a still lower equilibrium potential the passivation is not more possible. In fact this represents the case of corrosion of an active metal.

The following polarization parameters are obtained from the polarization curves of potential (E) versus the logarithm of current density (log i): corrosion potential (E_{corr}), corrosion current density (i_{corr}), potential at which pits are initiated (E_{pit}), potential at which pits repassivate (E_{prot}), potential at active peak (E_{max}), current density at active peak (i_{max}), current density in passive range (i_{pass}), Tafel coefficients (b_a , b_c), polarization resistance (R_p). The corrosion rates can be determined as follows by two methods: Tafel Plot and Polarization Resistance Plot.

Tafel Plot

A Tafel plot is obtained by potentiodynamic scanning within a range of +/-250 mV versus the corrosion potential (E_{corr}). An example is given in figure 17. The corrosion current (i_{corr}) is determined by superimposing the best straight line which fits the linear portion of the anodic or cathodic curve and is extrapolated through E_{corr} . The point of intersection at E_{corr} gives the i_{corr} value. Then the corrosion rate is calculated by the following equation:

$$v_{corr} = \frac{0.0033 \cdot i_{corr} \cdot (E.W.)}{d}$$

where:

v_{corr} = corrosion rate (mm/a)

E.W. = equivalent weight (g/eq.)

d = density (g/cm³)

i_{corr} = corrosion current density (μ A/cm²)

The slope of the best straight line fit is called Tafel constant. An anodic Tafel constant (b_a) is determined from the best fit of the anodic linear portion and a cathodic Tafel constant (b_c) is determined from the best fit of the cathodic linear region. The Tafel constants combined with the Polarization Resistance value (R_p) can be used to calculate the corrosion rate too.

Polarization Resistance Plot

The polarization resistance plot is generated by scanning within a range of +/-20 mV versus the corrosion potential (E_{corr}). The polarization resistance characterizes the resistance of the specimen against corrosion during the application of an external potential. The corrosion current density and the corrosion rate are directly related to the polarization resistance R_p .

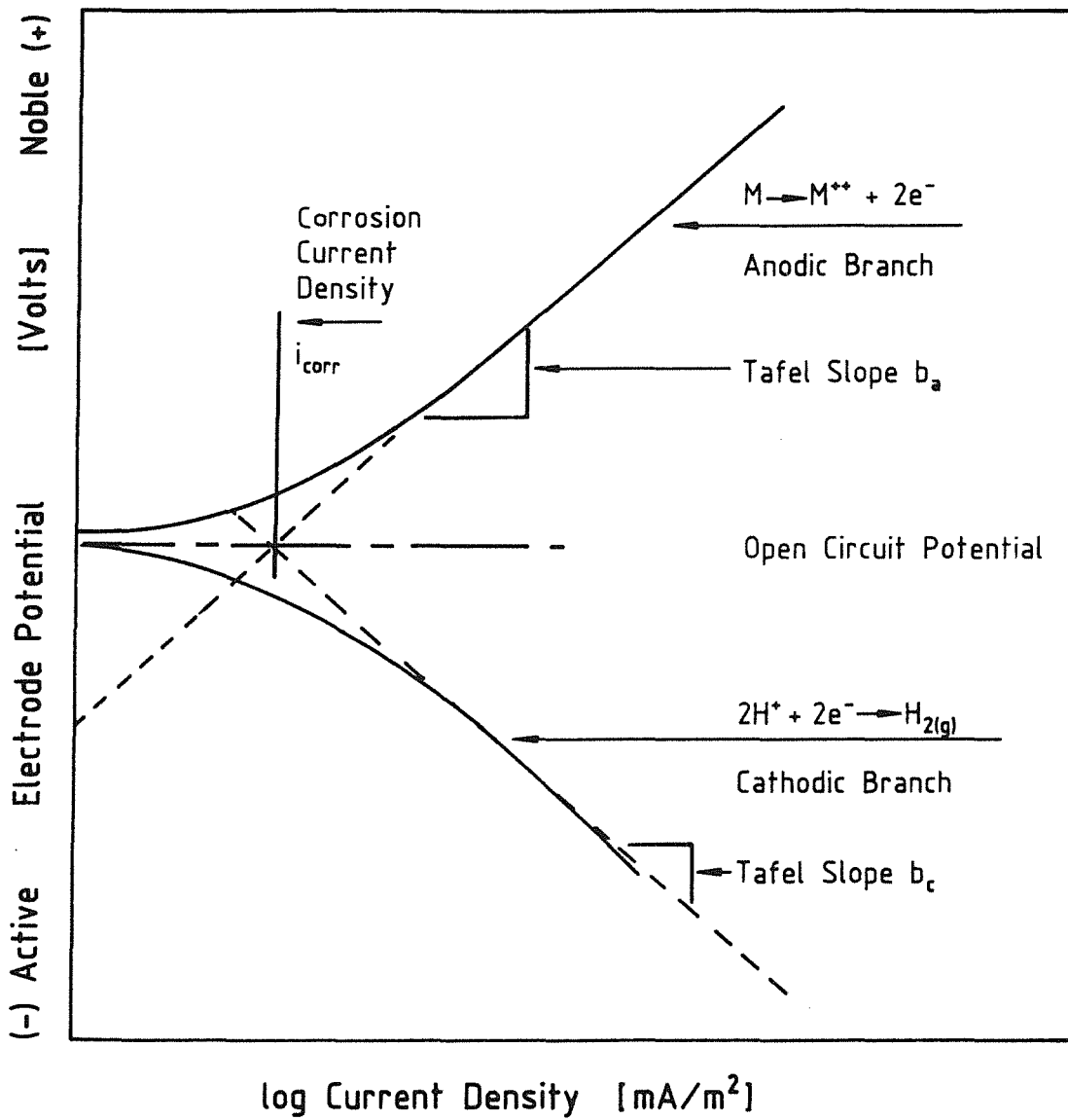


Fig. 17: Hypothetical cathodic and anodic polarisation diagram

$$R_p = \frac{\Delta E}{\Delta i} : \text{the slope of the linear region,}$$

$$i_{corr} = \frac{b_a \cdot b_c}{2.3 \cdot R_p \cdot (b_a + b_c)}$$

$$v_{corr} = \frac{0.0033 \cdot i_{corr} \cdot (E.W.)}{d}$$

where

v_{corr} = corrosion rate (mm/a)

R_p = polarization resistance ($K\Omega/cm^2$)

b_a, b_c = anodic and cathodic Tafel constants

i_{corr} = corrosion current density ($\mu A/cm^2$)

E.W. = equivalent weight (g/eq)

d = density (g/cm^3)

Furthermore, since the polarization resistance is inversely proportional to the corrosion current density, the polarization resistance characterizes the ability of the material to resist corrosion.

As some deviations from the Tafel behavior were recognized when the measured polarization curves are evaluated, the method how to calculate the corrosion rate has to be discussed in more detail. It is known, that a corroding metal is subjected to more than one electrochemical process, occurring on its surface at a measurable rate. It must be involved at least one anodic and one cathodic process. If an external current is applied to change the potential of the corroding metal it affects the rate of all electrochemical processes at the metal surface. In many real corroding systems, one of the cathodic and one of the anodic processes are predominant with respect to the competing ones. Then the cathodic and the anodic experimental curves show linear parts which coincide with the predominant cathodic and anodic partial current Tafel lines. The Tafel slopes can be then easily extrapolated from the experimental curve.

This method seems to fail for some corroding systems when, for example, the corrosion potential (E_{corr}) is too close to the partial corrosion potentials or because of an interfering electrochemical process. The theoretical linear $\log i$ vs E dependence is in those cases disturbed and the measurement of the Tafel curve and slopes are difficult. In a more general way, deviations from the Tafel behavior may be caused by local action currents, concentration polarization, IR

drop effects, by a change in the predominant electrode reaction or by a modification of the metal surface state.

- Concentration polarization occurs for example when the reaction rate is so high that the species being oxidized or reduced cannot reach the surface at a sufficiently high rate. The solution adjacent to the electrode then becomes depleted of the reacting ions, and consequently the rate is controlled by the diffusion of the reacting species to the metal surface (diffusion control). The shape of a curve, including both activation and concentration polarization, is illustrated by figure 18.

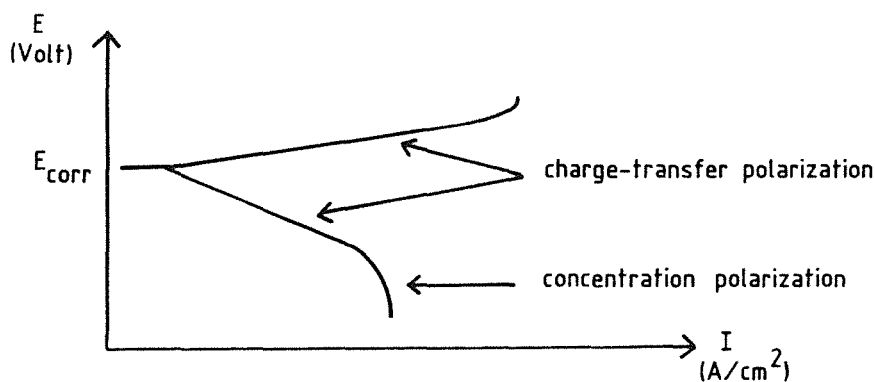


Fig. 18: Potentiodynamic polarization curve including charge-transfer and concentration polarization

The limiting diffusion current is a function of the concentration of the reacting species, the stirring rate of the solution and all the other factors which depress the maximum rate at which theoretically an ion can approach the metal surface. Examination of figure 18 shows that deviation from Tafel behavior caused by concentration polarization is quite marked. When concentration polarization occurs, the corrosion rate can be determined from the anodic Tafel value and from the polarization resistance value by the following equation:

$$i_{corr} = b_a / 2.3 R_p$$

- One additional factor is responsible for deviations from Tafel linearity in the low-current region: This is demonstrated when the corrosion potential of the system is not sufficiently far away from the equilibrium potentials of the different partial reactions. Then the other cathodic or anodic partial currents are not negligible and must be taken in account.

- Resistance between the reference electrode and the polarized metal surface contributes still as an additional term to the overvoltage, measured as a linear function of the current.
- Anodic metal dissolution at high potentials is often followed by passivation, which can distort the $\log I$ vs E plot before the linear Tafel region is completely established. The cathodic Tafel slope can still be obtained from the cathodic polarization curve provided the latter exhibits a linear $\log I$ vs E section. As only one of the two Tafel slopes is required for the determination of the corrosion current (if the corrosion potential is known precisely), the corrosion rate can be calculated any way.

However, other evaluation methods can be used simultaneously to the Tafel Plot and the Polarization Resistance Plot methods. These are the two-point or the three-point method developed by Barnartt et al. (66-67) for potentials near the corrosion potential to obtain both Tafel slopes and corrosion rates. For corroding electrodes on which both reactions are proceeding under charge-transfer control, the three-point method requires three current measurements at selected values of $\Delta E = (E - E_{\text{corr}})$: at ΔE , $2 \Delta E$, $-2 \Delta E$. The corrosion potential has to be far from the two partial corrosion potentials. As currents measured at large values of $(E - E_{\text{corr}})$ give no information about the cathodic Tafel slope, at least one of the three currents must be measured at $(E - E_{\text{corr}}) < 2.3 RT/F$. For corroding electrodes at which one of the reactions is under charge-transfer control and the other under concentration polarization respectively, the three-point method can be used only if the corrosion potential (E_{corr}) is close to the first partial corrosion potential (E'_{corr}). On the contrary, this method will often be not applicable because of severe interference from mass-transfer effects and competing reactions. In this case, it is better to use the two-point method at selected values of $\pm \Delta E$. ΔE will be small with respect to $(E_{\text{corr}} - E'_{\text{corr}})$.

4.3.2 Potentiostatic Polarization

In the potentiostatic polarization procedure the metal is quickly polarized and then the electrochemical potential is maintained constant. The evolution of the electrochemical current in function of time is registered. It can be correlated with the kinetics of different processes such as corrosion stabilization, porous layer formation, passivity, pit formation and propagation.

4.4. First Corrosion Results

At first, the free corrosion potentials as function of time and the potentiodynamic curves of Hastelloy C4, Incoloy 825 and the fine-grained structural steel DIN W.Nr. 1.0566 in acid and neutral solutions with different chloride ions contents were measured. These experiments were performed for calibration purposes and the comparison with the literature.

In figure 19, the potentiodynamic polarization curve of Incoloy 825 in a deaerated sulfuric acid solution (1m H₂SO₄) at 30°C is shown. The measured curve (a) is very similar to the one (b), reported previously by Bort (68). A corrosion potential of -695 mV was measured versus the Hg/Hg₂SO₄ reference electrode. Passivity is observed for anodic potentials from -470 to +380 mV. As Bort has shown (fig. 20 b), the passive range at 75°C is restricted by addition of chloride ions (1m H₂SO₄ + 0.5 M KCl) to the range of -460 to -100 mV (figure 20 a).

The tested steel DIN W.Nr. 1.0566 shows the ability to passivate by anodic polarization in a deaerated sulfuric solution (0.5 m H₂SO₄) at 25°C (figure 21). The current oscillations in the potentiodynamic curve during the active-passive transition were similar to those as observed for pure iron (69). When 250 mg/l chloride ions are added to this acid, passivity is not maintained (figure 22). Similarly, when anodically polarized at 25°C in a neutral, deaerated 0.5 m solution of Na₂SO₄, the low-carbon steel shows passivation at anodic potentials from -50 to +800 mV. In figure 24, the influence of an addition of 500 mg/l chloride ions to a deaerated neutral 0.5 m solution of Na₂SO₄ at 25°C on the decrease of the passive range is shown.

The following experiments were performed to compare the experimental results with those of the literature and to study the influence of some experimental parameters. The results are presented in figure 25-31.

DIN W.Nr. 1.0566 (Deaerated 0.5 m H₂SO₄, pH = 0.35)

The corrosion behavior of the fine-grained structural steel was initially examined in 1 n H₂SO₄ solution since a lot of results are published in the literature. In figure 25-26, the experimental potentiodynamic polarization curves and the corrosion rates from the polarization resistance and Tafel constant evaluations are presented. Our experimental results show good agreement with literature values (table 6 and figure 27). For example, Felloni (70) has measured the dissolution of iron in 0.5 m H₂SO₄. He registered a corrosion potential of -268 mV versus NHE (i.e. -916 versus Hg/Hg₂SO₄ electrode), an anodic Tafel slope of 31 mV/decade, a cathodic Tafel slope of -120 mV/decade and a corrosion current density of 120 μA/cm².

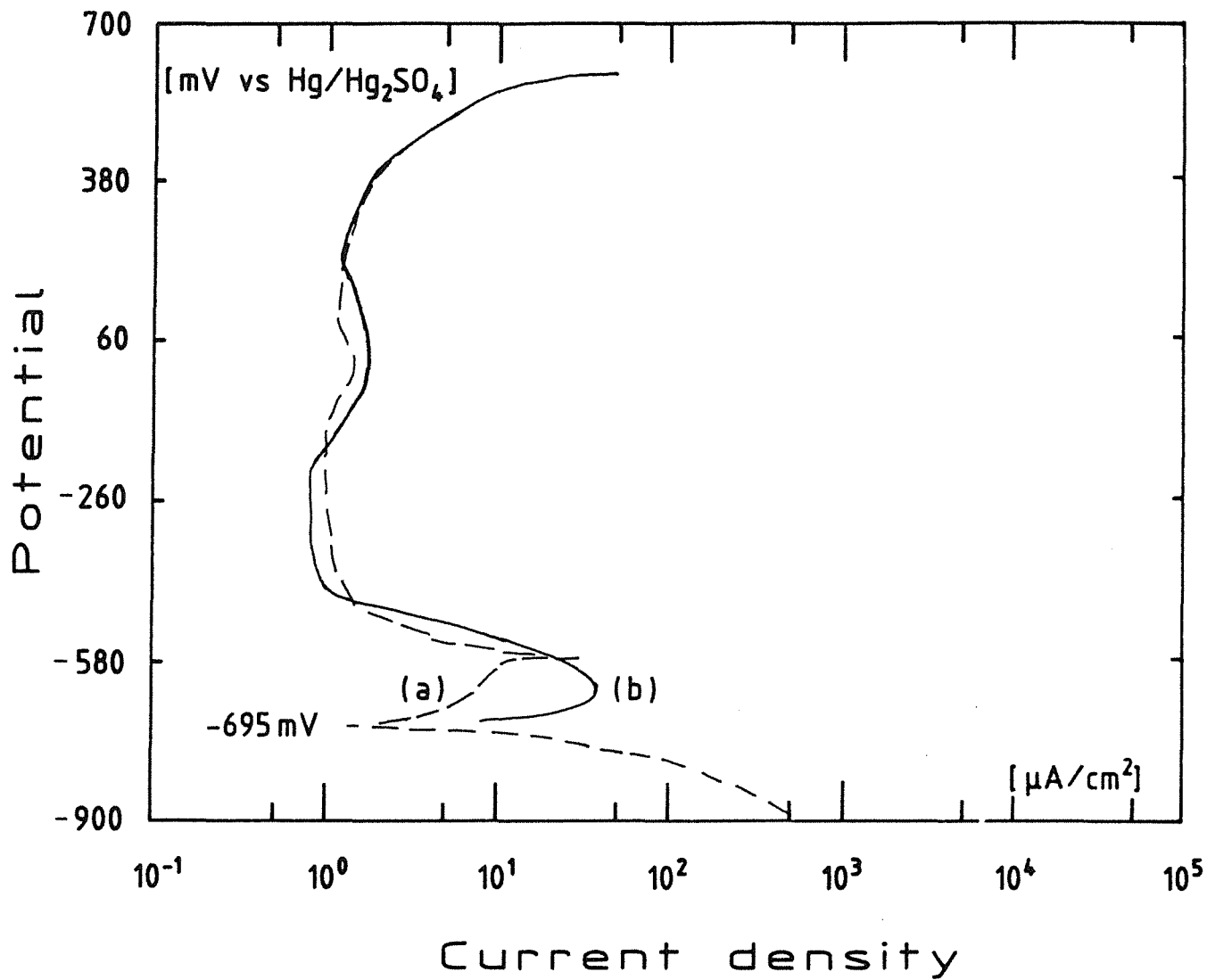


Fig. 19: Potentiodynamic polarization curves of Incoloy 825 in 1 m H₂SO₄ at 30°C
a) Own experiments
b) According to Bort (68)

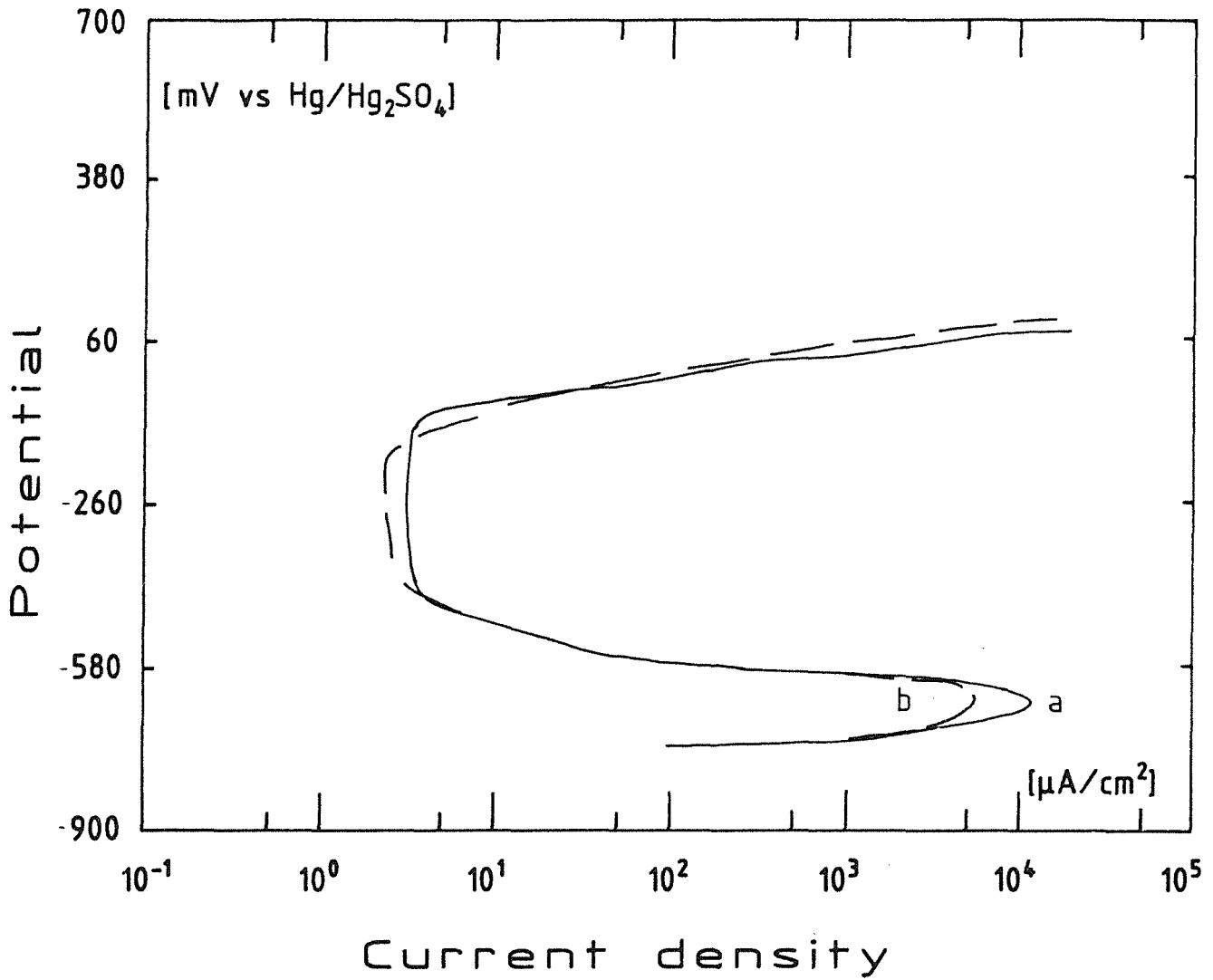


Fig. 20: Potentiodynamic polarization curves of Incoloy 825 in 1 m H₂SO₄ + 0.5 m KCl at 75°C
a) Own experiments
b) According to Bort (68)

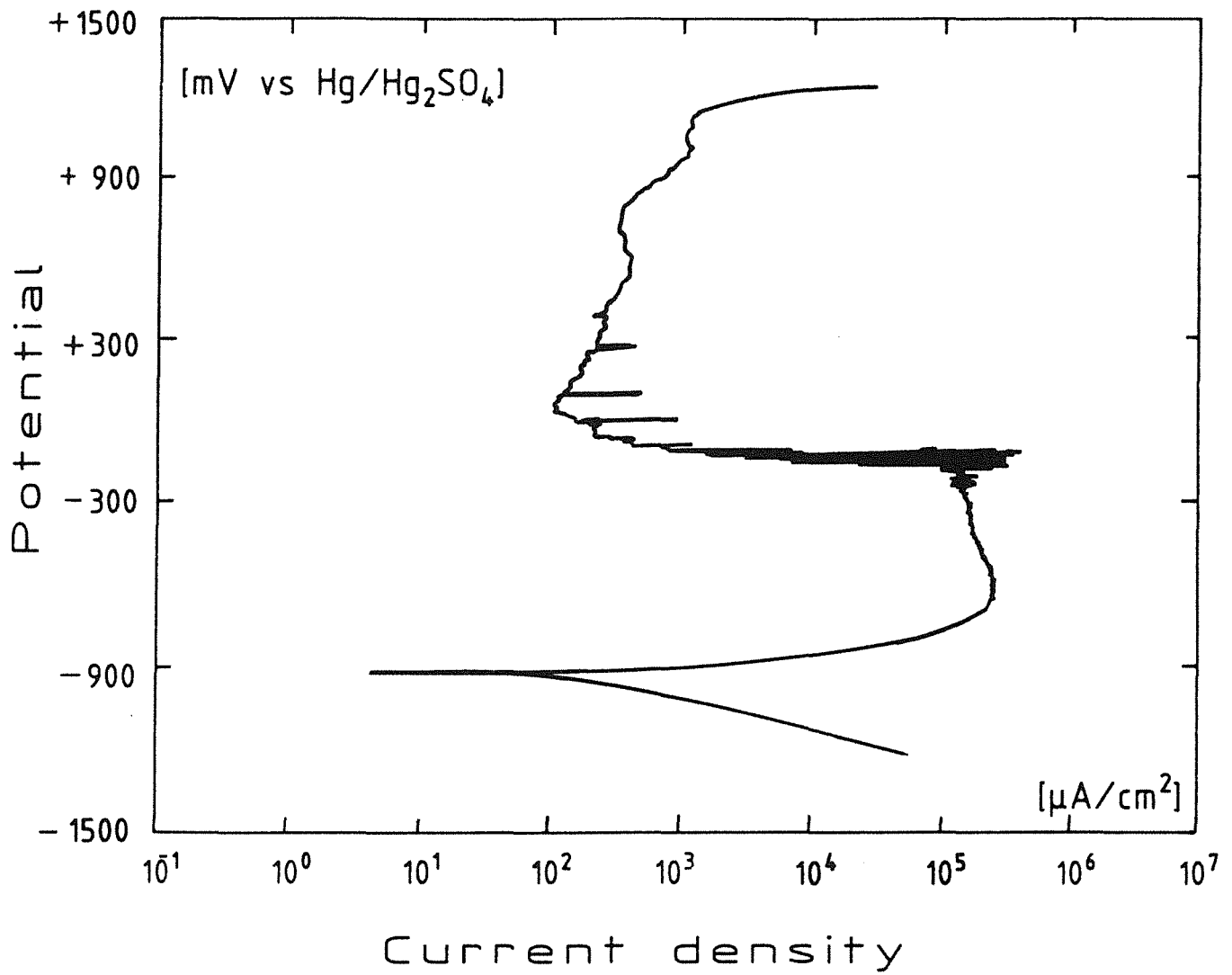


Fig. 21: Potentiodynamic polarization curve of the fine-grained structural steel DIN W.Nr. 1.0566 in 0.5 m H₂SO₄ at 25°C.

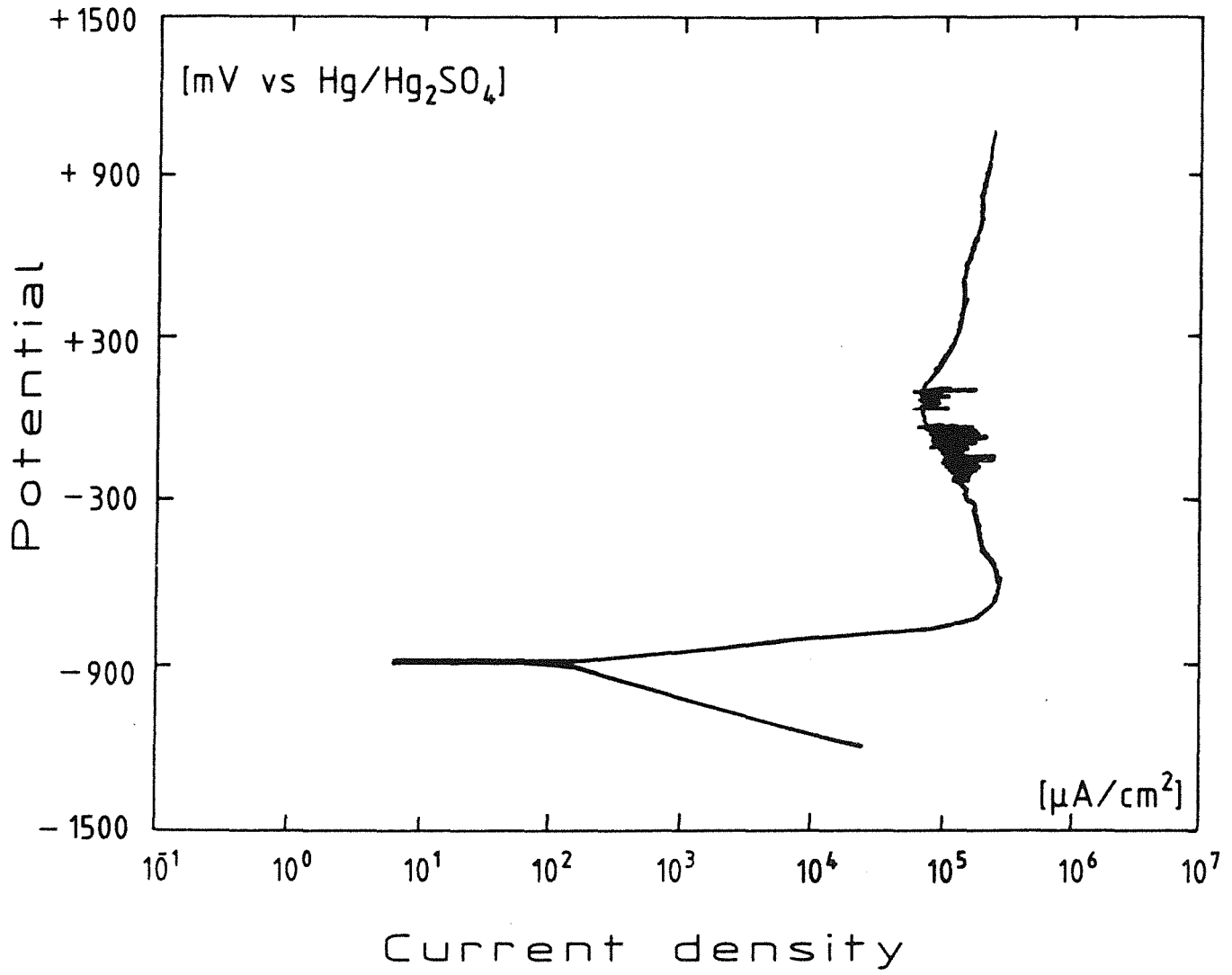


Fig. 22: Potentiodynamic polarization curve of the fine-grained structural steel DIN W.Nr. 1.0566 in 0.5 m H₂SO₄ and 0.007 m Cl⁻ at 25°C.

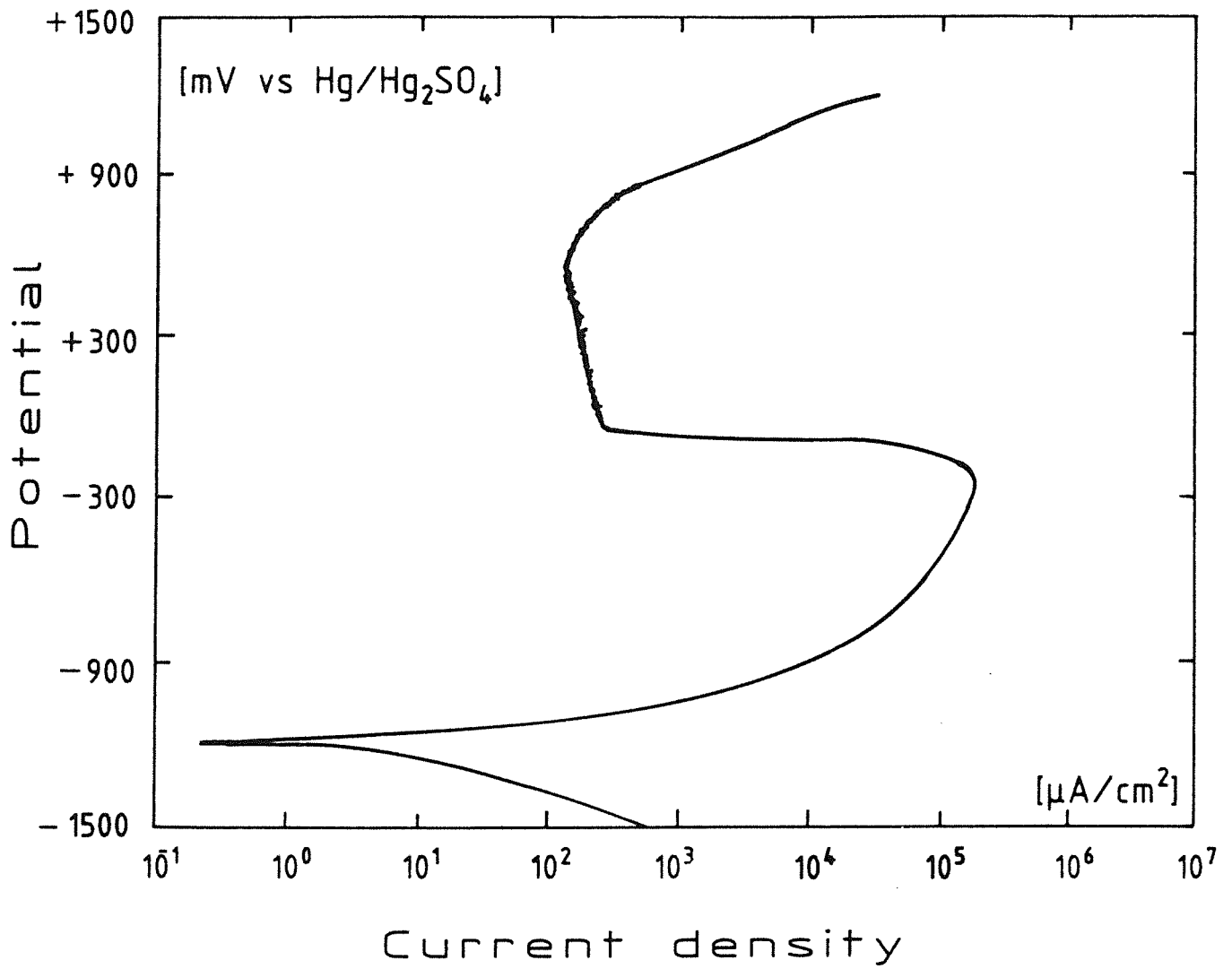


Fig. 23: Potentiodynamic polarization curve of the fine-grained structural steel DIN W.Nr. 1.0566 in 0.5 m Na₂SO₄ at 25°C.

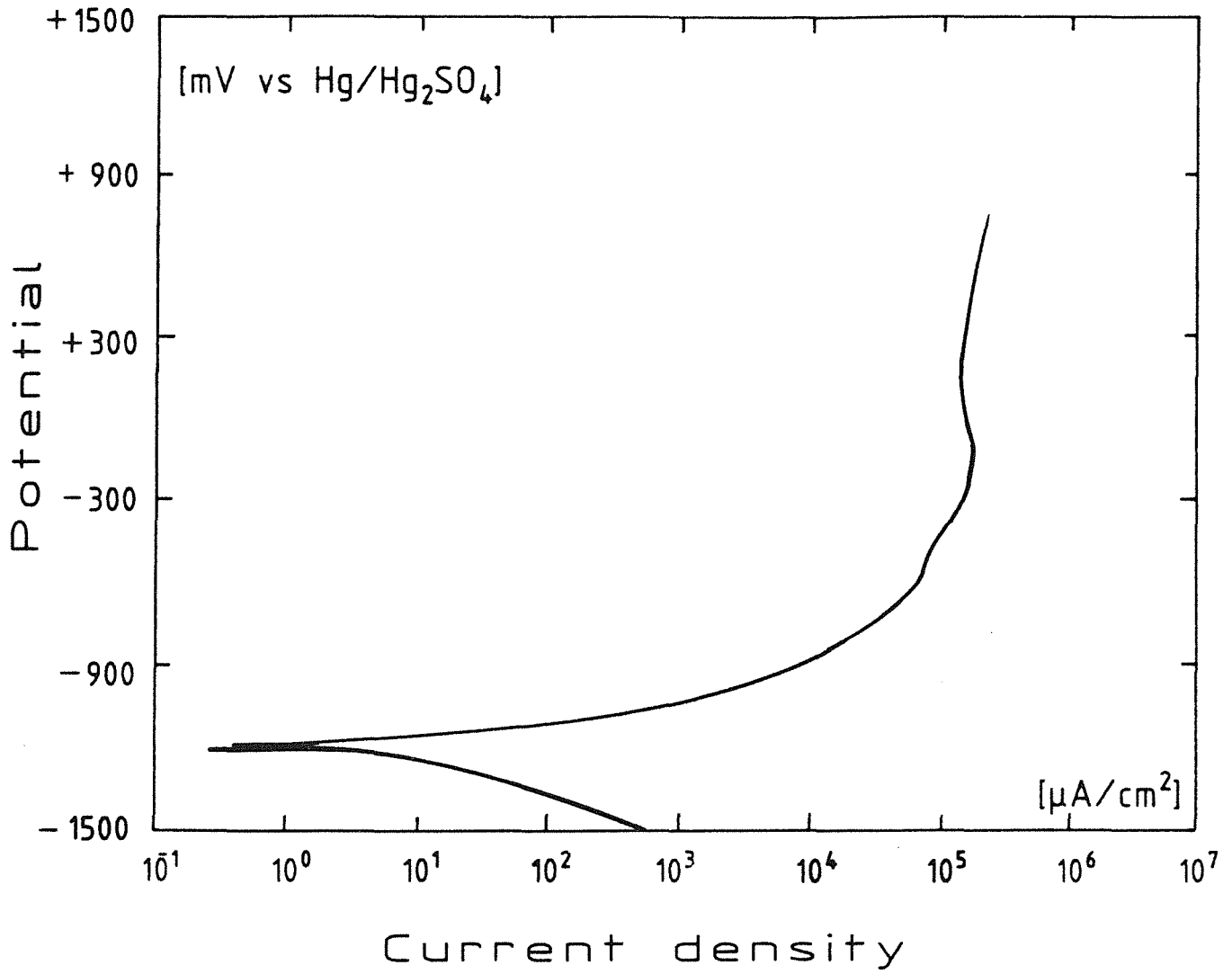


Fig. 24: Potentiodynamic polarization curve of the fine-grained structural steel DIN W.Nr. 1.0566 in 0.5 m Na₂SO₄ + 0.014 m Cl⁻ at 25°C.

In figure 25, additionally the influence of the scan rate on the potentiodynamic polarization curve is shown. The effects are smaller at low scan rate (< 0.5 mV/s), as shown in table 4. This proves that the experimental polarization curves and numerical analysis of such data can only be derived from experimental results if the scan rates are sufficiently slow.

The influence of the temperature on the reaction rate is much more important because the corrosion is a thermally activated process (figure 26). A comparison of our experimental results with some literature values (in respect to the temperature influence) is given in table 7 and figure 27 and shows good agreement.

In figure 28, the influence of chloride ion additions to the 0.5 m sulfuric acid at 50°C on the corrosion of the fine-grained structural steel is given. The most important effect is that no passivity can be achieved as long as a content of ≥ 100 mg/l chloride ions is present in the acid. When the concentration of chloride is raised from 0 to 100 mg/l the first appearance of passivity is retarded, the passive current density is increased and the passive potential range is shortened, as illustrated in figure 28.

DIN W.Nr. 1.0566 (Deaerated 0.5 m Na₂SO₄, pH = 5.7)

The fine-grained structural steel was studied at 50°C and neutral pH. In figure 29, the low influence of scan rate on the potentiodynamic curve at low scan rates (< 0.5 mV/s) can be recognized. As it can be seen in figure 30, the influence of chloride ions on the corrosion rate is small. The corrosion rate (table 10) is in this neutral solution much lower than below pH 4 due to the change of the cathodic reaction. Furthermore, it is shown that the passivity cannot be maintained at a neutral pH in the presence of 100 mg/l chloride ion additions.

DIN W.Nr. 1.0566 (Deaerated 3.5% NaCl Solution, pH = 7)

In figure 31 and table 11, our experimental potentiodynamic polarization curve of the fine-grained structural steel in 3.5% NaCl solution at ambient temperature and pH = 7 is compared with that of Marsh et al. (34) for a forged low-carbon steel BS 4360 43 A (table 2k). The corrosion potential difference can be due to the small difference in the material composition (table 2j) and in the experimental procedure. However, the Tafel constants, the corrosion currents and consequently the corrosion rates are similar.

Conclusion:

The above experimental results show that electrochemical methods can be successfully applied to study the corrosion behavior of the fine-grained structural steel DIN W.Nr. 1.0566 in salt brines.

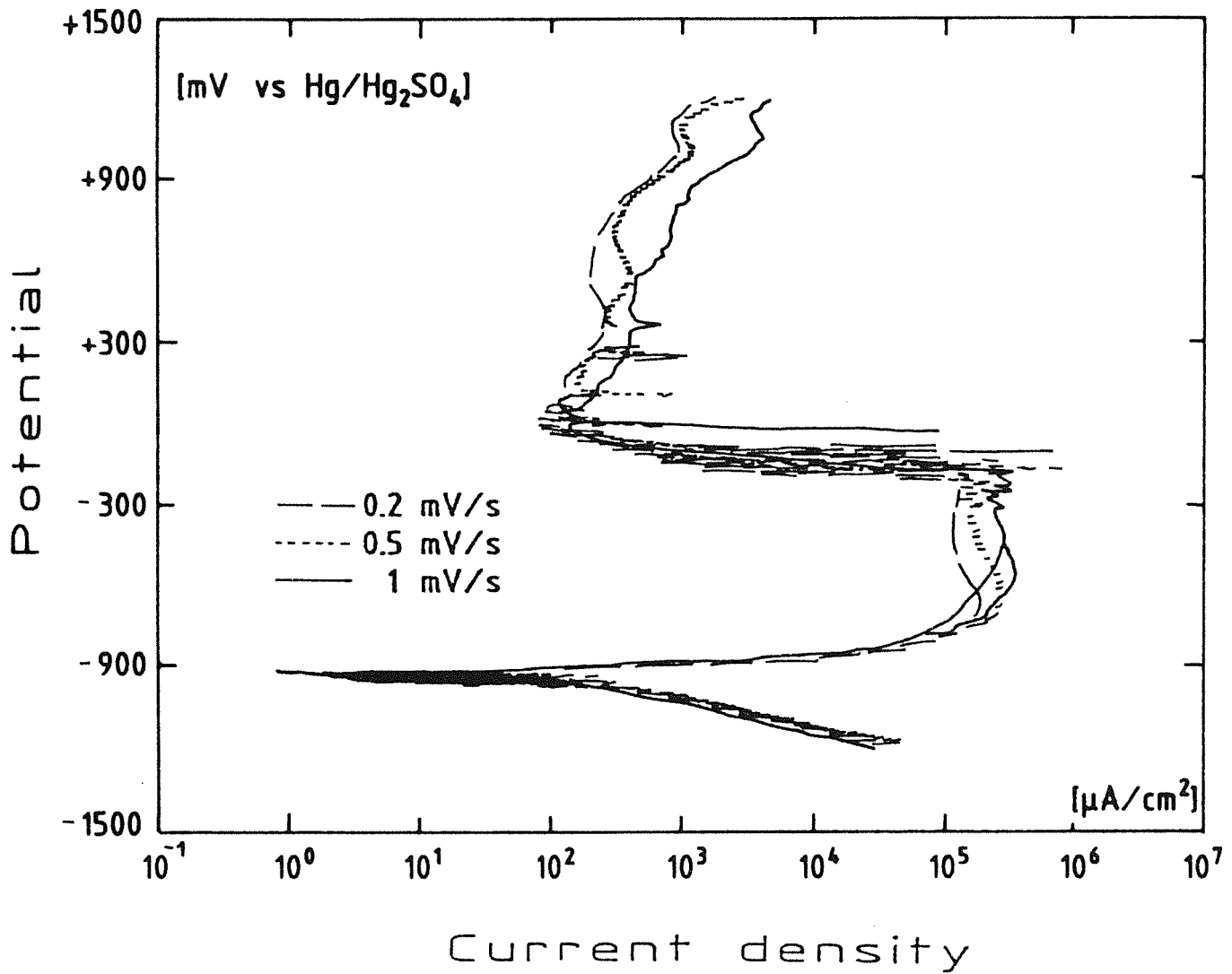


Fig. 25: Potentiodynamic polarization curves of the fine-grained structural steel DIN W.Nr. 1.0566 in 0.5 m H₂SO₄ at 25°C. Influence of scan rate.

Tab. 4:

Results	(mV/s)	0.2	0.5	1	1
corrosion potential	(mV vs Hg/Hg ₂ SO ₄)	-920	-917	-921	-921
cathodic Tafel constant	(mV)	104	101	104	110
anodic Tafel constant	(mV)	32	28	36	40
corrosion current density	(μA/cm ²)	130	120	105	105
corrosion rate	(mm/a)	1.5	1.4	1.2	1.2
corrosion potential	(mV vs Hg/Hg ₂ SO ₄)	-919	-920	-923	-924
polarization resistance	(KΩ/cm ²)	0.124	0.138	0.174	0.137
corrosion current density	((μA/cm ²)	86	81	67	93
corrosion rate	(mm/a)	1.0	1.0	0.8	1.1

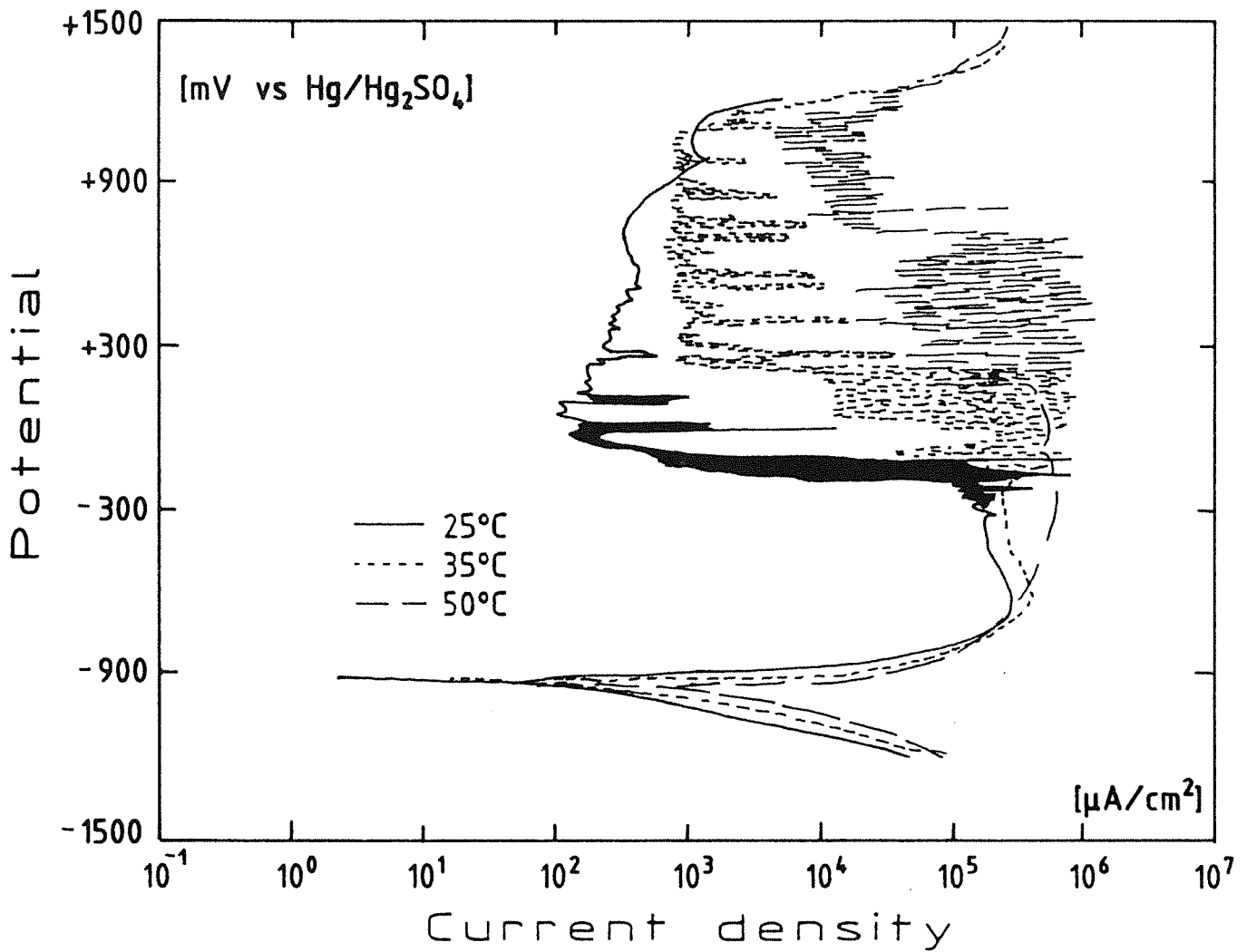


Fig. 26: Potentiodynamic polarization curves of the fine-grained structural steel DIN W.Nr. 1.0566 in 0.5 m H₂SO₄. Influence of Temperature.

Tab. 5:

Results	(mV/s)	25°C	35°C	50°C
corrosion potential	(mV vs Hg/Hg ₂ SO ₄)	-917	-921	-932
cathodic Tafel constant	(mV)	101	122	129
anodic Tafel constant	(mV)	28	33	30
corrosion current density	(μA/cm ²)	120	710	1400
corrosion rate	(mm/a)	1.4	8.2	16
corrosion potential	(mV vs Hg/Hg ₂ SO ₄)	-920	-924	-936
polarization resistance	(KΩ/cm ²)	0.138	0.0336	0.0094
corrosion current density	((μA/cm ²)	81	336	1095
corrosion rate	(mm/a)	1.0	3.9	13

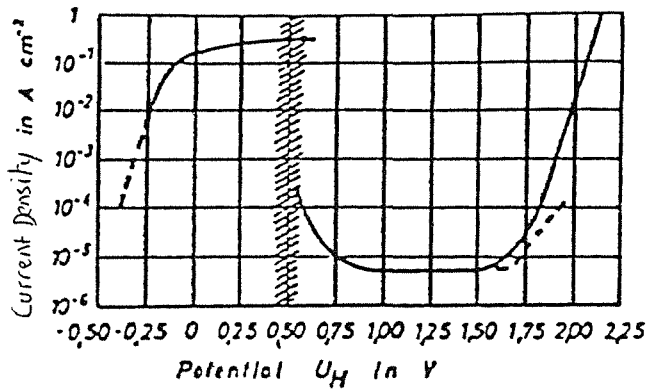


Fig. 27a: Potentiodynamic polarization of iron in 0.5 m H₂SO₄ at 25°C (71)

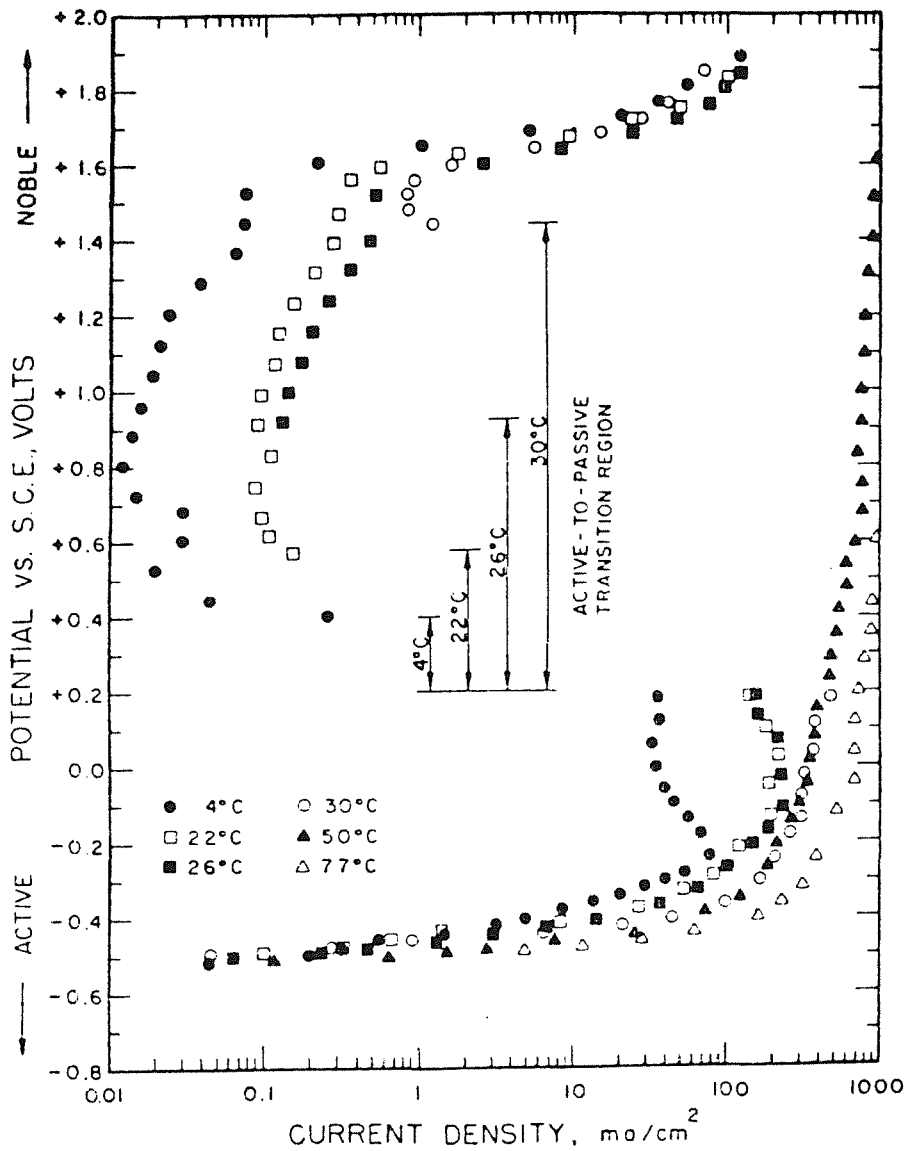


Fig. 27 b: Effect of temperature on the potentiostatic anodic polarization of iron in H₂ saturated, 0.5 m H₂SO₄ (72)

Table 6: Experimental and Literature results

	Experimental Values of DIN W.Nr. 1.0566	Literature Values of Pure Iron (70-75)
E corr (mV vs Hg/Hg ₂ SO ₄)	-920	-918 -914
b _a (mV/dec.)	34	30 42
b _c (mV/dec.)	105	126
I corr (μA/cm ²)	98	100
Corrosion rate (mm/a)	1.2	1.8

Table 7: Temperature Influence

Temperature		Experimental Values of DIN W.Nr.1.0566	Literature Values of Pure Iron (72)
22	E corr (mV vs Hg/Hg ₂ SO ₄)	-920	-914
	b _a (mV/dec.)	34	42
	Passive range (mV vs Hg/Hg ₂ SO ₄)	-500 to + 1100	+ 150 to + 1200
50	E corr (mV vs Hg/Hg ₂ SO ₄)	-934	-918
	b _a (mV/dec.)	30	29
	Passive range (mV vs Hg/Hg ₂ SO ₄)	+ 800 to + 1100	-

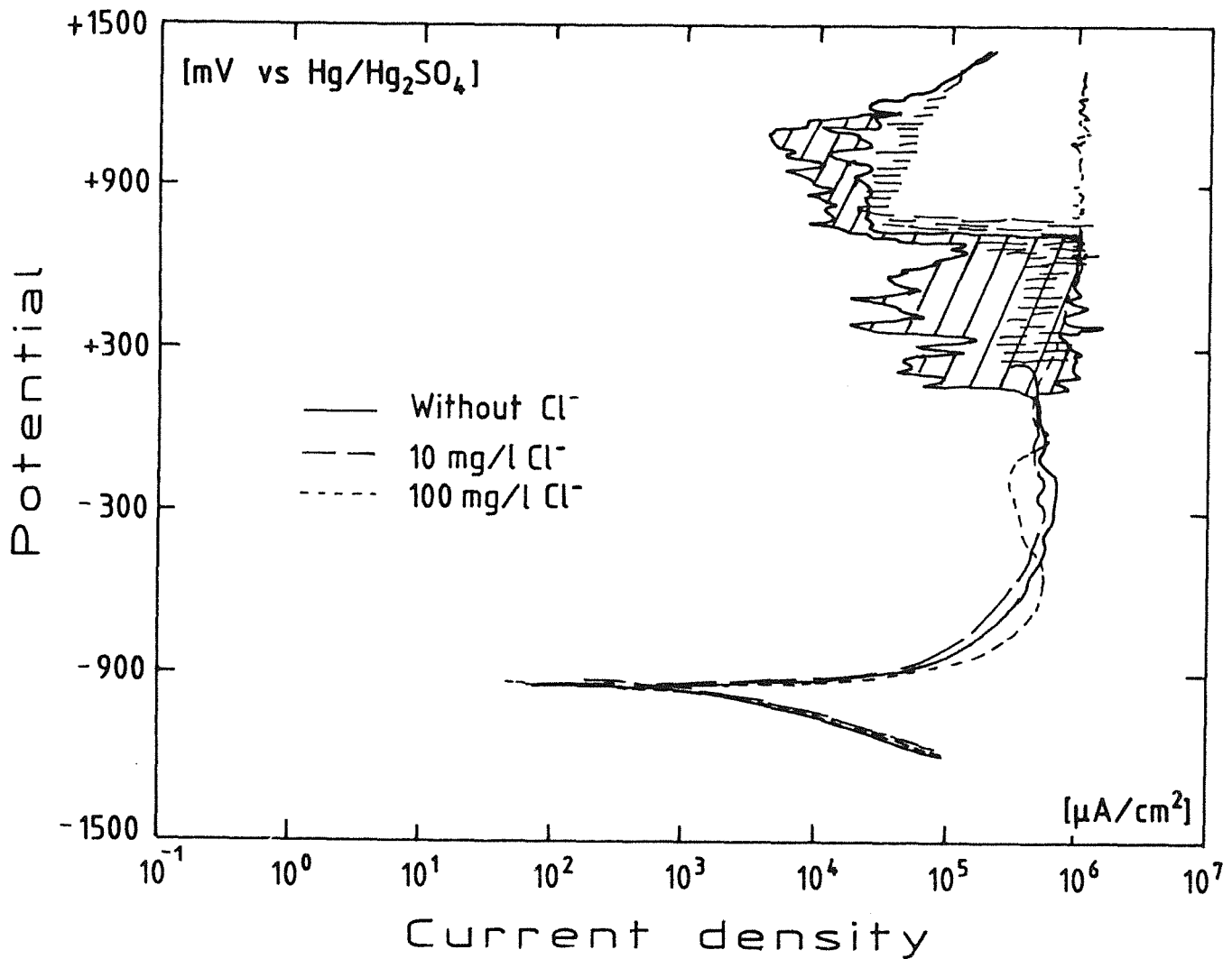


Fig. 28: Potentiodynamic polarization curves of the fine-grained structural steel DIN W.Nr. 1.0566 in 0.5 m H₂SO₄ at 50°C as influenced by chloride ion additions

Tab. 8:

Results	(Cl)	0 mg/l	10 mg/l	100 mg/l	
corrosion potential	(mV vs Hg/Hg ₂ SO ₄)	-932	-920	-922	-926
cathodic Tafel constant	(mV)	129	123	125	104
anodic Tafel constant	(mV)	30	28	33	29
corrosion current density	(μA/cm ²)	1400	2050	2000	1300
corrosion rate	(mm/a)	16	24	23	15
corrosion potential	(mV vs Hg/Hg ₂ SO ₄)	-936	-924	-926	-930
polarization resistance	(KΩ/cm ²)	0.0094	0.0049	0.0062	0.0084
corrosion current density	((μA/cm ²)	1095	2024	1831	1200
corrosion rate	(mm/a)	13	23	21	14

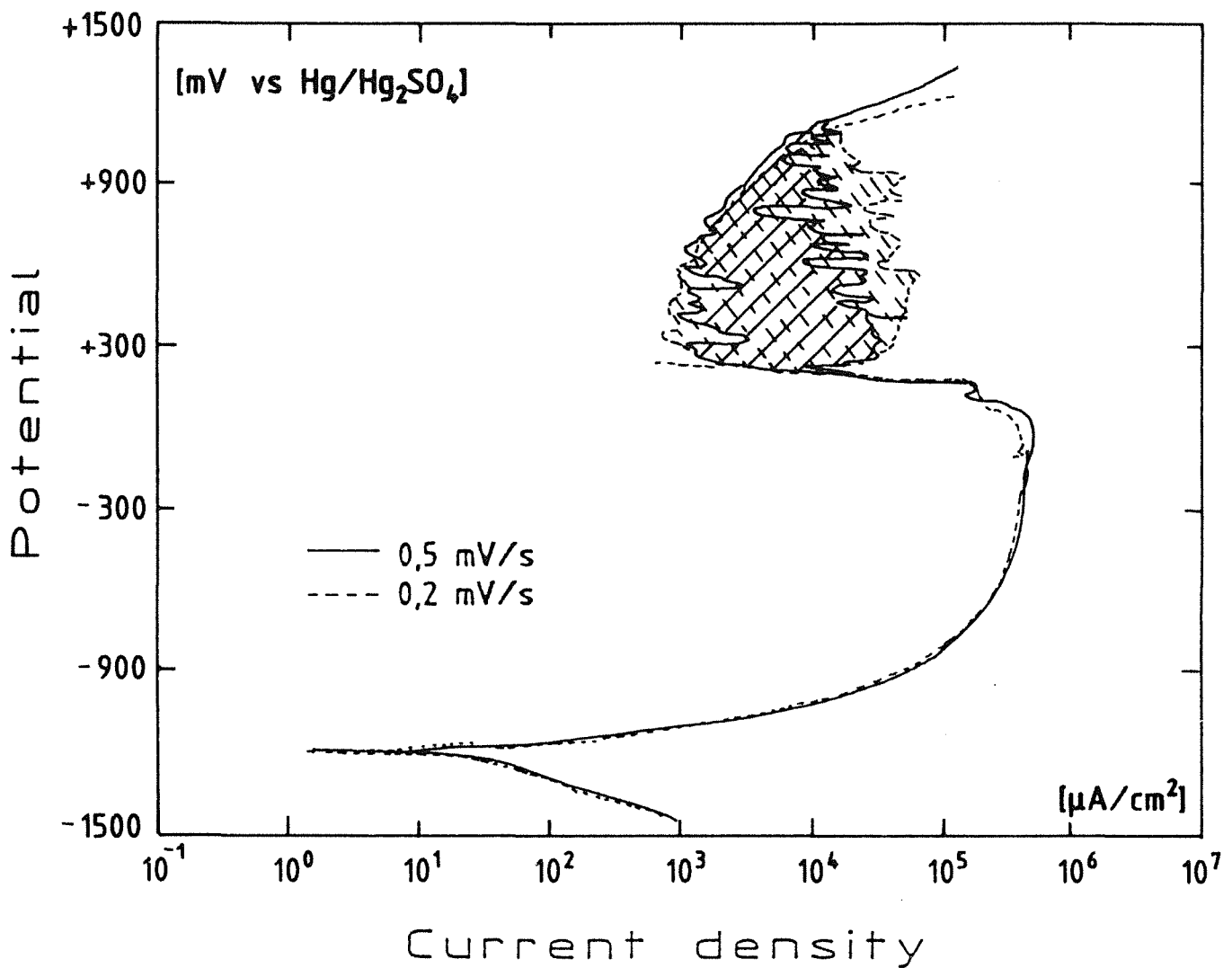


Fig. 29: Potentiodynamic polarization curves of the fine-grained structural steel DIN W.Nr. 1.0566 in 0.5 m Na₂SO₄ at 50°C and pH = 5.7. Influence of scan rate.

Tab. 9:

Results		
corrosion potential	(mV vs Hg/Hg ₂ SO ₄)	-1193
cathodic Tafel constant	(mV)	155
anodic Tafel constant	(mV)	50
corrosion current density	(μA/cm ²)	23
corrosion rate	(mm/a)	0.3
corrosion potential	(mV vs Hg/Hg ₂ SO ₄)	-1196
polarization resistance	(KΩ/cm ²)	0.533
corrosion current density	((μA/cm ²)	27
corrosion rate	(mm/a)	0.3

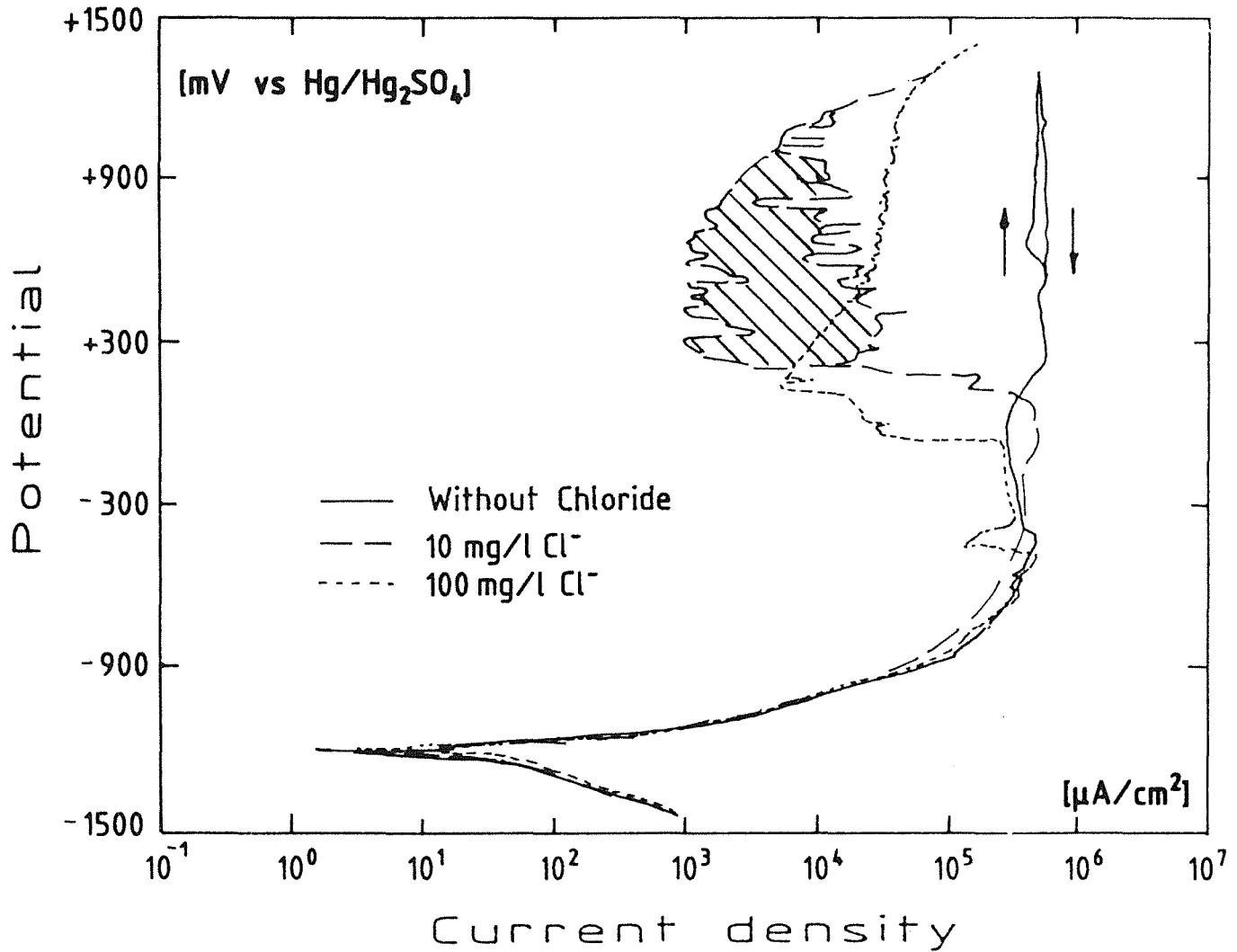


Fig. 30: Potentiodynamic polarization curves of the fine-grained structural steel DIN W.Nr. 1.0566 in 0.5 m Na₂SO₄ at 50°C and pH = 5.7
Influence of chloride ions on the passivity

Tab. 10:

Results	(Cl ⁻)	0 mg/l	10 mg/l	100 mg/l
corrosion potential	(mV vs Hg/Hg ₂ SO ₄)	-1193	-1191	-1199
cathodic Tafel constant	(mV)	155	157	177
anodic Tafel constant	(mV)	43	46	50
corrosion current density	(μA/cm ²)	23	28	31
corrosion rate	(mm/a)	0.3	0.3	0.4
corrosion potential	(mV vs Hg/Hg ₂ SO ₄)	-1196	-1194	
polarization resistance	(KΩ/cm ²)	0.533	0.483	
corrosion current density	((μA/cm ²)	27	32	
corrosion rate	(mm/a)	0.3	0.4	

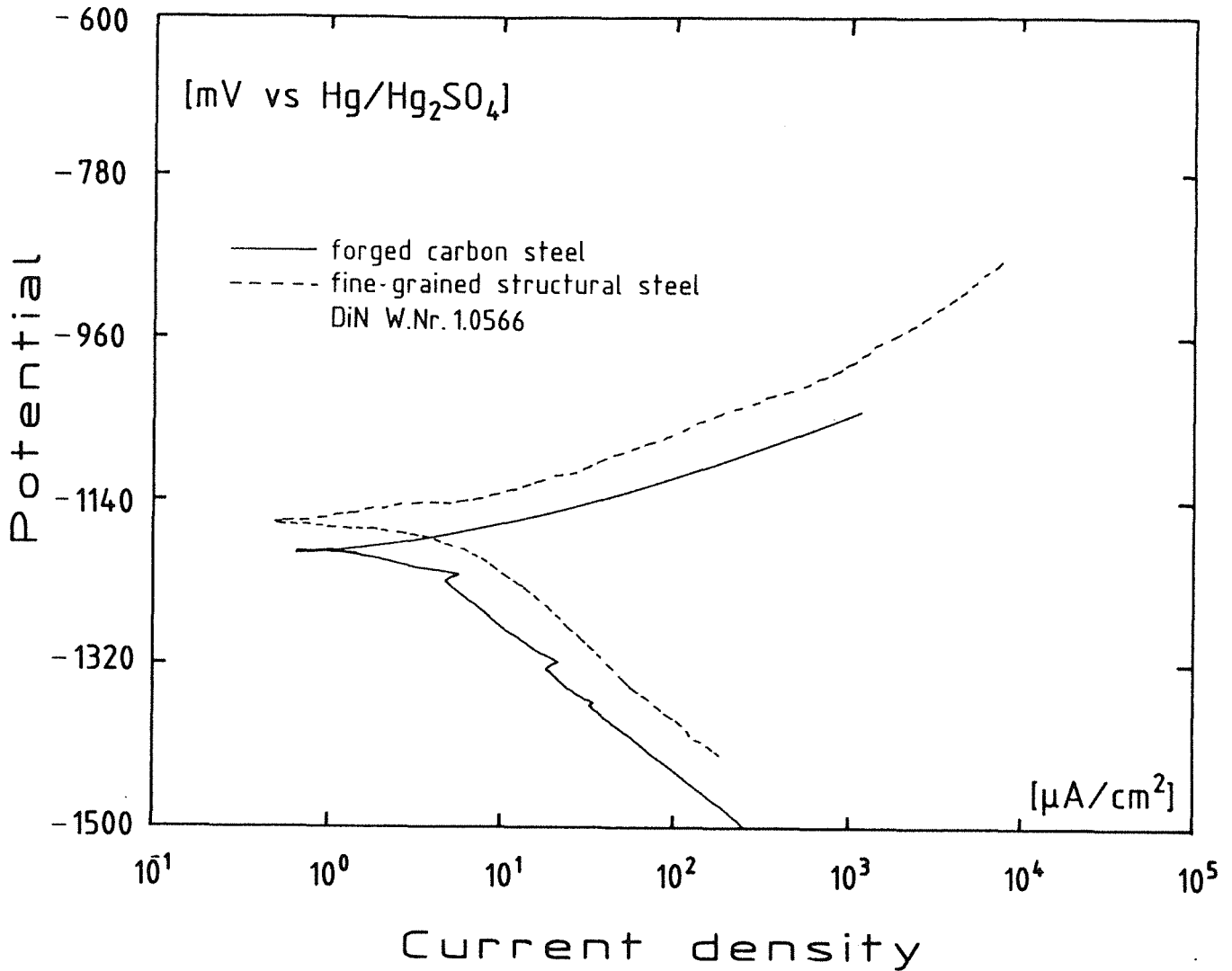


Fig. 31: Potentiodynamic polarization curves of the fine-grained structural steel DIN W.Nr. 1.0566 in deaerated 3.5 % NaCl solution at 25°C and pH = 7

Tab. 11:

Results		1.0566	forged carbon steel
corrosion potential	(mV vs Hg/Hg ₂ SO ₄)	-1166	-1216
cathodic Tafel constant	(mV)	159	160
anodic Tafel constant	(mV)	62	59
corrosion current density	(μA/cm ²)	4	3
corrosion rate	(mm/a)	0.046	0.035

5. Experimental Results

5.1 Free Corrosion Potential

At first, the free corrosion potential of the fine-grained structural steel in three salt brines (the brine composition is given in table 3) was registered as function of time at 55°C under aerated conditions. The concentration of dissolved oxygen in the brines 1-2-3 was low (<2ppm). No stirring was done. Results are presented in figure 32. After immersion in salt brines, the free corrosion potentials of the specimens became initially more negative until the brine was saturated with corrosion products. Then the free corrosion potential fluctuations decreased and its overall trend slowly became a little more positive. In the same time, an oxide layer composed of corrosion products grew on the surface of the fine-grained structural steel. The corrosion potentials of the fine-grained structural steel in the brines 1 + 2 were similar because their compositions and pH values are close to each other. In brine 3, the corrosion potential was more negative. A SEM study of the corroded specimens provided further informations (figure 33): As it can be seen on figure 33.1 which shows the microstructure of a non-corroded steel specimen, the microstructure of the studied material is composed of pearlite (black parts) and ferrite (white parts). SEM evaluations of the corroded specimens showed that corrosion in the three aerated salt brines had formed shallow pits (figure 33.2 to 7). Corrosion has occurred mainly at the sites of MnS inclusions, as shown in figures 33.3 to 4. Intergranular corrosion was found too. The corrosion rates of specimens immersed in brine 3 were smaller, as it can be seen on the pictures, due to the neutral pH.

Subsequently, the corrosion rates of the tested steel immersed in three different salt brines were measured in function of time under deaerated conditions. As shown in figure 34, the corrosion potentials became slowly more positive after their immersion in salt brines until they reached stabilization due to the formation of corrosion products on the steel surface. Free-corrosion potentials of -1073, -1034, -1157 mV vs the Hg/Hg₂SO₄ reference electrode were measured after one hour immersion at T = 55°C in brine 1, 2, 3 respectively.

5.2 Polarization behavior

Then, the polarization behavior of the fine-grained structural steel in deaerated salt brine was studied. In figure 35, the potentiodynamic polarization curve in Q-brine at 55°C is shown. A mean free corrosion potential of -1051 mV was found.

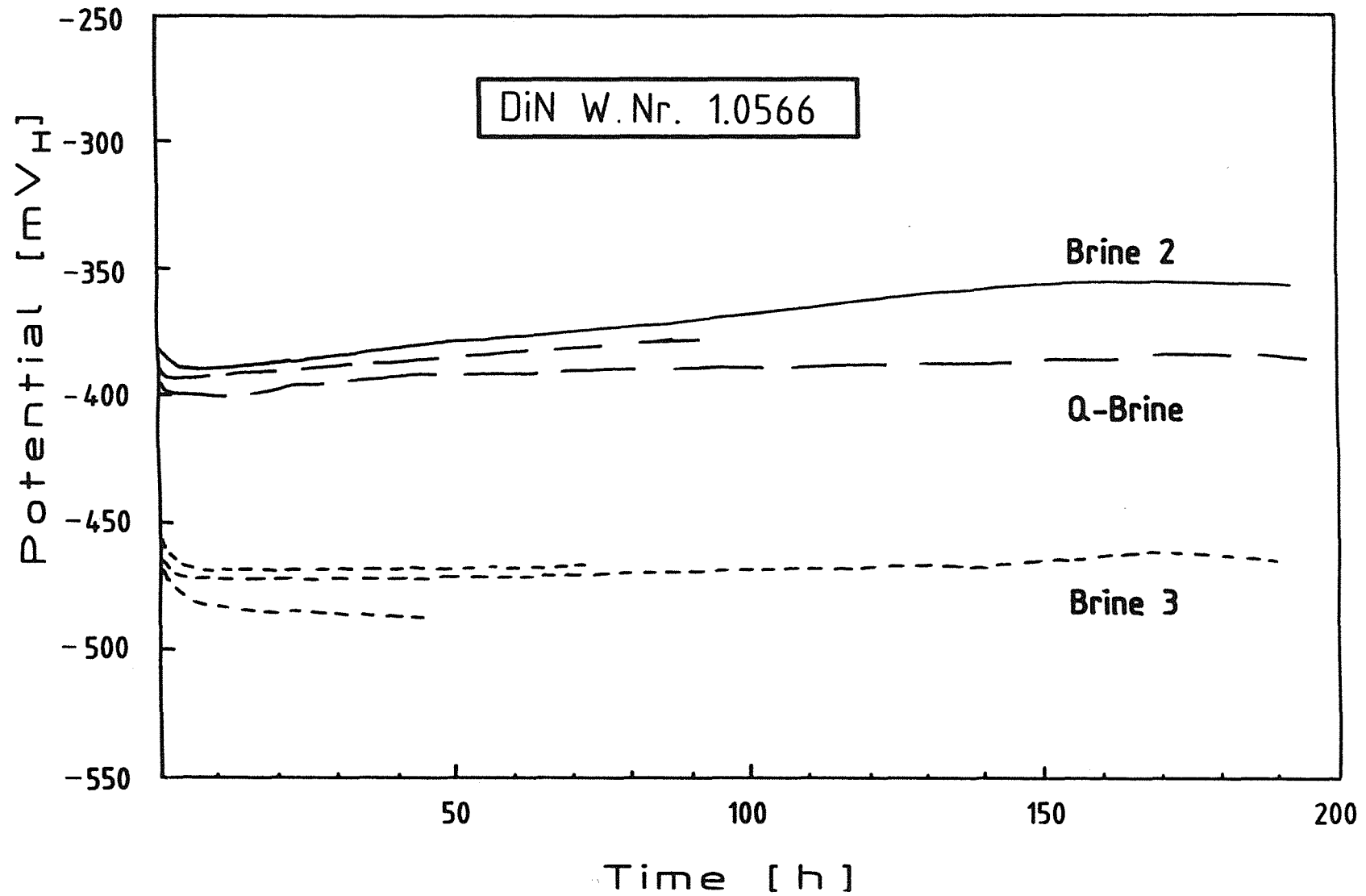


Fig. 32: Free corrosion potential of the steel DIN W.Nr. 1.0566 as function of time (55°C, no stirring, aerated)

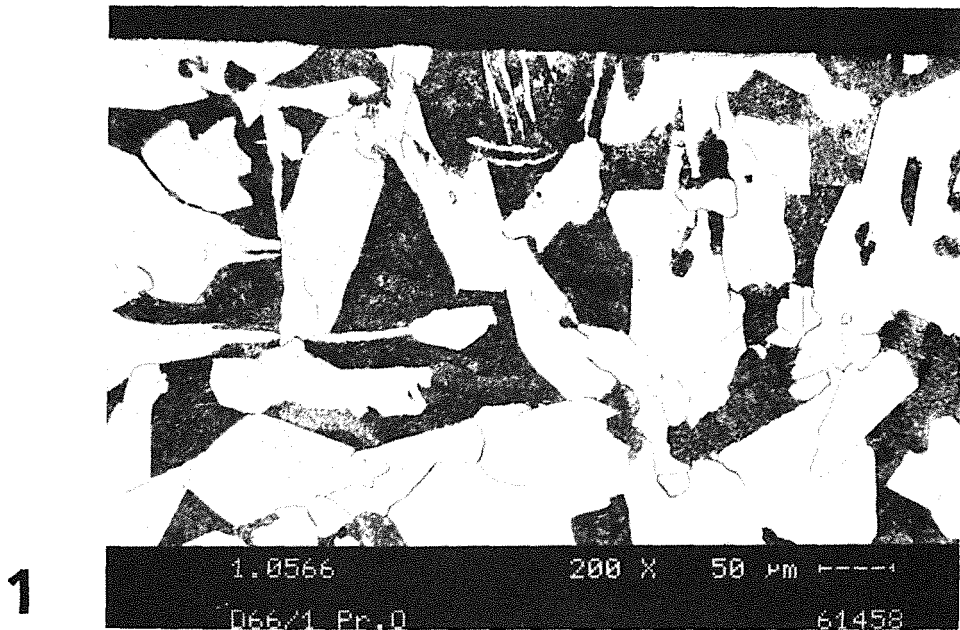


Fig. 33.1: Uncorroded Specimen of DIN W.Nr. 1.0566

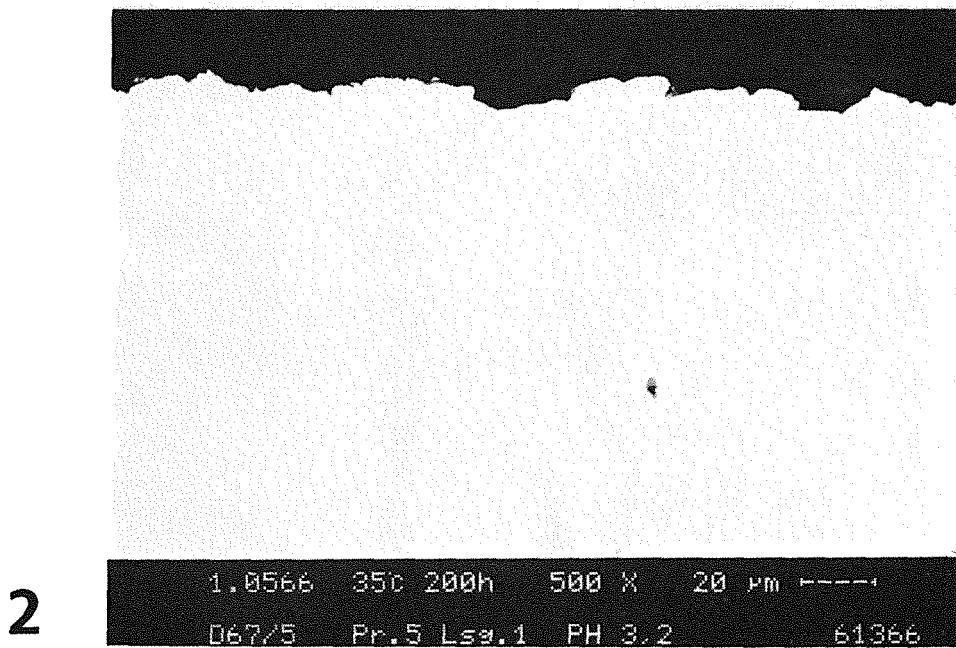
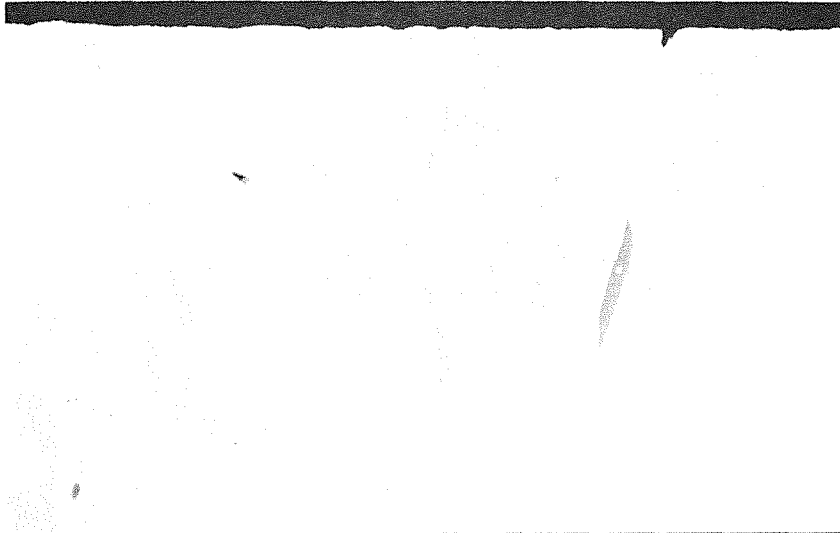
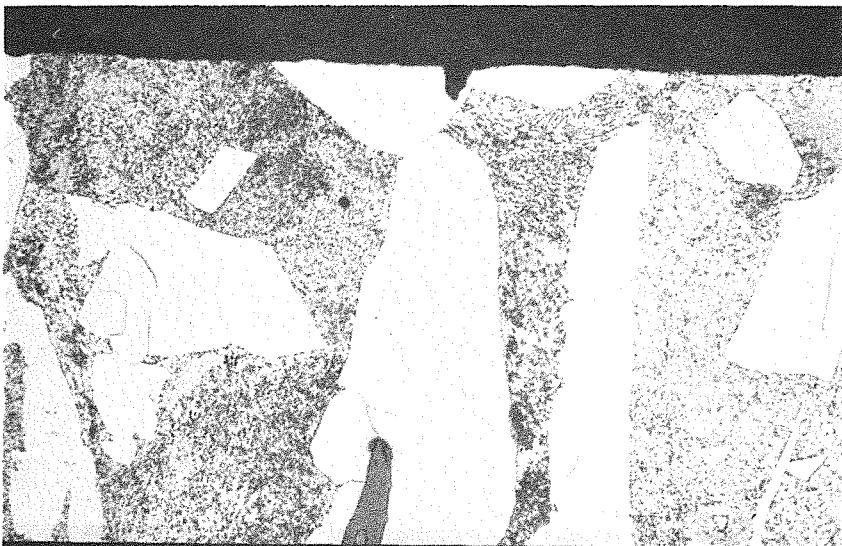


Fig. 33.2→7: Corroded Specimens of DIN W.Nr. 1.0566-
Sequence of informations as indicated on the
photographs: Temperature, Test Duration,
Magnification, Specimen No, Solution No, pH-
value)



3

7.0566 350 175h 200 X 50 µm F---
D67/6 Pr.6 Lsa.1 PH 5.5 61367



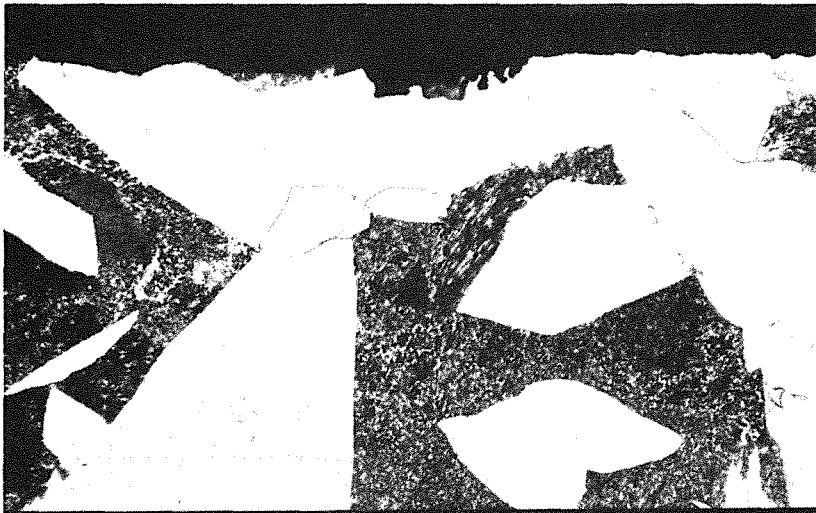
4

1.0566 350 175h 500 X 20 µm F---
D67/6 Lsa.1 PH 5.5 61443



5

1.0566 550 300h 500 X 20 μm -----
06777 Lsa.1 PH 4.2 61446



6

1.0566 550 350h 500 X 20 μm -----
06778 Lsa.2 PH 4.0 61451



7

1.0566 550 350h 500 X 20 μm -----
06779 Lsa.3 PH 7.1 61454

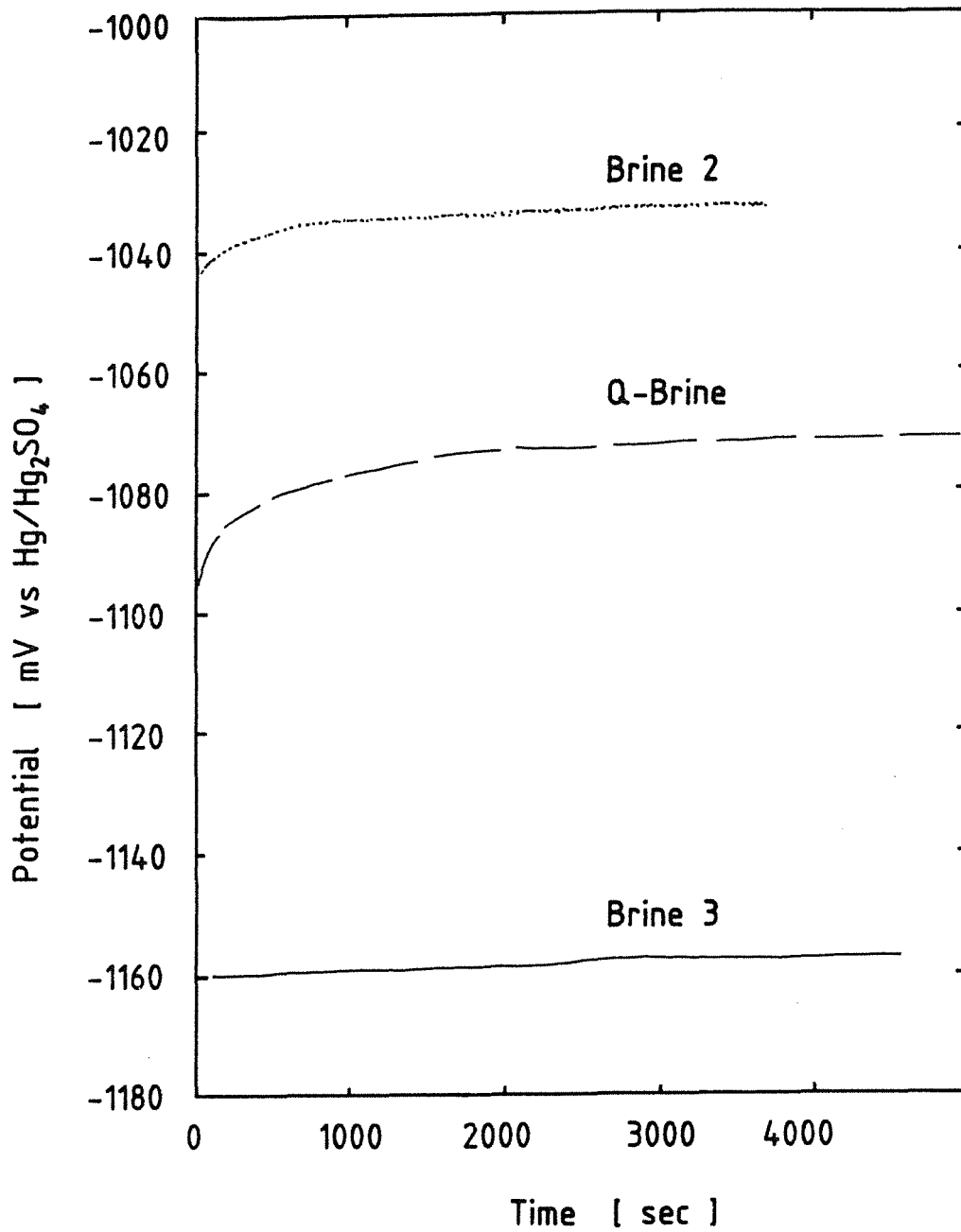


Fig. 34: Free corrosion potential as function of time of the fine-grained structural steel DIN W.Nr. 1.0566 in three salt brines at 55°C

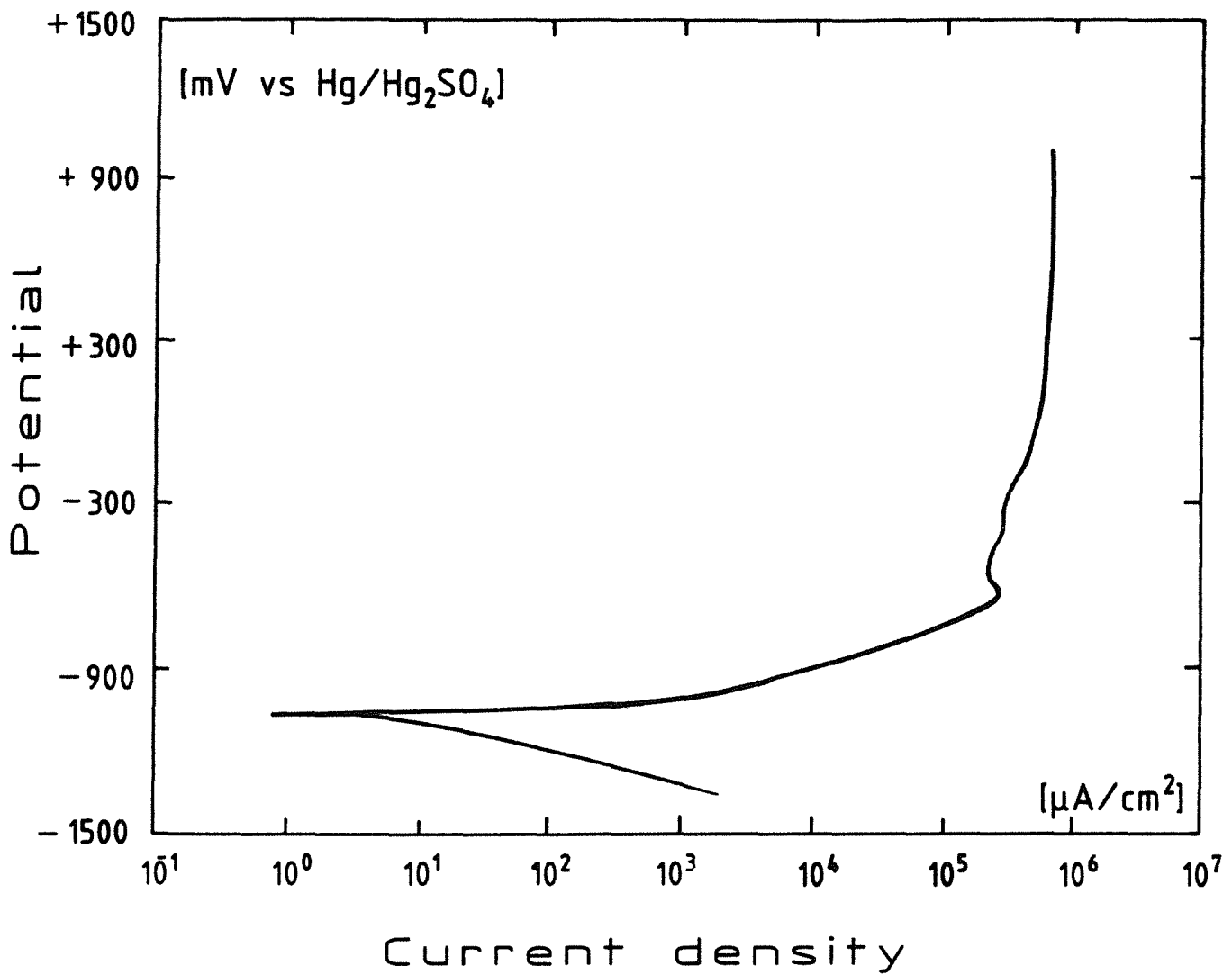


Fig. 35: Potentiodynamic polarization curve of the fine-grained structural steel DIN W.Nr. 1.0566 in Q-brine at 55°C, pH = 4.1

No passivity was observed at potentials from the corrosion potential to + 900 mV. The cathodic and anodic branches showed charge-transfer polarization. The corrosion rate was calculated by the Tafel Plot and the Polarization Resistance Plot methods. Reasonably good agreement was found. Results were compared with those published by Schmitt et al. (65) in table 12. Compared to our experimental results the difference can be related to the experimental procedure (stirring velocity, S/V ratio, gas environment, etc.). Full attention had to be paid to these parameters.

Table 12:

Results obtained with the low carbon steel 1.0566 in Q-Brine at T = 55°C, pH = 4.1 ± 0.1	Mean values	Mean values (Schmitt (65))
corrosion potential (mV vs Hg/Hg ₂ SO ₄)	- 1051 ± 15	- 1056 ± 20
anodic Tafel constant (V/dec)	0.035 ± 0.007	0.044 ± 0.023
cathodic Tafel constant (V/dec)	0.121 ± 0.009	0.125 ± 0.012
polarization resistance (KΩ/cm ²)	1.14 ± 0.63	3.45 ± 1.55
corrosion current density (μA/cm ²)	10.0 ± 7.5	4.8 ± 3.1
corrosion rate (mm/year)	0.12 ± 0.08	0.056 ± 0.037

5.3 Influence of Different Parameters on the Corrosion Behavior

5.3.1 Influence of Stirring Velocity

In order to check qualitatively the influence of the stirring velocity of the brine near the corroding metal surface on the corrosion behavior, polarization curves were measured in deaerated Q-brine at 55°C and pH = 4.1 (figure 36). It is shown that under the chosen experimental conditions, its influence on the polarization curve parameters and the corrosion rate is small. Similarly, Posey et al. (42) reported for a Type A212B carbon steel in deaerated 4 M NaCl solution between pH = 4 to 6 no significative dependence of stirring on the corrosion rate. As already shown by Kuo et al. (16) for anodic polarization of iron in concentrated chloride media, mass transport limited current levels are observed between -1000 and -800 mV versus Hg/Hg₂SO₄ reference electrode. The diffusion limiting species

can be the Fe^{2+} ions. The influence of the stirring velocity at $\text{pH} < 4$ will be tested in the near future.

5.3.2 Influence of Sampling Conditions

Samples were cut from the surface of each side of a metal plate. Under the same experimental conditions, polarization curves of these were registered. Corrosion results, as reported in figure 37, showed obviously no significant difference in the bulk structure of the metal samples.

5.3.3 Influence of Metal / Solution Interface

In figure 38, polarization curves measured at 55°C in the Q-Brine are presented. Results obtained by exposure of pre-corroded specimens differ from those in the as polished state (standard conditions) by small deformations of the cathodic and anodic branches of the polarization curves. Non-polished specimens showed no significant difference, since their surfaces were already smooth (figure 39). Two specimens were measured consecutively in the same solution (figure 38). During the second test, the solution contained a low concentration of corrosion products from the first test. The results showed a small influence on corrosion exerted by the low concentration of corrosion products in the brine. This can be correlated with the low values of the chosen experimental specimen surface to brine volume ratio (S/V : 0.0015 to 0.003 cm^{-1}).

5.3.4 Influence of Gaseous Environment

In figure 40, the polarization curves measured at 55°C and $\text{pH} = 4.1$ in inert gas, air, oxygen saturated Q-brines are presented. The differences observed between the curves are due to the fact that diffusion polarization prevails in the presence of oxygen, causing a change in the predominant mechanism of the cathodic reaction and an increase of the corrosion rates.

5.4 Influence of Temperature and Salt Brine Composition

Potentiodynamic polarization tests of the fine-grained structural steel were performed in three different salt brines at temperatures from 55 to 90°C . A set of anodic and cathodic polarization curves are shown in figures 41 to 44 for that steel. At 55°C free-corrosion potentials of about -1051 , -1025 , -1139 mV were

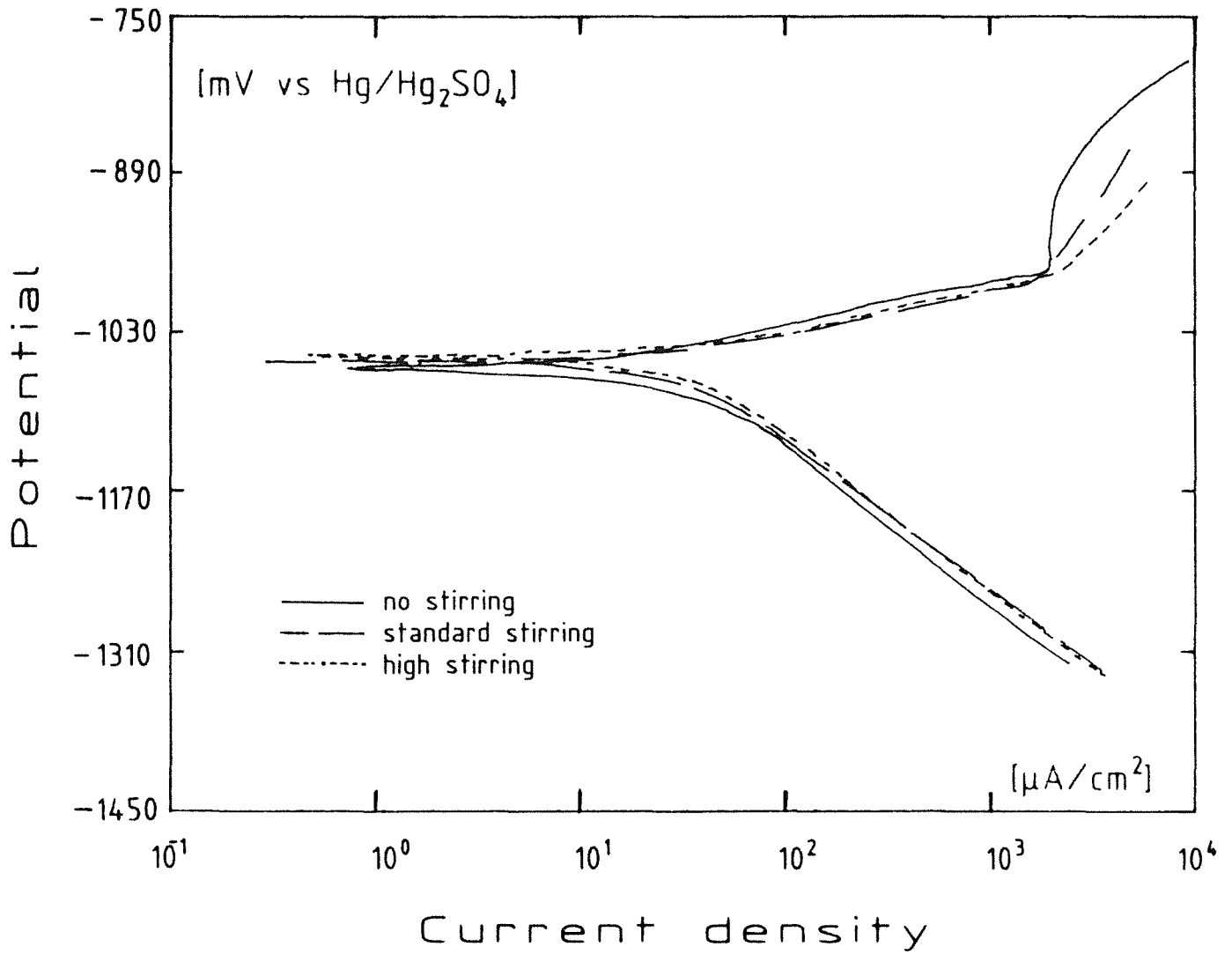


Fig. 36: Potentiodynamic polarization curve of the fine-grained structural steel DIN W.Nr. 1.0566 in Q-brine at 60°C, pH = 4.1. Influence of stirring.

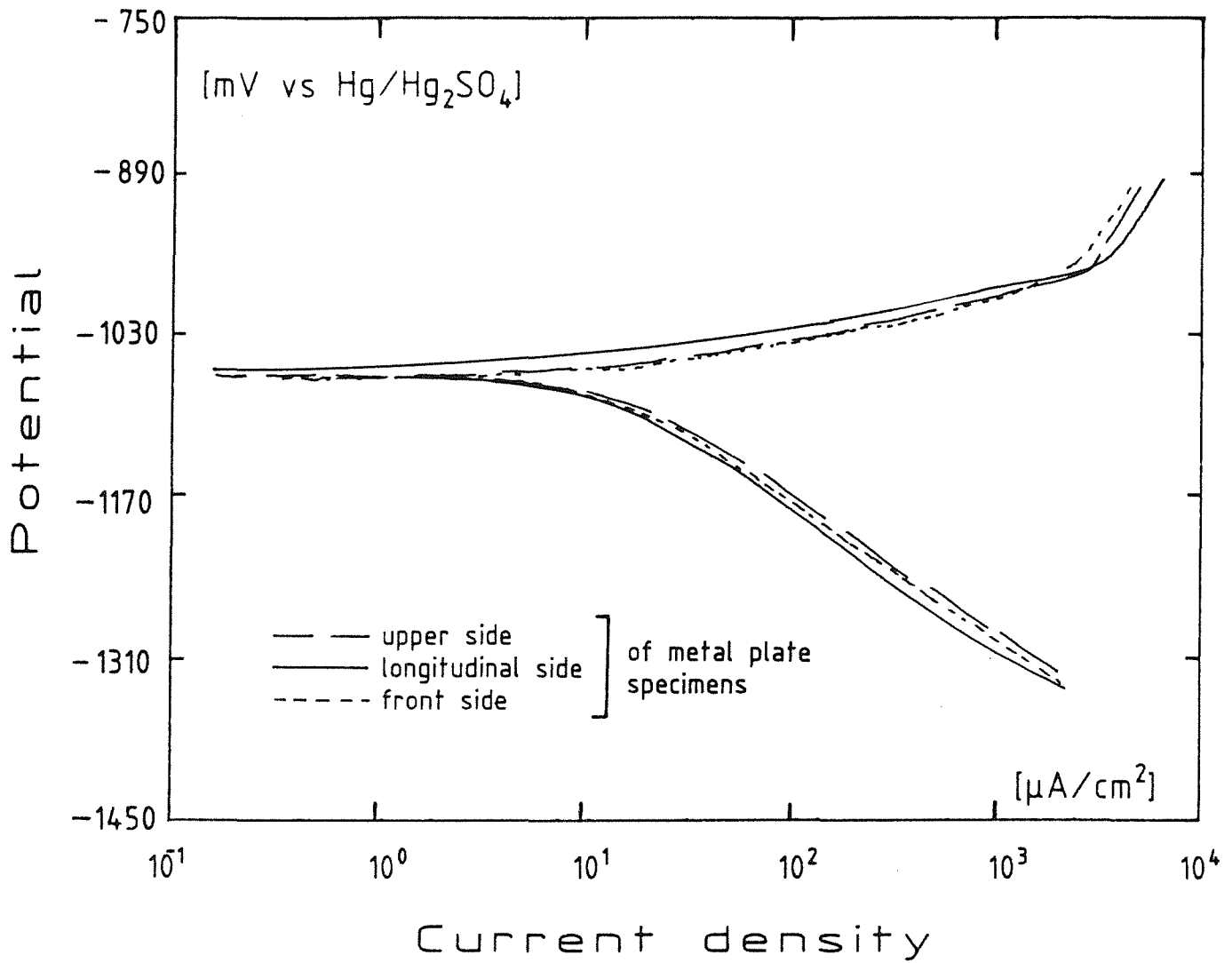


Fig. 37: Potentiodynamic polarization curve of the fine-grained structural steel DIN W.Nr. 1.0566 in deaerated Q-brine at 55°C, pH = 4.1 Influence of sampling.

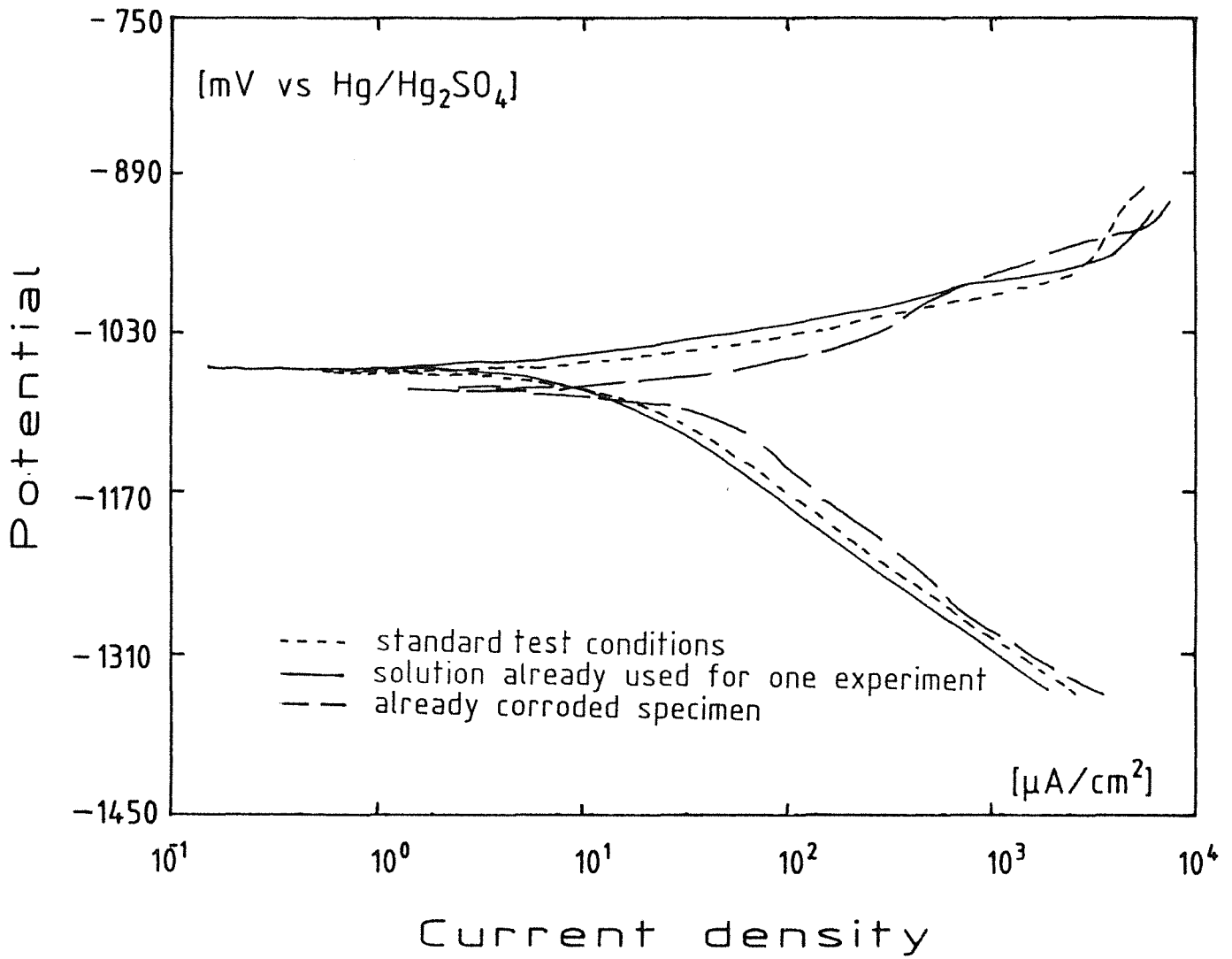


Fig. 38: Potentiodynamic polarization curve of the fine-grained structural steel DIN W.Nr. 1.0566 in deaerated Q-brine at 55°C, pH = 4.1. Influence of composition of solution and state of metal surface.

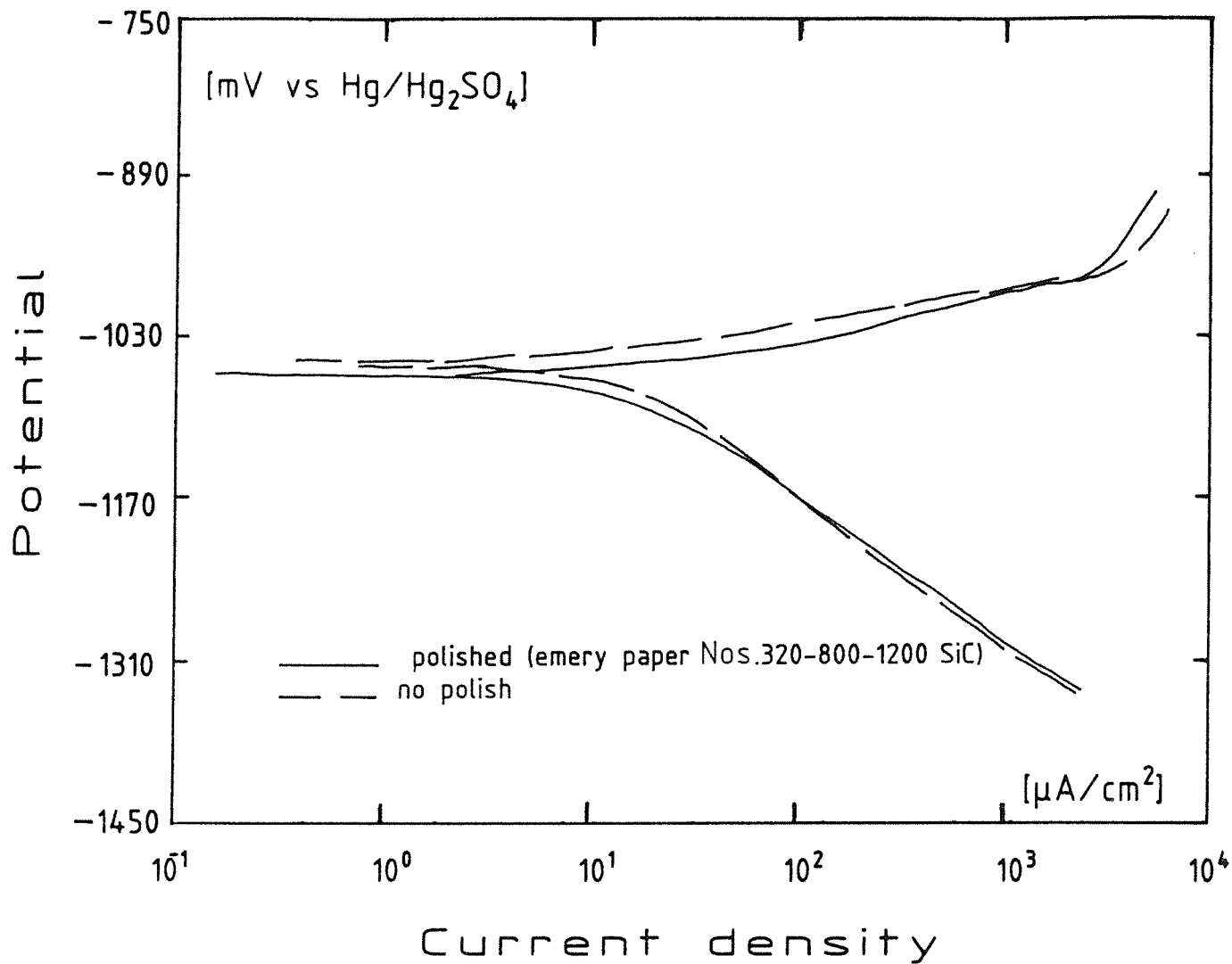


Fig. 39: Potentiodynamic polarization curve of the fine-grained structural steel DIN W.Nr. 1.0566 in deaerated Q-brine at 55°C, pH = 4.1. Influence of steel surface polish.

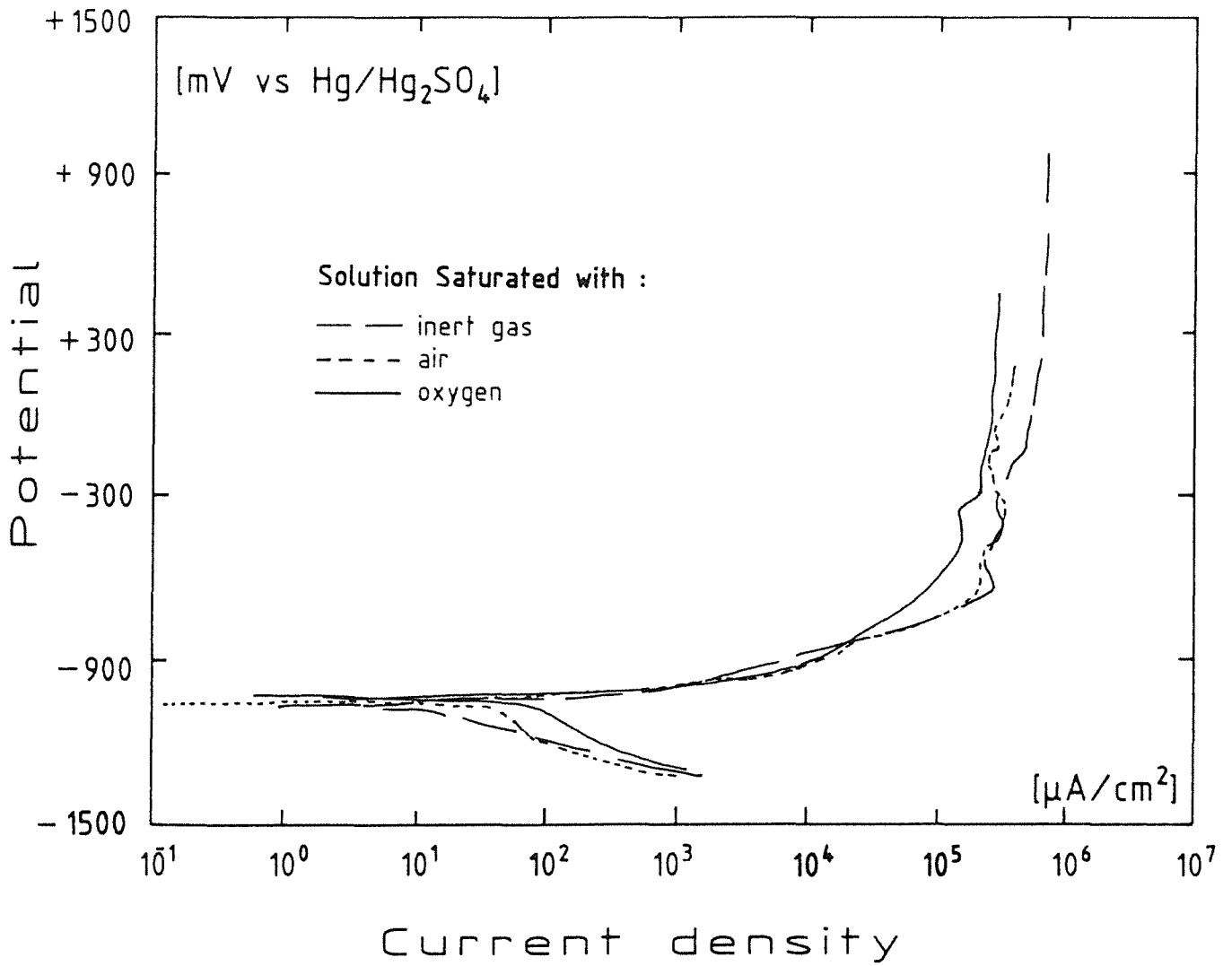


Fig. 40: Potentiodynamic polarization curve of the fine-grained structural steel DIN W.Nr. 1.0566 in Q-brine at 55°C, pH = 4.1. influence of dissolved oxygen content.

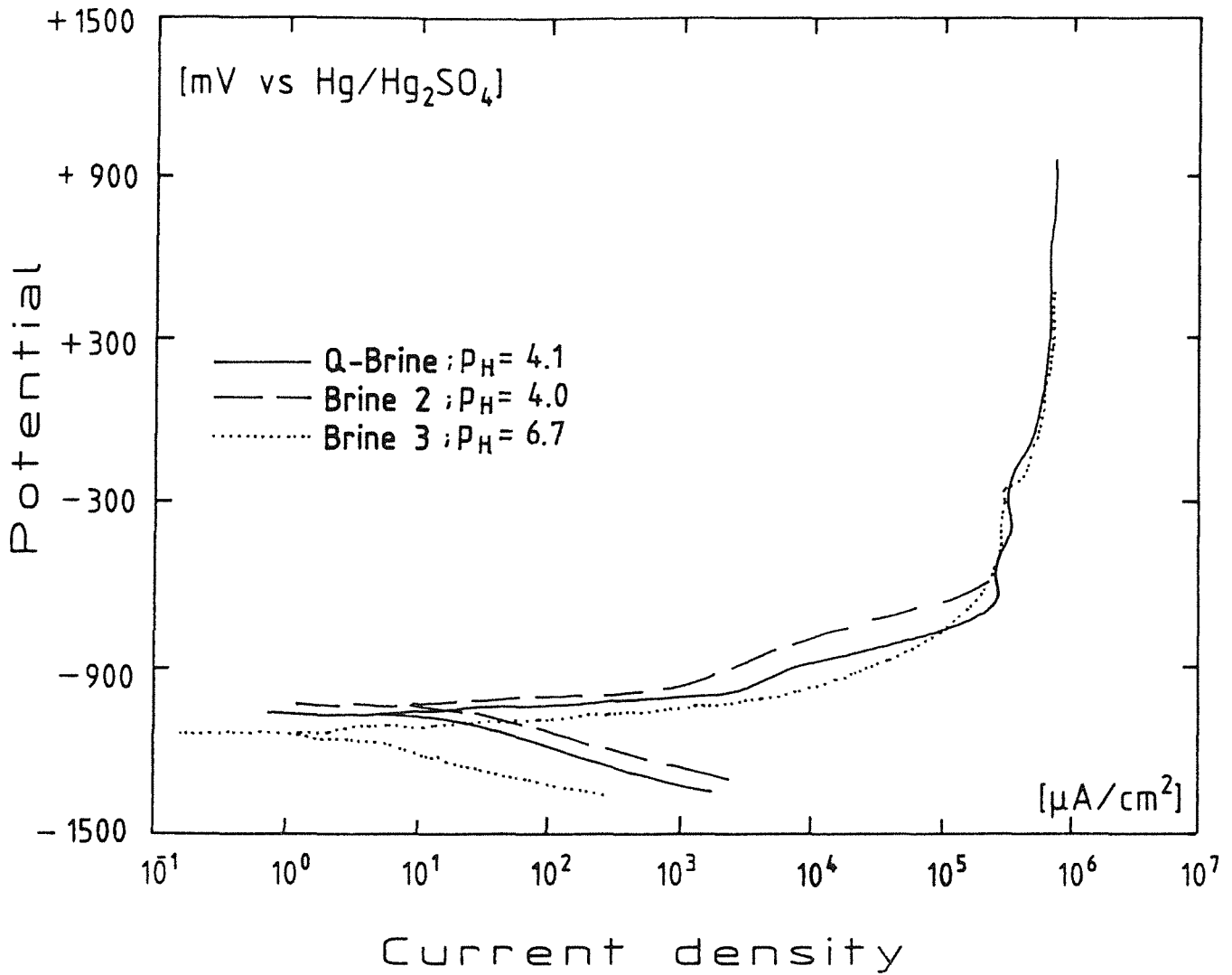


Fig. 41: Potentiodynamic polarization curve of the fine-grained structural steel DIN W.Nr. 1.0566 in the 3 different brines at 55°C. Influence of brine composition.

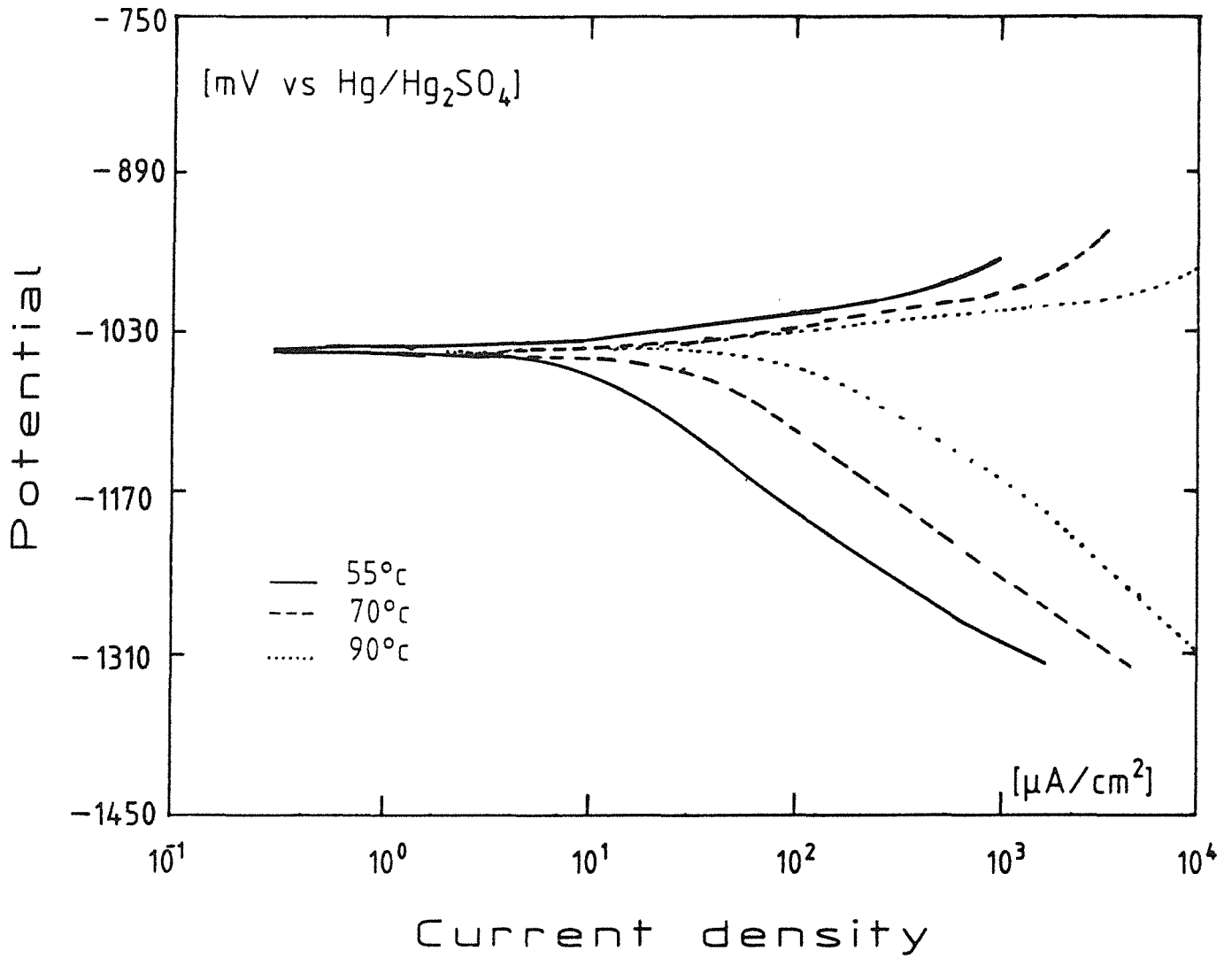


Fig. 42: Potentiodynamic polarization curve of the fine-grained structural steel DIN W.Nr. 1.0566 in deaerated Q-brine at 55-70-90°C. Influence of temperature.

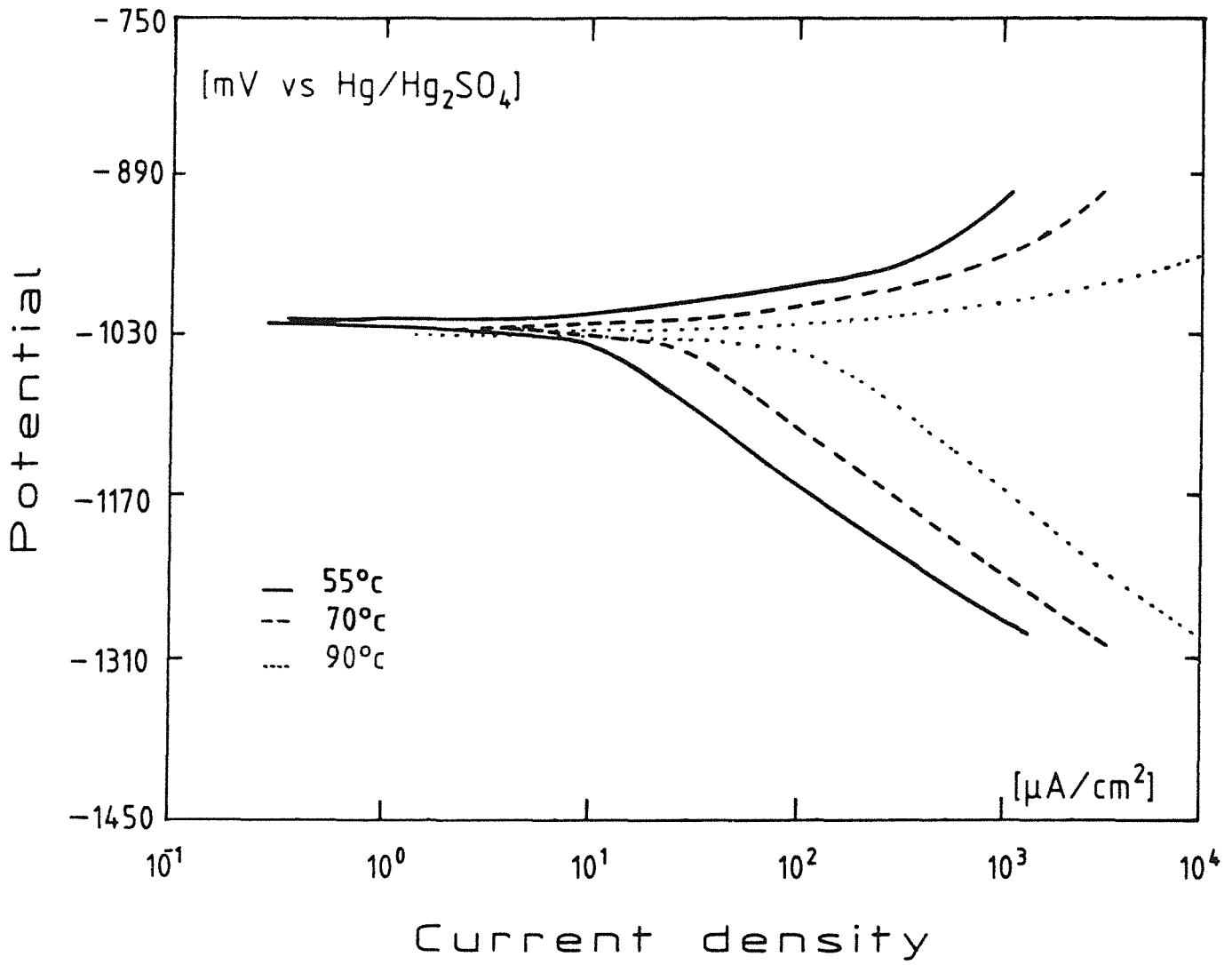


Fig. 43: Potentiodynamic polarization curve of the fine-grained structural steel DIN W.Nr. 1.0566 in deaerated brine 2 at 55-70-90°C. Influence of temperature.

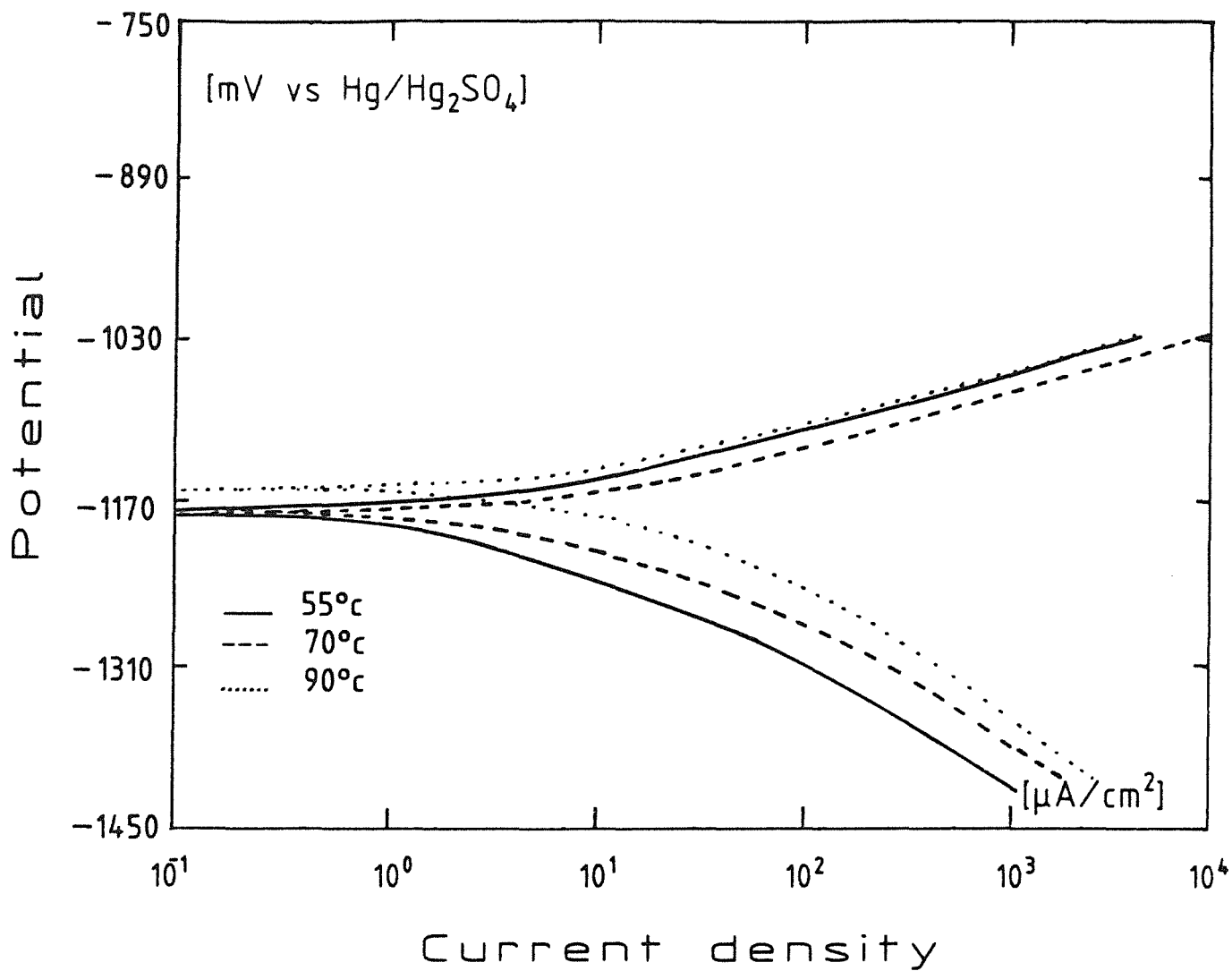


Fig. 44: Potentiodynamic polarization curve of the fine-grained structural steel DIN W.Nr. 1.0566 in deaerated brine 3 at 55-70-90°C. Influence of temperature.

obtained by the polarization method in the deaerated brine 1, 2, 3 respectively. These values differ from the others because of the applied polarization techniques. The measured free-corrosion potentials depend on experimental conditions, especially on the salt composition and concentration, besides the temperature of the salt brine and the state of the metal surface. In brine 1 and brine 2, the free-corrosion potentials are found similar. These two brines show a high content in $MgCl_2$. Their aggressivity is reinforced by the hydrolysis of $MgCl_2$ at the test temperature. Brine 3 is rich in $NaCl$ and has nearly a neutral pH (pH = 6.9). Temperature dependence of the free-corrosion potentials is not significant between 55 and 90°C, as shown by the results.

The reproductibility of the polarization tests was initially tested. A similar polarization behavior has always been observed. Especially active corrosion takes place in all tests - no passive range was detected. As shown in table 13, experimental results can vary from test to test and calculated corrosion current densities can differ to about a factor of 3. Consequently, each test was reproduced several times in order to determine mean values.

The results reported in table 13 were calculated by two methods: Tafel and Polarization Resistance Plot. Tafel Plot evaluation is effective in the potential ranges from +/-50 to +/-250 mV vs E_{corr} and Polarization Resistance Plot evaluation in the potential range +/-10 mV vs E_{corr} . In table 14, results obtained by these two methods are compared with those determined by the three-point method, developed by Barnartt et al. (66-67). A value of 30 mV was selected as potential difference ($E-E_{corr}$). Much more details about these methods have been given in part 4.3 of this report. Results have shown to be in good agreement. Each of the three methods can be applied for the determination of polarization parameters.

Finally, salt brine composition and temperature dependence of the polarization parameters in the three salt brine is summarized in table 15 and figure 45. Similar spontaneous corrosion rates: 0.12-0.15 mm/a at 55°C, 0.39-0.34 mm/a at 70°C, and 1.07-1.60 mm/a at 90°C were calculated for the exposure in the first two brines which are rich in $MgCl_2$. Brine 3, which is rich in $NaCl$, show lower spontaneous corrosion rates: 0.016 mm/a at 55°C, 0.033 at 70°C and 0.096 at 90°C.

The specimens have exhibited a similar polarization behavior from 55°C to 90°C in the three salt brines:

- All cathodic and anodic branches show under the applied experimental conditions charge-transfer polarization (taking-off or giving-off of electrons is rate-determining). No significative diffusion effect was observed.

Table 13: Results obtained by exposure of the fine-grained structural steel DIN W.Nr. 1.0566 in Q-Brine at different temperatures

Experimental Results as measured and/or calculated	Temperature [°C]					
	55		60		70	90
Corrosion Potential (mV vs Hg/Hg ₂ SO ₄)	-1041	-1066	-1047	-1052	-1048	-1039
	-1039	-1056	-1046	-1056		-1079
	-1042	-1066	-1060			-1074
	-1040	-1058	-1037			-1065
						-1060
Anodic Tafel Slope (mV/dec)	28	32	34	35	37	39
	38	35	36	36		37
	36	36	40			38
	36	41	34			35
						44
Cathodic Tafel Slope (mV/dec)	121	116	132	123	127	121
	127	115	120			118
	130	113	135	135		116
	128	121	116			114
						120
Polarization Resistance (kΩ/cm ²)	1.099	0.992	0.990	0.489	0.368	0.142
	1.034	1.770	0.561	0.728		0.113
	1.173	0.970	0.692			0.120
	1.034	1.080	0.511			0.233
						0.067
Corrosion Current Density (μA/cm ²)	8.1	10.5	10.0	22.1	33.4	95
	14.9	6.5	18.4	14.5		98
	10.8	11.1	16.0			102
	11.9	9.1	17.5			55
						110

Table 14: Results obtained by exposure of the fine-grained structural steel DIN W.Nr. 1.0566 in three different salt brines at 55°C (Evaluation performed by three methods).

Experimental Results as measured and/or calculated	Brine 1		Brine 2	Brine 3
<u>Tafel Plot Evaluation</u> Corrosion Potential (mV vs Hg/Hg ₂ SO ₄)	-1041 -1039 -1042 -1040	-1066 -1056 -1066 -1059	-1012 -1031 -1027	-1122 -1120 -1175
Anodic Tafel Slope (mV/dec)	28 38 36 36	32 35 36 31	30 30 40	43 42 42
Cathodic Tafel Slope (mV/dec)	121 127 130 128	116 115 113 121	126 114 122	88 112 83
Corrosion Current Density (μ A/cm ²)	7.4 17.5 11.1 12.0	10.0 6.5 10.0 9.5	7.7 12.0 13.5	0.8 1.7 1.9
<u>Polarization Resistance Plot</u> Polarization Resistance (k Ω /cm ²)	1.099 1.034 1.173 1.034	0.992 1.770 0.970 1.080	1.078 0.955 0.732	22.0 6.8 10.5
Corrosion Current Density (μ A/cm ²)	8.8 12.4 10.5 11.8	11.0 6.6 12.2 9.9	9.8 10.8 15.8	0.6 2.0 1.2
<u>3-Points Method</u> Corrosion Current Density (μ A/cm ²)	12.6 10.3 13.8 12.1	10.3 12.5 14.0 13.7	19.0 11.4 14.5	1.1 1.8

Table 15: Results obtained by exposure of the fine-grained structural steel DIN W.Nr. 1.0566 in three different salt brines in the temperature range 55-90°C (Mean Values)

Temperature [°C]	Brine 1	Brine 2	Brine 3
55	$E_{Corr} = -1051 \text{ mV vs. Hg/Hg SO}_4$ $b_a = 35 \text{ mV/dec}$ $b_c = 121 \text{ mV/dec}$ $R_p = 1.14 \text{ K}\Omega / \text{cm}^2$ $I_{Corr} = 10 \mu\text{A} / \text{cm}^2$ Corr.Rate = 0.12 mm/year	$E_{Corr} = -1023 \text{ mV vs. Hg /Hg}_2\text{SO}_4$ $b_a = 31 \text{ mV/dec}$ $b_c = 121 \text{ mV/dec}$ $R_p = 0.92 \text{ K}\Omega / \text{cm}^2$ $I_{Corr} = 13 \mu\text{A} / \text{cm}^2$ Corr.Rate = 0.15 mm/year	$E_{Corr} = -1139 \text{ mV vs. Hg /Hg}_2\text{SO}_4$ $b_a = 42 \text{ mV/dec}$ $b_c = 95 \text{ mV/dec}$ $R_p = 13.1 \text{ K}\Omega / \text{cm}^2$ $I_{Corr} = 1.4 \mu\text{A} / \text{cm}^2$ Corr.Rate = 0.016 mm/year
60	$E_{Corr} = -1050 \text{ mV vs. Hg/Hg SO}_4$ $b_a = 36 \text{ mV/dec}$ $b_c = 127 \text{ mV/dec}$ $R_p = 0.66 \text{ K}\Omega / \text{cm}^2$ $I_{Corr} = 16 \mu\text{A} / \text{cm}^2$ Corr.Rate = 0.19 mm/year	not measured	not measured
70	$E_{Corr} = -1048 \text{ mV vs. Hg/Hg SO}_4$ $b_a = 37 \text{ mV/dec}$ $b_c = 127 \text{ mV/dec}$ $R_p = 0.36 \text{ K}\Omega / \text{cm}^2$ $I_{Corr} = 33 \mu\text{A} / \text{cm}^2$ Corr.Rate = 0.39 mm/year	$E_{Corr} = -1030 \text{ mV vs. Hg/Hg SO}_4$ $b_a = 35 \text{ mV/dec}$ $b_c = 126 \text{ mV/dec}$ $R_p = 0.40 \text{ K}\Omega / \text{cm}^2$ $I_{Corr} = 30 \mu\text{A} / \text{cm}^2$ Corr.Rate = 0.34 mm/year	$E_{Corr} = -1177 \text{ mV vs. Hg/Hg SO}_4$ $b_a = 46 \text{ mV/dec}$ $b_c = 97 \text{ mV/dec}$ $R_p = 4.81 \text{ K}\Omega / \text{cm}^2$ $I_{Corr} = 2.9 \mu\text{A} / \text{cm}^2$ Corr.Rate = 0.033 mm/year
90	$E_{Corr} = -1063 \text{ mV vs. Hg/Hg SO}_4$ $b_a = 38 \text{ mV/dec}$ $b_c = 118 \text{ mV/dec}$ $R_p = 0.14 \text{ K}\Omega / \text{cm}^2$ $I_{Corr} = 92 \mu\text{A} / \text{cm}^2$ Corr.Rate = 1.07 mm/year	$E_{Corr} = -1030 \text{ mV vs. Hg/Hg SO}_4$ $b_a = 35 \text{ mV/dec}$ $b_c = 140 \text{ mV/dec}$ $R_p = 0.09 \text{ K}\Omega / \text{cm}^2$ $I_{Corr} = 138 \mu\text{A} / \text{cm}^2$ Corr.Rate = 1.60 mm/year	$E_{Corr} = -1155 \text{ mV vs. Hg/Hg SO}_4$ $b_a = 43 \text{ mV/dec}$ $b_c = 103 \text{ mV/dec}$ $R_p = 1.80 \text{ K}\Omega / \text{cm}^2$ $I_{Corr} = 8.3 \mu\text{A} / \text{cm}^2$ Corr.Rate = 0.096 mm/year

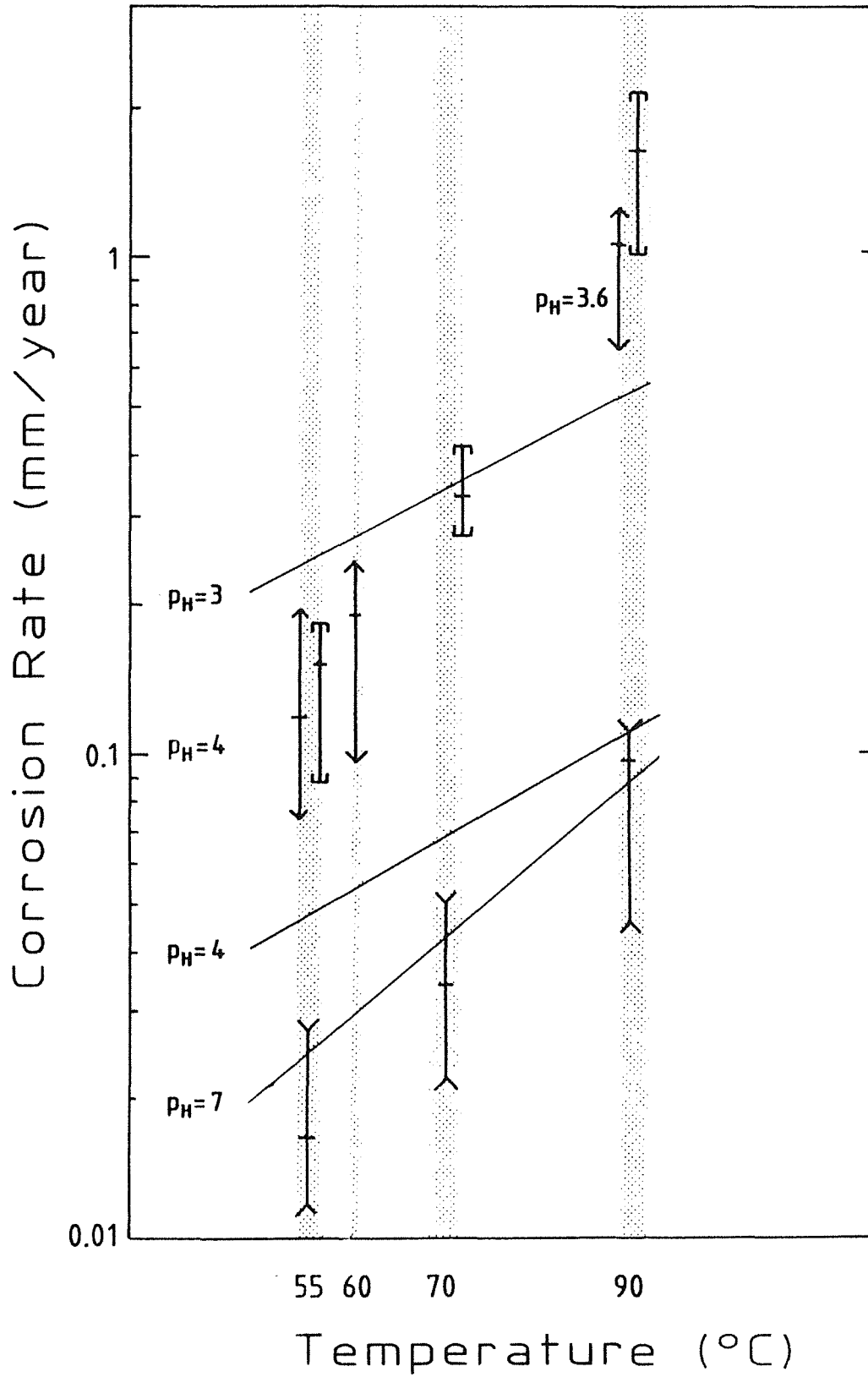


Fig. 45: Temperature dependence of corrosion rates of the fine-grained structural steel DIN W.Nr. 1.0566 in three different salt brines

- ↔ : Brine 1 (Q-Brine)
- ⌈⌋ : Brine 2
- ⌋⌈ : Brine 3
- ⊕ : Mean values
- : Results of Posey et al. (42)

- At the chosen pH-values (4 to 7), cathodic reactions are governed mainly by the reduction of water in molecular hydrogen. Anodic reactions consist in the oxidation of iron to Fe^{2+} .
- Active corrosion took place. No passivity of the specimens could be obtained in these aggressive environments: The formation of chloride complexes prevent the existence of really protective passive films on the surface of the steel. Consequently, no severe pitting corrosion was observed by post-test examination of the specimens. Corrosion has formed shallow pits on the surface of the samples.

5.5 Discussion

5.5.1 Experimental Results

In figure 45, broad scatter bands of results are obtained when the whole number of tests are taken into consideration. More experiments are not recommendable to increase the accuracy neither of the experiment procedure nor of the calculated average values. The reason for that was already mentioned: The complexity of a forced active metal dissolution leading to oxide layer formation caused by anodic and at least two possible cathodic processes which are highly sensitive to mass and charge transfer, boundary layer and bulk solution conditions. Another point to mention are the dimensions of the sample (surface area: 0.79 and 1.54 cm²). Since they are small, inhomogeneities of the metal surface can lead by general corrosion to much more fluctuations of metal dissolution e.g. corrosion rate results. That was indicated by the fluctuations of the corrosion potentials before the potentiodynamic experiments were started. Furthermore, low variations can be due to the sum of small differences in the experimental conditions as exemplified already for sampling conditions of the specimens or stirring of the brine.

The calculated broad scatter bands of results give - considering the calculated average values - a valuable indication of the parameter influences (temperature, salt brine composition) on steel corrosion. It was shown in figure 45 that the corrosion rates increase between 55°C and 90°C for each brine by a factor of 6 to 11. Furthermore the corrosion rates are found much higher in salt brines containing MgCl_2 (brine 1 and 2), principally due to the additional hydrolysis effect of MgCl_2 . The hydrolysis in these two simulated repository brines causes the acidification at higher temperatures which influences the corrosion mechanisms and the protective nature of the corrosion products (magnetite,

amakinite). For example, the pH of the Q-brine was found to decrease between 55 and 90°C from 4.1 to 3.6: This variation of the environment may cause a change of the corrosion process and rate at $\text{pH} < 4$. It is known that at $\text{pH} > 4$, the cathodic process is mainly the reduction of water to form molecular hydrogen. In moderately acidic brines ($\text{pH} = 2-3$), the cathodic process principally consists of hydrogen evolution from hydrogen ions.

5.5.2 Comparison with Results in the Literature

Schmitt et al. (figure 13) studied also by the potentiodynamic polarization method the corrosion of the fine-grained structural steel DIN W.Nr. 1.566 in the Q-brine between 55 and 90°C. Some difference in their experimental conditions compared to ours are reported: For example no stirring of the aerated solutions was done and before any potentiodynamic polarization was started, pretest time periods of 8 to 12 hours of specimen immersion at the corrosion potential were chosen. They reported lower mean values (factor 2), the broad scatter band however is partly in agreement with our results. These differences can be related to the already mentioned variations in the experimental conditions.

In figure 45, our results are compared to those of Posey and Palko (figure 8) obtained in deaerated 4 m NaCl as function of pH by the potentiodynamic polarization method. Results calculated for brine 3, which is rich in NaCl (table 3) can be easily compared to Posey results at $\text{pH} = 7$. Results show a good agreement. Results from brines 1 and 2, which show a more acidic pH, can be compared to those measured in 4 m NaCl at $\text{pH} = 3$ and $\text{pH} = 4$. The temperature dependence on the spontaneous corrosion rates was found to be higher in the brines 1 and 2 due to the MgCl_2 hydrolysis.

Finally, it must be stated also that the corrosion rates measured and calculated by polarization techniques differ from those of long-time immersion techniques. For example, Smailos (figure 10) reported corrosion rates of 30-40 $\mu\text{m/a}$ for the same fine-grained structural steel in the same Q-brine at 90°C but without stirring and with a another specimen surface to medium volume (S/V) of 0.2 cm^{-1} . Some reasons can be given to explain these differences:

- Lower surface to volume ratio (S/V of 8×10^{-4} to 4×10^{-3}) and stirring of the solution were applied for polarization measurements. It induces higher mass transport of the ferrous ions as corrosion product from the steel surface. Furthermore, the content of H^+ and of soluble corrosion products are more important in larger volumes.

- Immersion tests were performed in a closed system and polarization measurements in an open cell saturated with nitrogen.
- An important point to mention is that, as it can be seen from figure 10, corrosion rates decreased in function of exposure time, partly due to the formation of semi-protective layers of corrosion products.

On the contrary, polarization measurements give always the instantaneous state of the surface corrosion (spontaneous corrosion rate) and a pessimistic view on maximum corrosion by metal dissolution. So, the corrosion rates determined by the applied two techniques have to be understood according to their experimental boundary conditions.

5.5.3 Recommendation for Further Studies

The overall view on our work in respect to the "state of art" in the literature are summarized in table 16. The parameters are divided into three categories: metallurgical aspects, environmental and external parameters (variables).

In spite of the fact that many other data on the corrosion of low-carbon steels are still available from literature (as shown in table 16), electrochemical tests will be continued because

- they permit within an accelerated procedure to select the most important parameters in respect to their influence on corrosion rate and can serve vice-versa as reference basis for further long-time immersion testing. The measured values reflect the instantaneous corrosion rate of the tested steel,
- they provide additional information on the corrosion mechanisms because the cathodic and anodic processes are measured separately by polarization,
- the conditions under which passive behavior as well as local corrosion occur can be easily determined.

In addition to a systematic study of all parameters, listed in table 16, the further electrochemical studies will focus on the influence of

- the brine composition, especially the presence of salt impurities and the simulation of oxidizing radiolytic products,
- the metal surface state (study of corroded or passivated specimens),
- high temperatures ($T = 100$ to 250°C) which require electrochemical measurements in autoclaves. Doing that, special care has to be taken because of the aggressivity of the media and the use of special reference electrodes.

Table 16: Parameter Effects on Steel Corrosion

Variables	Effects on Corrosion		
	Literature Data	Short Notice	Experimental Results
<u>Metallurgical Variables</u>			
Variation of Metal Composition	weak	(+)	to be tested
Surface Area to Volume Ratio	variable	(+)	
Specimen Shape	open		
Surface Condition	open		
Surface Structure	local (presence of inclusions, dislocations)	(+)	
Weldments	weak	(+)	corrosion attack begins at inclusion sites intergranular corrosion
Sampling	weak	(+)	to be tested no significant effect
<u>Brine Variables</u>			
Brine Composition	important especially for (Cl ⁻) content	+	important especially in MgCl ₂ -containing brines
p _H	strong at p _H < 4	+	to be tested
Oxygen Content	modifies the cathodic process, induces pitting corrosion	+	modifies the cathodic process at p _H > 4 but no pitting corrosion
Brine Impurities	F ⁻ , Br ⁻ , I ⁻ , S ²⁻ ... can affect the corrosion behavior	(+)	to be tested
Brine Concentrations	weak	(+)	
Hydrogen Partial Pressure	important		
<u>External Variables</u>			
Temperature	important since thermally activated process	+	important as measured between 55 and 90°
Pressure	weak	(+)	to be tested
Brine Flow Velocity	important at p _H < 4 or in presence of oxygen (diffusion process)	+	no influence in deaerated Q-brine at p _H = 4
Interphase Steel/Brine	important when films or corrosion product layers present	+	important for pre-corroded specimens
Scan Rate	important at high scan rate	+	weak
Gamma Radiation	no noticeable influence at γ-dose rates of 1 and 100 Gy/h	(+)	at scan rate < 0.5 mV/s simulation tests of the presence of radiolytic products

+ : Strong effect
 (+) : Low or moderate effect
 : Not yet defined (tested)

6. Conclusions

The experimental results show that electrochemical methods can be successfully applied to study the corrosion of the fine-grained structural steel DIN W.Nr. 1.0566 in salt brines. Potentiodynamic polarization testing can be recommended as a suitable technique and a fast method to determine the influence of several parameters on metal corrosion. Literature results could be reproduced or at least directly related to our new results which now have been reported after tests under varying experimental conditions. The following statements from electrochemical tests - conducted in three different salt brines (brine 1, 2, 3) between 55 and 90°C - can be made:

- At 55°C for the brines 1, 2, 3 respectively, free corrosion potentials of -1051, -1025, -1139 mV vs the Hg/Hg₂SO₄ reference electrode (mean values) were measured by potentiodynamic polarization.
- The corresponding spontaneous corrosion rates (mm/a) were calculated to be within a range of 0,02-0,15 (55°C), 0,03-0,4 (70°C) and 0,1-1,6 (90°C), and proved to be highly dependent on MgCl₂ content (hydrolysis).
- Active metal corrosion, but no passivity and no pitting corrosion, was observed under all test conditions. Generally shallow pits were formed on the steel surface.
- Corrosion mechanisms in the three salt brines were found to be similar. Cathodic and anodic processes were governed by charge-transfer polarization. No significative diffusion process was observed. As cathodic reaction mainly the reduction of water forming molecular hydrogen, as anodic reaction the oxidation of iron to Fe²⁺ are assumed. If the pH of the brines becomes more acidic (pH = 2.3), the cathodic process may change to hydrogen evolution originating from the reduction of hydrogen ions.
- There is experimental evidence that the parameters temperature, pH, brine composition, oxygen content, metal surface state have much influence on the corrosion rate. Further experiments will focus on the influence of pH, S/V ratio, brine impurities and others.

References

- (1) Marsh G.P. et al.
EUR-10163, 314-330 (1986)
- (2) Smailos E., Schwarzkopf W., Köster R.
KfK 4426 (1988)
- (3) Natalie C.A.
BMI/ONWI/C--176 (1987)
- (4) Gellings P.J.
in "Introduction to Corrosion Prevention and Control for Engineers",
Delft University Press (1976)
- (5) Heusler K.E.
"Influence of Temperature and Pressure on the Kinetics of Electrode
Processes", in "High Temperature High Pressure Electrochemistry in
Aqueous Solutions", p 387, NACE-4 (1973)
- (6) Westermann R.E., Haberman J.H., Pitman S.G., Pool K.H., Rhoads K.C.,
Telander M.R.
PNL/SRP-6221 (1988)
- (7) Kesavan S., Mozhi T.A., Wilde B.E.
Corrosion NACE, 45 (3): 213-215 (1989)
- (8) Diercks D.R., Soppet W.K., Kassner T.F. et al.
ANL-IWPM-4/87 (1987)
- (9) Verink E.D.
Corrosion NACE, 38(6):336-347 (1982)
- (10) Kruger J., Rhyne K.
Nuclear and Chemical Waste Management, 3:205 (1982)
- (11) Strehblow H.H.
Werkst. Korros., 35:437 (1984)

- (12) Szklarska-Smialowska Z.
Pitting Corrosion of Metals, NACE (1986)
- (13) Reimus P.W.
PNL/SRP-6662 (1987)
- (14) Heusler K.E., Fischer L.
Werkst. Korros., 27:551 (1976)
- (15) Hoar T.P., Jacob W.R.
Nature 216:1299 (1967)
- (16) Foley R.T., Trzaskoma P.P.
In Passivity of Metals, ed. R.P. Frankenthal and J. Krüger, p. 337,
The Electrochemical Society Princeton (1978)
- (17) Pryor M.J.
In "Localized Corrosion", ed. R.W. Staehle et al., p. 2, NACE (1974)
- (18) Hoar T.P.
Corros. Sci., 7:341 (1967)
- (19) Sato N.
Electrochim. Acta, 16:1693 (1971)
- (20) Vetter K.J., Strehblow H.H.
In "Localized Corrosion", ed. R.W. Staehle et al., p. 240, NACE (1974)
- (21) Galvele J.R.
In "Passivity of Metals", ed. R.P. Frankenthal and J. Kruger, p. 337,
The Electrochemical Society Princeton (1978)
- (22) Kolotyркиn Y.M.
Corrosion, 19:261t (1963)
- (23) Wallwork G.R., Harris B.
in "Localized Corrosion", NACE-3, NACE, p. 292 (1974)

- (24) Kruger J.
J. Electrochem. Soc., 106:376 (1959)
- (25) Ives M.B., Srivastava S.C.
Corrosion, 43 (11):687-692 (1987)
- (26) Marsh G.P., Taylor K.J.
Corros. Sci., 28 (3):289-320 (1988)
- (27) Schwenk W.
Werkst. Korros., 19:741 (1968)
- (28) Marsh G.P., Taylor K.J., Sharland S.M., Tasker P.W.
Mat. Res. Soc. Symp. Proc., 84:227-238 (1987)
- (29) Wrangler G.
Corrosi. Sci., 14:331 (1974)
- (30) Reimus P.W.
PNL/SRP - - 6661 (1988)
- (31) Heitz E., Zur Megede D.
Technical Report 82-08, DECHEMA Frankfurt (1982)
- (32) Constantinescu E., Heitz E.
Corr. Sci. 16, 857 (1967)
- (33) Simpson J.P., Knecht B.
Proc. Intern. Sem. Radioactive Waste Products
Suitability for Final Disposal 10-13.6.1985 KFA Jülich, p 445
- (34) Marsh G.P., Harker A.H., Taylor K.J.
DOE/RW/97.074 AFRE-R 12510 (1987)
- (35) Marsh G.P., Bland I.D., Taylor K.J.
Br. Corros. J., 23(3):157164 (1988)

- (36) Marsh G.P., Taylor K.J., Sooi Z.
SKB Technical Report 88-09
Swedish Nuclear Fuel and Waste Management Co, Stockholm (1988)

- (37) Beavers J.A., Thompson N.G., Markworth A.J., Cialone H.J.,
Majundar B.S., McKoy J.K.
NUREG/CR--4955, Battelle Columbus Division, Columbus (USA) (1987)

- (38) Bakta P., Solomon A.
"Pitting Corrosion of Low-Carbon Steel - Nuclear Waste Canisters"
International NACE Conference on Localized Corrosion, Orlando,
June 1987

- (39) Heitz E., Manner R.
Werkst. Korros., 29:783-791 (1978)

- (40) Field P.
Corrosion, 8:123-136 (1950)

- (41) Chandler K.A., Bayliss D.A.
"Corrosion Protection of Steel and Structures"
Elsevier, London, p. 22 (1985)

- (42) Posey F.A., Palko A.A.
Corrosion NACE, 35(1):38-42 (1979)

- (43) Nachman J.F., Duffy E.R.
Corrosion, 30 (19), 357-365 (1974)

- (44) Lanza F., Manaktala H., Ronsecco C.
EUR-8586-EN (1983)

- (45) Fink F.W., White E.L., Boyd W.K., Gillamand W., Coley F.H.
Battelle Mem. Inst., OSW-PR-225 (1966)

- (46) Behrens H.C., Osborn O., Rice L., Schreiber C.F., Webb B.P.
W76-03146, OWRT/S-76/11 (1975)

- (47) Grauer R.
EIR-Report No. 523 (1974)
- (48) Alexander B.J., Foley R.T.
Corrosion 31, 148 (1975)
- (49) Goldberg A., Owen L.B.
Corrosion NACE, 35(3): 114-124 (1979)
- (50) Cramer S.D., Carter J.P.
ASTM/STP-717, 113-141 (1980)
- (51) Westerman R.E., Haberman J.H., Pitman S.G., Pool K.H., Rhoads K.C.,
Telander M.R.
PNL/SRP-6221 (1988)
- (52) Westerman R.E., Haberman J.H., Pitman S.G., Pulsipher B.A., Sigalla L.A.
PNL-5426 (1986)
- (53) Pulsipher B.A.
PNL/SRP-6637 (1988)
- (54) Griess J.C.
ORNL/TM-8351 (1982)
- (55) Molecke M.A., Ruppen J.A., Diegle R.B.
Nucl. Techn., 63:476-506 (1983)
- (56) Pool K.H., Frydrych D.J.
Milestone Letter Report - Status of Electrochemical Studies
Pacific Northwest Laboratory (1987)
- (57) Marsh G.P., Pinard-Legry G., Smailos E., Casteels F., Vu Quang K.,
Cripps J., Haijink B.
EUR-10163 (1986)
- (58) Smailos E., Schwarzkopf W., Köster R., Fiehn B., Halm G.
KfK-Report 4723 (1990)

- (59) Smailos E., Schwarzkopf W., Köster R., Gruenthaler K.H.
"Advanced Corrosion Studies on Selected Packaging Materials for Disposal of HLW Canisters in Rock Salt",
Proc. of Waste Management '88, Vol. 2, p. 985, Tucson, Arizona, USA (1988)

- (60) Smailos E., Schwarzkopf W., Köster R., Fiehn B.
KfK 4529 (1989)

- (61) Smailos E., Köster R.
IAEA-TECDOC-421, 7-24 (1987)

- (62) Heusler K.E., Gassen R.
Werkst. Korros., 38:12-19 (1987)

- (63) Heusler K.E.
personal communication, Technical University Clausthal, Germany (1990)

- (64) Manfredi C., Mozhi R.A., Wilde B.E.
Corrosion NACE, 45(2):172 (1989)

- (65) Schmitt R.E., Canadillas F., Köster R.
KfK 3729 (1984)

- (66) Barnartt S.
Electrochim. Acta, 15:1313-1324 (1970)

- (67) Barnartt S.
Corrosion NACE, Ed. R. Baboian: 1-10 (1977)

- (68) Bort H., Wolf I., Leistikow S.
J. Nucl. Mater., 149(2): 132-137 (1987)

- (69) Schwenk W.
Werkst. Korros., 15:741-749 (1968)

- (70) Felloni L.
Corros. Sci., 8:133-148 (1968)

- (71) Rahmel A., Schwenk W.
"Korrosion und Korrosionsschutz von Stählen"
Verlag Chemie Weinheim (1977)
- (72) Finley T.C., Meyers J.R.
Corrosion NACE, 26(12):544-546 (1970)
- (73) Lorenz W.J.
Corros. Sci., 21(9):647-672 (1981)
- (74) Bonhoeffer K.F.
Corrosion NACE, 11:304t-308t (1955)
- (75) Lorenz W.J., Heusler K.E.
"Anodic Dissolution of Iron Group Metals"
in "Corrosion Mechanisms",
F. Mansfeld Editor, Marcel Dekker, Inc. (1987)
- (76) Kuo H.C., Landolt D.
Electrochim. Acta, 20:393-399 (1975)